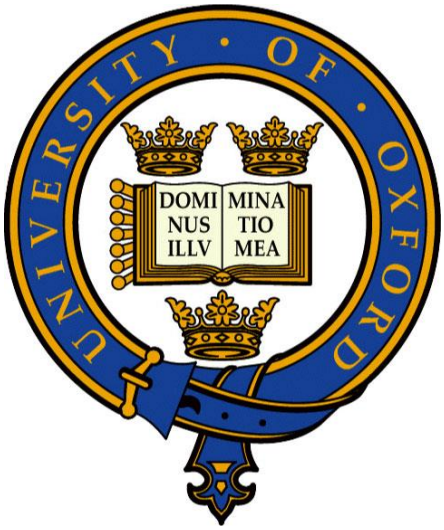
Functional evaluation of the human fat distribution *HOXC13* gene locus

A thesis submitted to the University of Oxford in candidature for the degree of Doctor of Philosophy



By

Feng-Chih Kuo

St Catherine's College, University of Oxford

Oxford Centre for Diabetes, Endocrinology and Metabolism

Radcliffe Department of Medicine

Trinity 2018

Memorandum

The work in this thesis is the original work of the author. Experiments were performed at the Oxford Centre for Diabetes, Endocrinology and Metabolism, University of Oxford, under the supervision of Professor Fredrik Karpe and Dr Katherine Pinnick. Funding was provided by the Tri-Service General Hospital, National Defence Medical Center, Taipei, Taiwan

I hereby state that no part of this thesis has been submitted for any other degree at this or any other university. This thesis is approximately 35,000 words (excluding references).

Functional evaluation of the human fat distribution *HOXC13* gene locus

Feng-Chih Kuo **St Catherine's College**

In candidature for the degree of Doctor of Philosophy Trinity 2018

Gynoid fat distinguishes from android fat in developmental origin and possesses metabolically protective roles, especially in women. Growing evidence supports that epigenetic modifications could potentially explain the regional differences between fat depots. Recent progress in transcriptome analysis has revealed that long non-coding RNAs (lncRNAs) play roles in epigenetic regulation, but their potential functions in fat depot-specific transcription remain largely unexplored. *HOX* transcript antisense RNA (*HOTAIR*) is a lncRNA that is expressed exclusively in the gluteal subcutaneous adipose tissue (GSAT); it is undetectable in the abdominal subcutaneous adipose tissue (ASAT) and locates under the fat distribution - genome-wide association studies (GWAS) locus near and around the *HOXC13* gene. Therefore, the aim of this project was to investigate the depot-specific functional roles of the *HOTAIR* gene.

GSAT *HOTAIR* expression was highly variable between individuals but generally expressed at lower levels in females compared with men. Detailed annotation of *HOTAIR*-haplotype tagging single nucleotide polymorphisms (SNPs) identified the minor allele of rs76084431 as a GSAT *HOTAIR* expression quantitative trait locus (eQTL) associated with increased android to gynoid fat mass ratio in females. Comparison of histone marks between abdominal and gluteal preadipocytes showed that rs76084431 is positioned in an open chromatin region and which could be considered as a *HOTAIR* enhancer in gluteal preadipocytes. *HOTAIR* stable knockdown and constitutive overexpression in human adipocytes provided further evidence that the *HOTAIR* gene is essential for the gluteal adipocytes, but anti-adipogenic for abdominal adipocytes. Weighted Gene Co-expression Network Analysis (WGCNA) of RNA-seq from *HOTAIR* knockdown cells data suggested regulation a number of regulated pathways: extracellular matrix and protocadherin genes appear to be predominant *HOTAIR* downstream pathways in the gluteal preadipocytes. *CEBPD*, *PTEN* and *PCDH10* were shown to be epigenetically regulated by *HOTAIR* during adipogenic differentiation of the gluteal preadipocytes.

Overall, these data suggests that *HOTAIR* is a novel and dynamic regulator of the adipocyte epigenome with functional importance for regional human adipose tissues.

Acknowledgements

I want to take this opportunity to express my appreciation to my colleagues at the Tri-Service General Hospital, who encouraged me to go for a Ph.D. degree abroad. My parents and whole family have provided their full support, especially my lovely wife and two sons who willingly moved from Taiwan to the UK and endured 4 years accompanying me. Without their support, it would not have been possible to complete my DPhil studies in Oxford.

Four years ago, it came as a great and unexpected gift that my supervisors, Professor Fredrik Karpe and Dr Katherine Pinnick, let me join their prestigious Metabolic Research Group (MRG) in OCDEM. They have guided me step by step into basic science research of determinants of human fat distribution. I also would like to thank many other friends and colleagues in OCDEM; Sandy Humphreys and Amy Barrett provided laboratory assistance to ensure all machines and consumables ordering worked smoothly; Matt Neville has guided me in performing genetic analyses; Nellie Loh taught me cell transfection and western blotting work; Marijana Todorčević helped me to measure adipocyte size in histological samples; Nathan Denton as the more senior graduate student always inspired me when I encountered difficulties; Anne Clark provided expert advice in immunohistochemistry staining; Costas Christodoulides gave me his insightful and candid advice. The clinical research nurses, especially Jane Cheeseman, helped me to recruit many research volunteers for my studies. Also, I would like to thank Professor Philippe Collas, Dr. Nolwenn Briand and Dr. Anita Sørensen in University of Oslo, who collaborated with me and performed the chromatin immunoprecipitation of histone marks in human immortalised preadipocytes; Dr. Agata Wesolowska-Andersen in the Wellcome Trust Centre for Human Genetics, who helped me analyse the RNA-sequencing data.

I am eternally grateful to all these people and many others who have made my DPhil period full of enjoyable memories. This thesis would not have been possible without their support and encouragement over time.

Table of Contents

Chapter 1 Introduction 18

1.1 Adiposity, body shape and metabolic disorders 19

1.1.1 Obesity and metabolic disorders 19

1.1.2 Body fat distribution and metabolic disorders 20

1.1.3 Determinants of upper-body and lower-body fat distribution 21

1.2 Genome-wide association studies (GWAS) of body fat distribution 23

1.2.1 Common genetic variability and human fat distribution 23

1.2.2 How can results from GWAS of fat distribution be used to understand the mechanism underlying the phenotypic variation? 24

1.2.3 Local adipose tissue function plays a role in body fat distribution 25

1.3 Depot-specific differences between abdominal and gluteal subcutaneous adipose tissue 26

1.3.1 Adipose tissue is a heterogeneous organ 26

1.3.2 Depot-specific differences in adipose tissue expandability 27

1.3.3 Depot-specific differences in fatty acids metabolism 29

1.3.4 Depot-specific differences in the sex hormone function and adipokine secretion 30

1.3.5 Depot-specific differences in developmental gene expression 34

1.3.6 Potential functional roles of developmental genes on body fat distribution 36

1.4 Epigenetic regulation in adipose tissue 37

1.4.1 Nuclear architecture 37

1.4.2 DNA methylation and histone modification 38

1.4.3 Long non-coding RNA 39

1.4.4 *HOTAIR* (*HOX* transcript antisense RNA) 40

1.5 Aims 41

Chapter 2 Methods 43

2.1 The Oxford Biobank 44

2.2 Handling of human abdominal and gluteal subcutaneous adipose tissues.... 45

2.2.1 Core needle biopsy for adipose tissue histology 45

2.2.2 Needle aspiration biopsy to recover whole adipose tissue 45

2.2.3 Extraction of genomic DNA from human adipose tissue or cells 46

2.2.4 Homogenizing human adipose tissue with TRIzol for RNA extraction..... 46

2.2.5 Isolation of stromal vascular fraction cells from human adipose tissue..... 46

2.2.6 Immortalised human subcutaneous abdominal and gluteal preadipocytes..... 47

2.3 Cell culture of human primary or immortalised preadipocytes..... 47

2.3.1 Maintenance of human primary or immortalised preadipocytes..... 47

2.3.2 Adipogenic differentiation of human primary or immortalised preadipocytes 48

2.3.3 Estimating cell proliferation..... 48

2.4 Gene expression analysis..... 49

2.4.1 RNA extraction..... 49

2.4.2 Complementary DNA synthesis 49

2.4.3 Quantitative real-time PCR 50

2.5 Quantification intracellular total protein and triglyceride contents..... 51

2.6 Western blotting..... 51

2.6.1 Extraction and quantification of cellular protein..... 51

2.6.2 Gel electrophoresis and wet transfer 52

2.6.3 Enhanced chemiluminescence..... 53

2.6.4 Densitometric analysis of Western blot images..... 53

2.7 Statistical analysis..... 54

Chapter 3 Intrinsic/dynamic *HOTAIR* expression patterns and its genetic variation for identification of phenotypic eQTLs 55

3.1 Introduction 56

3.1.1 Aims 58

3.2 Methods 59

3.2.1 Collection of paired abdominal and gluteal subcutaneous adipose tissues 59

3.2.2 Isolation of adipose-derived stromal vascular fraction cells 59

3.2.3 Maintenance and differentiation of human primary or immortalised preadipocytes 59
3.2.4 Administration of dexamethasone or oestradiol 59
3.2.5 Measurement of *HOTAIR* gene expression 60
3.2.6 Selection of predominant SNPs in *HOTAIR* locus (Haplotype map/1000 Genome data) 60
3.2.7 KASP^{TM} genotyping of *HOTAIR* SNPs 62
3.2.8 Estimation of *HOTAIR* haplotypes by using PHASE program 63
3.2.9 Chromatin immunoprecipitation for exploring the histone marks 63
3.2.10 Bisulfite conversion and pyrosequencing of genomic DNA 64
3.2.11 Statistical analysis 66
3.3 Results 67
3.3.1 *HOTAIR* expression presents gluteal depot-specific pattern with gender difference 67
3.3.2 *HOTAIR* expression is negatively correlated with age in males 68
3.3.3 *In vitro* gluteal preadipocytes maintain the intrinsic *HOTAIR* expression, which changes during adipogenic differentiation 69
3.3.4 *HOTAIR* expression was enhanced by dexamethasone, but not by oestradiol in the *in vitro* cellular model 70
3.3.5 Two haplotype-tagging SNPs have eQTLs with opposite directional effects .. 71
3.3.6 Females carrying the *HOTAIR* transcript-lowering SNP have significantly higher android to gynoid fat ratio 74
3.3.7 Recruiting rs76084431 TT genotype females to validate the eQTL effects and exploring the histone modifications/DNA methylation around rs760844431 76
3.4 Discussion 82
3.4.1 rs76084431 is not in the same LD with the lead SNPs of the GWAS identified *HOXC13* fat distribution locus 82
3.4.2 The potential mechanisms for regulating *HOTAIR* gene expression by intronic SNPs 83

3.4.3 Hypothesizing *HOTAIR* function in gluteal adipose tissue based on the genotype-phenotype associations 84
3.4.4 Concluding statements 84

Chapter 4 Phenotypic effect of modulating *HOTAIR* expression *in vitro* and *in vivo* 85

4.1 Introduction 86
4.1.1 Aims 88
4.2 Methods 89
4.2.1 Generation of stable *HOTAIR* knockdown in immortalised human gluteal preadipocytes 89
4.2.2 Cloning of *HOTAIR* construct into pEGFP-Lv105 vector 89
4.2.3 Generation of lentivirus particles containing pEGFP-Lv105-*HOTAIR* vector and pEGFP-Lv105 empty vector 91
4.2.4 Generation of constitutive *HOTAIR* overexpression in immortalised human gluteal and abdominal preadipocytes 91
4.2.5 Separation of nuclear and cytoplasmic total RNA 91
4.2.6 Custom TaqMan assay design 92
4.2.7 Anti-H3K27me3 and anti- suppressor of zeste 12 (SUZ12) chromatin immunoprecipitation 92
4.2.8 Western blotting for phosphorylated Akt (pAkt) and total Akt (tAkt) proteins 94
4.2.9 Transfecting with siRNA oligos 94
4.2.10 Bisulfite pyrosequencing for measuring DNA methylation status in the *PTEN* promoter region 96
4.2.11 Recruitment of OBB subjects based on genotype and previous GSAT *HOTAIR* levels 96
4.2.12 Gene expression analysis 97
4.2.13 Statistical analysis 97
4.3 Results 98
4.3.1 Evaluation of *HOTAIR* knockdown efficiency between stable *HOTAIR*

knockdown and scramble control gluteal preadipocytes 98
4.3.2 Assessing the functional effects of *HOTAIR* stable knockdown in gluteal preadipocytes 103
4.3.3 Assessing the functional effects of *HOTAIR* constitutive overexpression in abdominal and gluteal preadipocytes 106
4.3.4 Exploring interactions between *HOTAIR* and two potential target genes (*CEBPD* and *PTEN*) 108
4.3.5 Comparing the adipocyte sizes between females carrying rs76084431 TT and CC genotype 113
4.3.6 Recruiting subjects in whom tissue *HOTAIR* abundance has already been quantified to evaluate the *in vivo* functional roles of *HOTAIR* gene 114
4.3.7 Comparing regional fat distribution in women with differential GSAT *HOTAIR* levels. 115
4.4 Discussion 117
4.4.1 Difficulties quantifying the knockdown effect of *HOTAIR* in gluteal sh*HOTAIR* preadipocytes during adipogenesis 117
4.4.2 Depot-specific functional roles of *HOTAIR* gene in human preadipocytes 118
4.4.3 Limited evidence of phenotypic effect shown in *in vivo* studies of *HOTAIR* gene 120
4.4.4 Concluding statements 120
Chapter 5 Identifying novel *HOTAIR* targets using an unbiased approach of RNA-sequencing 122
5.1 Introduction 123
Aims 125
5.2 Methods 126
5.2.1 Gene expression analysis 126
5.2.2 RNA-sequencing for global transcriptome comparison 126
5.2.3 Chromatin immunoprecipitation in the *PCDH10* promoter region 127
5.2.4 Bisulfite pyrosequencing for measuring DNA methylation status 127

5.2.5 Western blotting of PCDH10 protein 128
5.2.6 Transfecting with siRNA oligos 128
5.2.7 Statistical analysis 129
5.3 Results 130
5.3.1 RNA-sequencing for comparing global transcriptome between gluteal sh*HOTAIR* and gluteal shControl cells during adipogenesis 130
5.3.2 *PCDH10* gene was epigenetically regulated by *HOTAIR* through both histone modifications and DNA methylation 133
5.3.3 Transiently knocking down the *HOTAIR* candidate target gene *PCDH10* in gluteal sh*HOTAIR*/shControl preadipocytes to evaluate its influence on *in vitro* adipogenesis 137
5.4 Discussion 139
5.4.1 Impact of transiently knocking down individual *HOTAIR* target genes 139
5.4.2 Functional roles of *PCDH10* gene 140
5.4.3 Extracellular matrix and adipogenesis 142
5.4.4 Concluding statements 142
Chapter 6 General discussion 144
6.1 From GWAS identification of the fat distribution *HOXC13* locus to functional evaluation of *HOTAIR* in human gluteal fat 145
6.2 Summary of main findings 146
6.3 Strengths and limitations 148
6.4 Future avenues of the research 150
Reference: 152

List of figures

Figure 1-1: The differential expression of HOX genes between gluteal and abdominal subcutaneous adipose tissues in four independent studies. 34

Figure 3-1: Selection of predominant SNPs based on LD maps and common haplotypes (<1%) in the *HOTAIR* locus constructed from HAPMAP and 1000 Genome data..... 61

Figure 3-2: Fat depot-specific and gender-specific differences in *HOTAIR* expression 67

Figure 3-3: *In vitro* dynamic *HOTAIR* expression during adipogenic differentiation..... 69

Figure 3-4: *HOTAIR* expression in the gluteal preadipocytes was enhanced by dexamethasone, but not oestradiol in the *in vitro* cellular model..... 70

Figure 3-5: Two haplotype-tagging SNPs have eQTLs with opposite directional effects 72

Figure 3-6: Females carrying rs76084431 TT genotype have significant lower *HOTAIR* expression in gluteal adipose tissue than females with CC genotype 76

Figure 3-7: Patterns of histone modification across the *HOTAIR/HOXC* locus in gluteal and abdominal preadipocytes 77

Figure 3-8: Evaluation of the *in vivo HOTAIR* DNA methylation status in genotype-recruited gluteal subcutaneous adipose tissue 80

Figure 4-1: Transducing *HOTAIR* shRNA lentivirus in gluteal cells interferes the *HOTAIR* expression with counterintuitively elevated levels during adipogenesis 98

Figure 4-2: Using designed TaqMan assay to assess the cleavage of *HOTAIR* mRNA by shRNAs and evaluate *HOTAIR* knockdown efficiency in cytoplasmic and nuclear components 100

Figure 4-3: *HOXD8* and *HOXD10* genes were de-repressed and *HOTAIR* function was suppressed in the gluteal sh*HOTAIR* cells 101

Figure 4-4: Cell proliferation rate and adipogenesis were impaired in the gluteal sh*HOTAIR* preadipocytes 103

Figure 4-5: Expression of master adipogenic transcription genes and early adipogneic genes were influenced in the gluteal sh*HOTAIR* cell 104

Figure 4-6: The gluteal sh*HOTAIR* cell becomes relatively insulin resistant with increased *PTEN* expression in the late phase of differentiation 105

Figure 4-7: Cell proliferation rate was increased in both *HOTAIR* preadipocytes and adipogenesis was suppressed specifically in the abdominal *HOTAIR* cell 106
Figure 4-8: Overexpression of *HOTAIR* in the abdominal preadipocytes significantly suppresses the adipogenic differentiation 107
Figure 4-9: Overexpression of *HOTAIR* in human gluteal preadipocytes suppresses *PTEN* and *CEBPD* levels during cell proliferation 108
Figure 4-10: The presence of H3K27me3 or SUZ12 in the *CEBPD* and *PTEN* promoter regions were significantly reduced in gluteal sh*HOTAIR* cells..... 109
Figure 4-11: Methylation of the *PTEN* promoter is not regulated by *HOTAIR* in proliferating cells condition. 110
Figure 4-12: Transient suppression of *CEBPD* expression in gluteal sh*HOTAIR* and gluteal shControl cells during *in vitro* adipogenesis 111
Figure 4-13: Transient suppression of *PTEN* expression in gluteal sh*HOTAIR* and gluteal shControl cells during *in vitro* adipogenesis 112
Figure 4-14: Comparison of gluteal and abdominal adipocyte size distribution between rs76084431 TT genotype and CC genotype females 113
Figure 4-15: Current GSAT *HOTAIR* expression retains positive correlation with previous expression levels only in males, but not in females 114
Figure 4-16: GSAT *HOTAIR* expression between premenopausal and postmenopausal women..... 115
Figure 5-1: Comparing the transcriptome profiling between gluteal sh*HOTAIR* and shControl cells during adipogenesis 130
Figure 5-2: Weighted Gene Co-expression Network Analysis (WGCNA) highlights 135 genes maintain significant increased expression in the gluteal sh*HOTAIR* cells..... 132
Figure 5-3: Real-time qPCR confirms *HOXD3*, *HOXD9*, *PAX3* and *PCDH10* genes maintain increased expression in the gluteal sh*HOTAIR* cells through adipogenesis..... 133
Figure 5-4: Overexpression of *HOTAIR* in the human gluteal preadipocytes reduces the abundance of PCDH10 protein 134
Figure 5-5: The presence of H3K27me3 and SUZ12 on the promoter region of *PCDH10*

were significantly reduced in the D0 gluteal sh*HOTAIR* preadipocytes 135
Figure 5-6: Evaluation of the DNA methylation status in the *PCDH10* promoter region between gluteal sh*HOTAIR* and shControl preadipocytes under proliferation 136
Figure 5-7: GSAT *PCDH10* expression is negatively correlated with GSAT *HOTAIR* expression 137
Figure 5-8: Transient suppression of *PCDH10* expression in gluteal sh*HOTAIR* and gluteal shControl cells through adipogenesis 137
Figure 6-1: Summary of *HOTAIR* functional effects in regional adipose tissue 148

List of Tables

Table 2-1: Reverse-transcription reaction volumes for cDNA synthesis 50

Table 2-2: Solutions for Preparing Gels for Tris-glycine SDS-Polyacrylamide Gel Electrophoresis..... 52

Table 3-1: ChIP primers for exploring histone marks in the *HOTAIR/HOXC* locus..... 63

Table 3-2: Composition for bisulfite PCR reactions 64

Table 3-3: Bisulfite PCR primers and their optimal conditions..... 65

Table 3-4: Sequencing primers for bisulfite pyrosequencing 66

Table 3-5: Spearman correlation coefficients between GSAT *HOTAIR* expression and anthropometric or biochemical variables in OBB subjects (105 females and 99 males)..... 68

Table 3-6: GSAT *HOTAIR* levels among rare versus other genotype groups of *HOTAIR* 9 tagging SNPs..... 72

Table 3-7: GSAT *HOTAIR* levels among genotype groups of rs1443512, rs76084431 and rs12427129..... 73

Table 3-8: Body fat distribution among TT+TC versus CC genotype of *HOTAIR* transcript-lowering variant (rs76084431) in females 74

Table 3-9: Body fat distribution among TT+TC versus CC genotype of *HOTAIR* transcript-elevating variant (rs12427129) in females..... 75

Table 3-10: The interpretation of the histone marks for recognising promoter/enhancer..... 78

Table 4-1: Primers designed for cloning *HOTAIR* construct..... 90

Table 4-2: Custom TaqMan assays designed for the promoter regions of genes 93

Table 4-3: Bisulfite PCR primers and their optimal conditions..... 96

Table 4-4: Sequencing primers for bisulfite-pyrosequencing 96

Table 4-5: Body fat distribution among females with differential GSAT *HOTAIR* 116

Table 5-1: Custom TaqMan assay designed for the promoter regions of *PCDH10* gene 127

Table 5-2: Bisulfite PCR primers and their optimal conditions..... 127

Table 5-3: Sequencing primers for bisulfite-pyrosequencing 128

Abbreviation

ATBF Adipose tissue blood flow

ASAT Abdominal subcutaneous adipose tissue

BMI Body mass index

ChIP Chromatin immunoprecipitation

CTs Chromosome territories

DEGs Differentially expressed genes

DXA Dual-energy x-ray absorptiometry

ECL Enhanced chemiluminescence

ECM Extracellular matrix

eQTL Expression quantitative trait locus

ER Oestrogen receptor

EREs Oestrogen response elements

EZH2 Enhancer of zeste homolog 2

FDR False discovery rate

FISH Fluorescence in situ hybridization

GFP Green fluorescent protein

GIANT Genetic investigation of anthropometric traits

GR Glucocorticoid receptor

GSAT Gluteal subcutaneous adipose tissue

GTEx Genotype-tissue expression

GWAS Genome-wide association studies

HAPMAP Haplotype map

hASCs Human adipose-derived stem cells

HBSS Hanks' balanced salt solution

HDL High density lipoprotein

hnRNP Heterogeneous nuclear ribonucleoproteins

HOMA-IR Homeostatic model assessment of insulin resistance

HOTAIR HOX transcript antisense RNA

HOX Homeobox

HRP Horseradish peroxidase

HREs Hypoxia response elements

KASP Kompetitive allele specific PCR

LADs Lamin-associated domains

LB Lysogeny broth

LD Linkage disequilibrium

LncRNA Long non-coding RNA

LPL Lipoprotein lipase

LSD1 Lysine-specific histone demethylase 1

MAF Minor allele frequency

MSCs Mesenchymal stem cells

NEFA Non-esterified fatty acid

NTC No template control

OBB Oxford biobank

PBS Phosphate-buffered saline

PHASE Phylogenetics and sequence evolution

PRC2 Polycomb repressive complex 2

PVDF Polyvinylidene difluoride

qPCR Quantitative polymerase chain reaction

RISC RNA-induced silencing complex

SNP Single nucleotide polymorphism

SUZ12 Suppressor of zeste 12

TAG Triglyceride

TBST Tris-buffered saline containing 0.1% Tween-20

TPM Transcript per million

TSS Transcription start site

WGCNA Weighted gene co-expression network analysis

WHR Waist-to-hip ratio

Chapter 1
Introduction

1.1 Adiposity, body shape and metabolic disorders

1.1.1 Obesity and metabolic disorders

Obesity arises from a long-term imbalance between caloric intake and energy expenditure with the consequence of excess energy stored as fat. This is reflected by an increase in body weight relative to height. The accumulation of adipose tissue is often accompanied by a low-grade, chronic and systemic inflammatory status. Obesity is associated with metabolic disorders including type 2 diabetes mellitus, cardiovascular disease, and also some cancers (Williams, et al., 2015). It is also related to lower quality of life (Vallis, 2016) and higher all-cause mortality (Global, et al., 2016). According to the World Health Organization, being overweight is defined as body mass index (BMI) $\geq$ 25 kg/m^2 whereas the cut off for obesity is BMI $\geq$ 30 kg/m^2. The prevalence of obesity was estimated to be 13% of the world's adult population in 2016 with more than 650 million adults being obese. Correspondingly, overweight adults were 39% for men and 40% for women (WHO, 2017). Furthermore, it has been forecasted that 57.8% (3.3 billion people) of the world's adult population will be overweight by 2030 (Finkelstein, et al., 2012; Kelly, et al., 2008). Therefore, obesity-related metabolic disorders are expected to increase continuously in the coming decades.

The reasons for the rise in obesity prevalence are complex and multifactorial. Several factors that influence human behaviours such as socioeconomic status, environment, neural or endocrine network systems and genetic/epigenetic heritability need to be taken into account (Gonzalez-Muniesa, et al., 2017). Hence, approaches to tackle the current obesity trends require multiple strategies including lifestyle modification, dietary adjustment, physical activity, medical management and most extremely bariatric surgery. However, most commonly used therapeutic approaches have a low or variable effect. Tight adherence to caloric restriction is required for the long-term success of maintained weight loss, which is difficult to implement due to strong feedback loops favouring energy conservation in human evolution. Although

bariatric surgery has been proven to be an effective treatment to achieve weight loss or even remission of obesity-related metabolic comorbidities (Nguyen and Varela, 2017), it is mainly used in subjects with severe obesity. The risk of surgical complications or the requirement for lifelong nutritional support should also be considered. Therefore, novel therapeutic approaches to ameliorate metabolic disorders in obesity are still required.

1.1.2 Body fat distribution and metabolic disorders

When considering the metabolic disorders predisposing to type 2 diabetes or cardiovascular disease, body fat distribution should not be ignored. Most of human body fat (80-90%) is stored in the subcutaneous areas and this can generally be divided into upper-body and lower-body subcutaneous depots. Anatomically they can be referred to as abdominal subcutaneous adipose tissue and gluteofemoral subcutaneous adipose tissue, respectively. Generally, women have higher total body fat and a greater proportion of lower-body fat compared with men and thereby a tendency towards a pear-shaped body (Fried, et al., 2015). The circumference around the waist and the hip can be used as an approximate measure of regional fat content. The waist-to-hip ratio (WHR) has been shown to have stronger and more consistent positive association with obesity-related diseases than body fatness *per se.* For example, comparing BMI and WHR, the risk for myocardial infarction is higher for WHR than for BMI in the INTERHEART study (Yusuf, et al., 2005). Similarly, WHR is independently associated with the incidence of type 2 diabetes mellitus (Vazquez, et al., 2007). Using Mendelian randomization techniques it has been possible to demonstrate a causal relationship with higher WHR and increased risks of cardiovascular events (Emdin, et al., 2017). Hence, these studies provide strong evidence that fat distribution is associated with increased risk of metabolic disorders independent of overall fatness and could be a major driver of disease risk.

Separating the components of WHR, i.e. waist circumference and hip circumference, to search for independent relationships to metabolic disorders, some

studies have suggested that the lower-body fat has an independent "protective" property. In the INTERHEART study, hip circumference showed an association with decreased risk of myocardial infarction and this effect became stronger after adjustment for BMI and height (Yusuf, et al., 2005). The EPIC study showed that waist and hip circumference displayed independent and opposite associations with coronary artery disease after adjustment for BMI and cardiovascular risk factors (Canoy, et al., 2007). Accumulation of lower-body subcutaneous fat is also associated with lower likelihood of type 2 diabetes mellitus independent of overall adiposity in both sexes (Livingston, 2006). By using dual-energy X-ray absorptiometry (DXA) scans to precisely quantify regional fat mass, the group of my supervisors have demonstrated that gynoid fat mass, after adjustment for total fat mass, is inversely associated with insulin resistance and dyslipidaemia in both genders (Pinnick, et al., 2014). There are functional differences between abdominal and gluteofemoral subcutaneous adipose tissue. For example, the gluteofemoral tissue possesses increased expandability during weight gain and has a higher capacity to sequester lipids for long-term storage. Therefore, lower-body fat depots can be considered as a metabolic sink that prevents insulin-sensitive tissues from excessive fatty acid exposure and so-called ectopic fat accumulation (Karpe and Pinnick, 2015). Factors including age, gender, steroid hormones, drugs and genetics also influence fat depot-specific biological function. Thus, when discussing the impact of body fat distribution on metabolism, these factors also need to be considered.

1.1.3 Determinants of upper-body and lower-body fat distribution

The noticeable sex-specific android and gynoid fat distribution pattern becomes apparent at puberty. Sex steroids play key roles during this period; testosterone primarily helps build up lean mass in boys and oestrogen increases the regional fat mass in girls (Hattori, et al., 2004; Maynard, et al., 2001; Wells, 2007). With the decline of testosterone and oestrogen during menopause, accumulation of central adiposity is seen in both sexes (Allan, et al., 2008; Lovejoy, et al., 2008; Stevens, et al., 2010).

Hormones, such as glucocorticoids and growth hormone are also known to influence body fat distribution. Chronic exposure to excessive glucocorticoids, such as patients with Cushing's syndrome or under long-term pharmacological use of corticosteroids, causes central obesity with adverse cardiometabolic outcomes (Burt, et al., 2006; Lee, et al., 2014). Subjects with growth hormone deficiency present with increased total body fat, decreased lean mass but increased abdominal fatness. Replacement of growth hormone can reduce the central adiposity (Bengtsson, et al., 1993; Burt, et al., 2006; Roemmich, et al., 2001). Few other drugs affect body fat distribution but the group of insulin sensitizers (Thiazolidinediones, TZDs), targeting peroxisome proliferator-activated receptor-γ (PPARγ), can affect body fat distribution. Basically, TZDs can reduce visceral and ectopic fat accompanied by expansion of subcutaneous adipose tissue, preferentially in the lower-body (Rasouli, et al., 2005; Shadid and Jensen, 2003). In HIV-infected patients, fat redistribution has also been associated with long-term antiretroviral therapy. The fat redistribution could be peripheral lipoatrophy in the face, limbs and buttocks or lipohypertrophy particularly in the breasts, dorsocervical and visceral fats (Carr, 2003).

Genetics is also considered as a major determinant of body fat distribution. Several twin studies have been performed to estimate the heritability of fat distribution by measuring the within-pair correlation of WHR. However, there is a wide range of estimated heritability, ranging from 6-89% in different twin studies (Lehtovirta, et al., 2000; Poulsen, et al., 2001; Selby, et al., 1990). One possible reason for this substantial variation could be the way regional adiposity is measured where WHR is an imprecise tool whereas methods employing direct quantification of regional fat masses might show stronger associations. The same research group which initially published low heritability estimates (6%) of abdominal obesity re-examined and reported that there is actually a strong genetic heritability in regional fat distribution (71-85%) when combining the use of DXA scan and biometric modelling to quantify the regional fat mass more precisely. Moreover, the high heritability is similarly observed within

young twins as well as in elderly twins (Malis, et al., 2005). In addition, there is strong evidence from monogenic disorders in which mutations in a limited number of genes (*CIDEC, PLIN1, AKT2, PPARG, LMNA*) cause partial lipodystrophy, which is characterized by selective loss of regional white adipose tissue (Garg, 2011). These studies have provided convincing evidence that regional fat distribution is strongly influenced by genetic factors. Additional evidence comes from genome-wide association studies of fat distribution, results of which have been a theme in my thesis.

1.2 Genome-wide association studies (GWAS) of body fat distribution

1.2.1 Common genetic variability and human fat distribution

With the introduction of large-scale and easily accessible genotyping platforms, genome-wide association studies (GWAS) were first introduced in 2005 (Klein, et al., 2005). This allowed for testing associations between complex traits and common genetic variability, which mainly focussed on single nucleotide polymorphisms (SNPs) with minor allele frequency (MAF) >5%. Due to the massive multiple testing there has been strict attention to statistical robustness. As of 1st September 2016, more than 24,000 SNPs have been associated with one or more complex traits in more than 2,500 publications (MacArthur, et al., 2017). For fat distribution the only traits available so far in very large cohorts have been BMI, waist and hip circumference. By using WHR adjusted for BMI as the surrogate of body fat distribution, meta-analysis of 32 GWAS (comprising up to 77,167 participants) was executed in 2010 and 14 SNPs were found to be associated with WHR adjusted for BMI at genome-wide statistical significance (Heid, et al., 2010). More recently, an even larger meta-analysis of 57 GWAS and 44 Metabochip studies (comprising up to 224,459 individuals) for the WHR adjusted for BMI trait was conducted in 2015 with the identification of 49 independent gene loci (33 new) (Shungin, et al., 2015). Twenty of these 49 loci show a significant sexual dimorphism and most of them (n = 19) have a stronger effect in women. Despite this large and impressive discovery work, only a small fraction of total variation (2.4%) in WHR adjusted for BMI is explained in females and even less in men (0.8%). The

proportion of trait variability explained by common genetic variants and estimated heritability (71-85%) (Malis, et al., 2005) is unusually large for fat distribution compared with other complex traits. This 'heritability' gap could be due to a number of different reasons. It could be that the heritability has been overestimated in the first place as it is often performed in twins for which it is sometimes difficult to separate the heritable and environmental components. It has been suggested that undiscovered low frequency/ rare SNPs could impact on the phenotypic variability (Cirulli and Goldstein, 2010; Wang, et al., 2016). There could be a 'long tail', i.e. despite the very large numbers available in existing GWAS meta-analyses, these studies are still underpowered to detect many additional contributing genetic loci. It has been suggested that some variation could be epigenetic and thus possibly counted into heritability as the foetal environment is shared between twins and some epigenetic signatures can be established at this stage. Finally, it is possible that the phenotype as such (quantifying fat distribution) is imprecise using conventional methods (WHR) compared with more sophisticated ways of assessing fat distribution, such as DXA scanning, which has been employed in some heritability studies.

1.2.2 How can results from GWAS of fat distribution be used to understand the mechanism underlying the phenotypic variation?

GWAS have helped distil several genetic loci that potentially have individual or synergistic influence on the trait of interest. Although the impacts of individual GWAS loci on the phenotypic trait are small, their influence on molecular mechanisms explaining the complex trait could be significant (Visscher, et al., 2017). Currently, functional studies to link GWAS identified loci to the biological or molecular levels are still very limited and the fact that the vast majority (more than 90%) of GWAS lead SNPs map within non-coding sequence further impedes the functional interpretation (Maurano, et al., 2012).

Although it is arduous to gain biological insights from GWAS identified loci, there are some methods or strategies that can help in prioritising possible gene candidates.

Detection of enriched pathways and pinpointing the tissues/cell types that are likely to be involved in the trait of interest can be helpful. For example, the framework of DEPICT (Data-driven Expression Prioritized Integration for Complex Traits) can identify likely causal genes by reconstituting gene sets in different loci that share similar predicted functions and select implicated tissues or cell types by assessing the enriched expression for genes from associated loci (Pers, et al., 2015). Since the GWAS-identified lead SNPs are most often only likely to serve as proxies for the functional SNPs within the haplotype block, further dense genotyping and linkage disequilibrium (LD) calculation could be applied to refine the associated SNPs. Moreover, the combined approaches to identify either cell-type specific expression-associated SNPs or regulatory SNPs that lie within promoters, enhancers, high chromatin accessibility or CpG dinucleotides regions can help identifying functional SNPs (Tak and Farnham, 2015).

Methods for identification of the open chromatin include DNase-sequencing, which finds areas that are accessible to DNase I digestion (Boyle, et al., 2011) and Assay of Transposase Accessible Chromatin sequencing (ATAC-seq), which uses an engineered Tn5 transposase for efficiently cutting exposed DNA (nucleosomes-free) regions. Therefore, ATAC-seq can be performed with fewer cells (500-50,000 cells) and it is thought to be less noisy than DNase-seq (Buenrostro, et al., 2013). More specifically, Chromatin ImmunoPrecipitation sequencing (ChIP-seq) uses an antibody of either a specific histone mark or a transcription factor to immunoprecipitate its presence on the DNA regions. Mapping the chromatin accessibility with the associated SNPs helps select candidate functional SNPs. Furthermore, novel genome–editing tools, such as CRISPR Cas9 can be applied to validate the phenotypical effects of candidate SNPs.

1.2.3 Local adipose tissue function plays a role in body fat distribution

In order to define GWAS-identified loci as expression quantitative trait loci (eQTLs) or evaluate if the associated SNPs map with regulatory elements, it is important to use specific tissues/cell types that are relevant to the trait of interest. However, for many

complex traits (e.g. for height or longevity) or many complex diseases (for example neurodegenerative diseases), the relevant tissue or cell type is either difficult to identify or inaccessible (Paul, et al., 2014). This is certainly less of a problem for tissues/cell types determining the body fat distribution trait. Intuitively, depot-specific subcutaneous adipose tissues, with its specific adipocytes, are considered the predominant tissues/cell type determining regional fat distribution. Indeed, this was supported by the recent meta-analysis of GWAS on WHR adjusted for BMI (Shungin, et al., 2015), which explored the possible biological mechanisms of identified gene loci using the frameworks of GRAIL (Raychaudhuri, et al., 2009), MAGENTA (Segre, et al., 2010) and DEPICT (Pers, et al., 2015), which indicated the involvement of adipocyte-related tissues, including abdominal subcutaneous fat as enriched for the expression of genes in or near the fat distribution GWAS loci. It has (Karpe and Pinnick, 2015; Pinnick, et al., 2014) also been pointed out that the gluteofemoral and abdominal subcutaneous adipose tissues possess depot-specific intrinsic differences in both biological function and show distinct differences in the expression of developmental genes. Therefore, further experimental analysis using regional adipose tissues-centred approaches will be valuable and can potentially decipher the mechanisms underlying the phenotypic variation in body fat distribution.

1.3 Depot-specific differences between abdominal and gluteal subcutaneous adipose tissue

1.3.1 Adipose tissue is a heterogeneous organ

Comparative studies of regional adipose tissues have revealed that the tissues are different in terms of both cell morphology and biological function. There is an overall divide between white and brown adipose tissue based on its colour on the gross appearance. The brown colour is due to the high density of mitochondria and numerous small lipid droplets within individual adipocytes (Enerback, 2009). Brown adipose tissue is thermogenic and plays a role in maintaining body temperature in newborns. The brown fat is mainly located in the neck, in the interscapular and suprascapular

region, it also surrounds the kidneys and is found along the spinal cord (Gesta, et al., 2007). The small remnants remaining in adult humans decline with age, but studies have also identified ‘beige’ or ‘brite’ adipose tissue that is interspersed within white adipose tissue in adults. This can be trans-differentiated from white adipose tissue by repeated cold exposure and akin to the classic brown stores it is activated by adrenergic stimulation (Enerback, 2009; Petrovic, et al., 2010; Wu, et al., 2012).

White adipose tissue is the dedicated organ for storage of excess energy and thus plays a key role in fatty acid metabolism. It is also known as an endocrine organ with bioactive peptide secretion and steroid hormone metabolism (Mohamed-Ali, et al., 1998). Importantly, different white adipose tissue depots have different biological functions which impact on the systemic energy homeostasis with consequences on diabetes and cardiovascular risk. The majority of studies on depot-specific white adipose tissue focus on the visceral and abdominal subcutaneous adipose tissue. Visceral/ectopic fat is thought of as an ‘unhealthy’ fat depot which releases a large amount of free fatty acids, adipocytokines and inflammatory factors, the flux of which feeds directly into the liver via the portal vein, leading to hepatic insulin resistance and metabolic disorders (Wang and Li, 2017). In contrast, the gluteofemoral subcutaneous adipose tissue depot is considered to be protective against cardiometabolic disorders, possibly due to its capacity to safely sequester fat away from spilling over to other tissues, for example liver and muscle. However, functional studies of this depot are sparse. The underling molecular mechanism that makes it a ‘healthy’ fat depot is still poorly understood. Therefore, I will focus on some detailed aspects of the depot-specific differences between abdominal subcutaneous and gluteofemoral subcutaneous adipose tissue.

1.3.2 Depot-specific differences in adipose tissue expandability

As white adipose tissue serves to safely store excess energy in the form of triglycerides, its capability for expansion when facing continued positive energy balance becomes a crucial factor to counteract systemic lipotoxicity and maintain

metabolic homeostasis (Gray and Vidal-Puig, 2007). This 'expandability theory' was first formulated by Eliot Danforth Jr (Danforth, 2000) and is supported by some examples of altered adipose tissue function/amount in both animal models and human states. In the adiponectin transgenic *ob/ob* mice, the expandability of subcutaneous adipose tissue was massively increased and led to weight gain in the absence of diet-induced insulin resistance (Kim, et al., 2007). The corresponding condition in humans has been denoted 'metabolically healthy obesity'. The variability between individuals to develop obesity-induced insulin resistance, suggests there is variation in the adipose tissue expandability, which in turn determines the metabolic consequences when encountering body weight gain. An opposite extreme example is with the rare forms of partial lipodystrophy caused by autosomal dominant mutations in *LMNA* and *PPARG*, such as Dunnigan-Kobberling syndrome which displays selective loss of subcutaneous adipose tissue in arms and legs but excess fat accumulation on the face and neck region. These patients suffer from severe insulin resistance and metabolic disorders (Schmidt, et al., 2001). Moreover, in the transgenic mice with lipoatrophic diabetes, transplantation of functional adipose tissue can partially reverse metabolic abnormalities (Gavrilova, et al., 2000). The study on lipodystrophy further consolidates the theory that maintenance of a fully functional and expandable fat depot can ameliorate metabolic risks when there is an excessive demand for fat storage. This is probably particularly pertinent to the lower-body fat (gluteofemoral subcutaneous adipose tissue). Indeed, the cellular responses of upper-body and lower-body subcutaneous fat depots during overfeeding in healthy, normal weight adults have been investigated and lower-body fat shows a hyperplasic response during weight gain whereas the upper-body fat response is hypertrophy of adipocytes (Tchoukalova, et al., 2010). The hyperplasic response generates new adipocytes in the gluteofemoral adipose tissue and provides a well-controlled fat storage environment avoiding the hypoxic and inflammatory microenvironment that is seen with hypertrophy (Engin, 2017).

1.3.3 Depot-specific differences in fatty acids metabolism

During day-to-day metabolism, the lipid handling in regional adipose tissue shows depot- and gender-specific characteristics. The amount of regional white adipose tissue is dynamically controlled by the balance between release of non-esterified fatty acid (NEFA) via lipolysis and the uptake/storage of fatty acids through the lipoprotein lipase (LPL)-mediated mechanism from chylomicron and very-low-density lipoprotein or direct uptake of circulating NEFA. This dynamic balance is turned towards uptake/storage after meals, which is triggered by the inhibition of intracellular lipolysis by insulin concomitantly with the increased activity of LPL promoting fat uptake. A contributory factor could also be the meal induced increase in adipose tissue blood flow (ATBF) (Manolopoulos, et al., 2010; Thompson, et al., 2012). By using radio-labelled NEFA *in vivo*, it has also been suggested that there is direct uptake of circulating NEFA by subcutaneous adipose tissue and that this is greater in women than men both in the post-prandial and post-absorptive states (Koutsari, et al., 2008; Shadid, et al., 2007). From a regional fat redistribution point of view it has also been noted that in the post-prandial period, the abdominal subcutaneous fat takes up NEFA more avidly than lower-body subcutaneous fat in both sexes (Koutsari, et al., 2008). Nevertheless, post-absorptively, men maintain preferential storage of fatty acids in the abdominal subcutaneous fat; women show equivalent storage of NEFA in both upper-body and lower-body fats, which subsequently increases the lower-body fat deposition (Shadid, et al., 2007). Also, *in vitro* studies in abdominal and gluteal subcutaneous adipose tissues of non-obese individuals found men have higher LPL activity in the abdominal fat, whereas women have higher LPL activity in the gluteal fat (Arner, et al., 1991). Overall, these studies provide plausible explanations on how differences in body fat distribution are maintained between genders and also point to the fact that the main function of abdominal subcutaneous fat is to provide an effective storage compartment for meal-derived fatty acids (Manolopoulos, et al., 2010).

The major stimulus for lipolysis in abdominal adipose tissue is adrenergic, whereas

the gluteofemoral tissue is largely unresponsive to adrenaline. The absence of this 'fight and flight' response suggests a specific ability for long-term fatty acid storage. In this context it is interesting to note that the role of leg fat as a contributor to systemic provision of NEFA during physical exercise is largely unexplored. (Manolopoulos, et al., 2010; Thompson, et al., 2012). The differential lipolytic response between the tissues observed *in vivo* is confirmed *in vitro* and explained by the different abundance of lipolytic (beta 1- and beta 2-adrenergic) and anti-lipolytic (alpha 2-adrenergic) adrenergic receptors on the surface of the regional human white adipocytes (Arner, et al., 1990; Lafontan and Berlan, 1993; Wahrenberg, et al., 1989). Also, in the obese premenopausal women, gluteal adipocytes present higher sensitive to the anti-lipolytic effect of insulin than abdominal adipocytes (Johnson, et al., 2001). In summary, upper- and lower-body fat depots possess distinct properties relating to fatty acid uptake and lipolysis. The abdominal depot acts as a buffer for the influx of dietary fatty acids on a short-term basis. In contrast, the gluteofemoral depot reacts more passively toward lipolysis and exerts its protective properties as a metabolic sink for long-term entrapment of fatty acids. Therefore, well-functioning lower-body fat tissue can prevent excessive exposure of lipids to insulin sensitive tissues such as liver, muscle and pancreas (Karpe and Pinnick, 2015).

1.3.4 Depot-specific differences in the sex hormone function and adipokine secretion

Due to the appearance of sexual dimorphic adiposity and changes in fat distribution during puberty, regulation of regional adipose tissue by sex hormones becomes an intriguing research topic. Generally speaking, oestrogens are thought to increase total adiposity with preferential lower-body fat deposition during the growth and development of female adolescents (Wells, 2007). In oestrogen deficiency, such as after menopause, central adiposity is increased with subsequent metabolic disorders in the postmenopausal women (Stevens, et al., 2010). Based on two independent studies in postmenopausal women with either long-term oral supplement of oestrogen (Lindberg, et al., 1990) or short-term intravenous injection of conjugated oestrogens

(Van Pelt, et al., 2006), oestrogens appear to suppress lipolysis in the subcutaneous adipose tissue with higher effects on the gluteal depot than abdominal depot. These findings are compatible with the proposed concept that oestrogens preserve the lower-body fat deposition and also suggest oestrogens may mediate anti-lipolysis through both genomic and non-genomic mechanisms (Mayes and Watson, 2004). Research in transsexuals undergoing cross-sex hormone therapy also support the anti-lipolytic effect of oestrogens. One year long administration of oestrogens in male to female transsexuals can increase the fat cell size and inhibit *in vitro* basal lipolytic activity in both abdominal and gluteal subcutaneous fat depots (Elbers, et al., 1999). The differential effect of oestrogen in the regional fat tissues could be explained by differences in oestrogen receptor (ER) protein content; there is higher abundance of ER-beta and lower abundance of ER-alpha in the gluteal subcutaneous adipose tissue compared to the abdominal subcutaneous adipose tissue (Gavin, et al., 2013). Although studies with oestrogen receptor knockout mice suggested the ER-alpha is involved in reduction of fat mass whereas ER-beta may counteract the functions of ER-alpha (Mayes and Watson, 2004), but the actual roles of these two ERs in human regional adipose tissue are still unclear and future investigation is needed to decipher their depot-specific functions. Furthermore, experiments using human adipose-derived stem cells (hASCs) from either abdominal subcutaneous fat or thigh fat revealed that *in vitro* administration of oestradiol can increase cell proliferation and adipogenic differentiation (Hong, et al., 2007; Luo, et al., 2013; Razavi, et al., 2015). To connect the influence of oestrogen replacement therapy to the cell biology in regional adipose tissue, one randomized, cross-over design, with 2 week application of transdermal oestradiol, or placebo patches, was performed in postmenopausal women (Cox-York, et al., 2017). After each treatment, paired abdominal and femoral subcutaneous hASCs were isolated and cultured to evaluate *in vitro* proliferation and differentiation. This study showed that femoral hASCs, but not abdominal hASCs, had a significantly enhanced adipogenic differentiation after transdermal oestradiol. These *in vitro* studies are also in line with the finding that oestrogens seem to increase general adiposity and

gynoid fat deposition in females. Although it has been suggested that oestrogens can also influence LPL activity in regional human adipose tissue, results in the literature are inconsistent. For example, application of transdermal oestradiol patch in premenopausal women suppressed local LPL activity in the gluteal fat depot (Price, et al., 1998), but oral co-supplementation with oestrogens and progestins in postmenopausal women (Rebuffe-Scrive, et al., 1987) or local percutaneous application of progesterone in premenopausal women (Rebuffe-Scrive, et al., 1983) increased LPL activity in femoral subcutaneous adipocytes/adipose tissue. These divergent results may be due to different concentrations/routes of oestrogens administration (Palin, et al., 2003). Other unresolved issues are whether progestins differentially regulate depot-specific LPL activity (Mayes and Watson, 2004).

A key role for androgens in normal physiology is to help accumulate lean body mass during the pubertal development in boys (Wells, 2007). It is also negatively correlated to central adiposity in men based on the cross-sectional (Pasquali, et al., 1991) and longitudinal observational studies (Gapstur, et al., 2002). This concept was also supported by studies in two special examples: men with hypogonadism and female to male transsexuals. In men with hypogonadism, restoring testosterone levels to the normal physiological range can improve the glucose homeostasis, increase lean mass and reduce the waist circumference (Saad, 2017). In female to male transsexuals, one year long administration of testosterone was found to decrease the subcutaneous fat and fat cell size at both gluteal and abdominal depots and increase basal lipolysis in the abdominal depot, but not in the gluteal depot (Elbers, et al., 1999). However, it is worth noting that in the long-term hyper-androgenic status, androgens appear to cause adverse consequences with accumulation of visceral adipose tissue, such as women with polycystic ovary syndrome (Dunaif, 1997) and 3 years administration of testosterone in female to male transsexuals (Elbers, et al., 1997). Experiments using hASCs show that androgens can suppress adipogenic differentiation in the abdominal subcutaneous and visceral fat depots (Blouin, et al., 2010; Chazenbalk, et al., 2013).

These results are in agreement with the normal physiological effect on androgens showing a decrease in central fat accumulation and therefore suggest a narrow range in androgenic tone to achieve this. In term of the effects of androgens on LPL activity in regional adipose tissue, different studies showed inconsistent results and are probably complicated by the aromatization of androgen to oestrogen (Mayes and Watson, 2004).

White adipose tissue can also secrete adipokines that can influence the systemic metabolic status. Leptin and adiponectin have higher mRNA expression in subcutaneous adipose tissue compared to visceral adipose tissue (Fisher, et al., 2002; Hube, et al., 1996). By using the western analysis to evaluate the adiponectin protein content, the subcutaneous adipose tissue showed higher protein amounts than omental adipose tissue. In the gluteal fat, non-diabetic subjects had higher adiponectin content compared to diabetic subjects (Fisher, et al., 2002). The secretion of leptin is higher in subcutaneous abdominal adipocytes compared with omental adipocytes in women (Van Harmelen, et al., 1998). Women have higher plasma concentrations of both leptin and adiponectin compared with men (Nishizawa, et al., 2002; Saad, et al., 1997). Based on these findings, it is tempting to suggest that the adipokine release pattern from gluteofemoral subcutaneous adipose tissue is more metabolically advantageous compared with abdominal subcutaneous adipose tissue. However, *in vivo* arterio-venous sampling across these two fat depots has shown no significant difference in the secretions of leptin and adiponectin. However, it has been found that lower-body adipose tissue releases higher amounts of the insulin-sensitising lipokine palmitoleate and lower amounts of the pro-inflammatory cytokine interleukin-6 (Pinnick, et al., 2012; Pinnick, et al., 2014).

1.3.5 Depot-specific differences in developmental gene expression

A

Studies that comparing two subcutaneous depots	high in gluteal	high in abdominal
Pinnick *et al.* (2014)	★	★
Karastergiou *et al.* (2013)	■	■
Gehrke *et al.* (2013)	◆	◆
Passaro et al. (2017)	✚	✚

B

	Rostral HOX groups			Central HOX groups					Caudal HOX groups				
HOXA	1 ★	2 ★■◆	3 ★■◆✚	4 ◆	5 ★■◆✚	6 ★	7 ★◆		9 ★■	10 ★■	11 ★✚		13 ✚
HOXB	1	2	3	4	5	6 ◆	7 ★■◆✚	8 ★■✚	9				13
HOXC				4	5	6		8 ■	9	10 ★◆✚	11 ★◆	12 ◆✚	13 ■
HOXD	1		3	4				8 ◆	9	10	11	12	13

Figure 1-1: The differential expression of HOX genes between gluteal and abdominal subcutaneous adipose tissues in four independent studies.

A. The HOX genes with higher expression in gluteal or abdominal fat are presented with blue or red colours, respectively and different symbols were matched to individual studies.

B. Abdominal fat mainly expresses higher levels in the rostral groups (HOX 1-3) or central groups (HOX 4-8) of *HOXA* and *HOXB* clusters, but gluteal fat presents higher expression only in the caudal groups (HOX 9-13) of *HOXA* and *HOXC* clusters.

Currently, direct comparisons of tissue-specific transcriptome profiling between abdominal and gluteofemoral subcutaneous adipose tissues have been performed in four independent research groups (Gehrke, et al., 2013; Karastergiou, et al., 2013; Passaro, et al., 2017; Pinnick, et al., 2014). Consistent between these studies is the demonstration that developmental genes were differentially expressed between the two fat depots. This includes the homeobox (HOX) genes in the four HOX clusters, HOX cofactors (for example, *PBX1*, *PBX3* and *MEIS1*), other HOX-domain encoding genes (for example, *IRX1*, *IRX2* and *SHOX2*) and T-box genes (for example, *TBX5* and *TBX15*). In the human genome, there is a total of 39 HOX genes which are divided into four HOX clusters each containing 9-11 genes. The HOX clusters are found on chromosome 7 (*HOXA*), 17 (*HOXB*), 12 (*HOXC*), and 2 (*HOXD*), and the genes they

contain can be grouped into 13 paralogous groups based on sequence alignment which are numbered 1 to 13 from the 3' end to the 5' end of gene sequence (Scott, 1992). In many animals, the organization of the HOX genes in the chromosome displays co-linearity with the same order of their expression along the anterior-posterior body axis (Carroll, 1995; Pearson, et al., 2005). Interestingly, the expression pattern of HOX genes in abdominal and gluteofemoral subcutaneous adipose tissues also follows this co-linearity with very consistent findings in four independent studies (Figure 1-1). Abdominal subcutaneous adipose tissue mainly expresses higher levels in the rostral groups (HOX 1-3) or central groups (HOX 4-8) of *HOXA* and *HOXB* clusters, but gluteofemoral subcutaneous adipose tissue has higher expression of HOX genes in the caudal groups (HOX 9-13) in the *HOXA* and *HOXC* clusters. Particularly intriguing, in the *HOXC12-HOXC13* locus area, Passaro et al. and Gehrke et al. found that *HOXC12* was more highly (50-fold) expressed in the gluteal depot compared with abdominal (Gehrke, et al., 2013; Passaro, et al., 2017). Karastergiou et al. showed that *HOXC13* was exclusively expressed in the gluteal depot and undetectable in the abdominal samples (Karastergiou, et al., 2013). The group of my supervisors identified the *HOX* transcript antisense RNA (*HOTAIR)*, a long non-coding RNA, as exclusively expressed in the gluteal depot and the most differentially expressed gene between the two fat depots (Pinnick, et al., 2014). *HOTAIR* is located within the large and complex *HOXC13* locus which is identified in GWAS of human body fat distribution (Shungin, et al., 2015).

In order to understand how these developmental genes are controlled in the regional adipose tissue, Gehrke et al. performed genome-wide DNA methylation analysis and demonstrated that the majority of the depot-differential HOX genes showed depot-specific methylation differences (Gehrke, et al., 2013). It has also been shown that abdominal preadipocytes have significantly higher DNA methylation in the *HOTAIR* promoter compared with gluteal preadipocytes, which is consistent with its depot-differential expression: the tissue with hypermethylation showed little or no expression

of *HOTAIR* (Pinnick, et al., 2014). Moreover, there was memory of the depot-specific transcriptional profile which was retained *in vitro* both in primary human preadipocytes and hTERT/HPV16-E7 human preadipocyte cell lines (Pinnick, et al., 2014). All these results suggest that these two fat depots have divergent developmental origins, which are tightly regulated by epigenetic mechanisms. It is also tempting to propose that the depot-specific functional characteristics of these two adipose depots is determined by their distinct developmental gene expression profiles. There is circumstantial evidence that genes located within the *HOXC13* locus play a role in body fat distribution but studies are now needed to determine the functional importance of these genes (e.g. *HOTAIR*) and addressing this question has been the focus of my thesis.

1.3.6 Potential functional roles of developmental genes on body fat distribution

The protein products of homeobox and T-box genes can behave as transcription factors since they possess either homeodomain or T-box domains as the DNA binding motifs (Holland, et al., 2007; Papaioannou, 2014). Their putative functions are not only limited to embryonic development, but also appear to be involved in adult tissue plasticity. For example, several HOX genes are regulated by endocrine systems and are necessary for functional differentiation in the female reproductive tract and the hematopoietic system (Daftary and Taylor, 2006). Studies focusing on regional adipose tissues also point to several developmental genes that are implicated in the regulation of the body fat distribution. Firstly, *HOXA5* and *TBX15* levels in the visceral and abdominal subcutaneous adipose tissues have been shown to correlate with BMI and WHR (Gesta, et al., 2006). Secondly, several homeobox genes (including *IRX3*, *IRX5*, *HOXA5*, *HOXA9*, *HOXB5*, *HOXC6*, *EMX2* and *PRRX1*) in the abdominal subcutaneous adipose tissue were upregulated after bariatric surgery induced profound weight loss (Dankel, et al., 2010). In mouse cells and animal models, *Shox2* and *Tbx15* are important regulators of adipocyte function, development and heterogeneity (Gburcik, et al., 2012; Gesta, et al., 2011; Lee, et al., 2017; Lee, et al., 2013). In human

preadipocytes, interference of the *TBX5* or *HOTAIR* expression has been found to influence the *in vitro* adipogenic differentiation (Divoux, et al., 2014; Pinnick, et al., 2014). Furthermore, GWAS studies have identified several loci in the developmental genes (*TBX15, HOXC13, HOXA11* and *MEIS1*) that were associated with body fat distribution (Shungin, et al., 2015). However, functional gene variants within the GWAS identified loci, such as the *HOXC13* locus are still obscure. Variation in coding regions in genes at this locus has been excluded so the focus on identifying functional variants will be within regions conveying transcriptional regulation. A starting point is the identification of tissue-specific eQTL SNPs and subsequently work on further fine mapping and functional evaluating of potential candidate genes (for example, the *HOTAIR* gene).

1.4 Epigenetic regulation in adipose tissue

1.4.1 Nuclear architecture

During the last decades, the knowledge on epigenome regulation has been broadened from DNA methylation and histone modifications to also include the role of nuclear architecture involving the interactions between nuclear environment and 3D chromatin structures/chromosome positions (Charo, et al., 2016). The nuclear environment includes nuclear lamina and nuclear matrix, which are important for establishing the 3D genome organization inside the nucleus. The nuclear lamina is a meshwork of A- and B- type lamins that line the nucleoplasmic surface of the nuclear envelope (Fawcett, 1966; Patrizi and Poger, 1967). In general, the nuclear lamina plays a role in anchoring the interphase chromosomes to the nuclear envelope. The anchoring sites, known as lamin-associated domains (LADs) are characterized by low levels of gene-expression (Akhtar, et al., 2013) and usually display a repressive chromatin environment (Yokochi, et al., 2009). The importance of nuclear lamina in adipogenesis was highlighted by the identification of mutations in lamin A/C (LMNA) gene, which cause partial lipodystrophy (Vigouroux, et al., 2001). The detailed mechanism by which the structural changes in lamin A/C interacts with transcriptional control is not

well understood, but using the human gluteal preadipocytes expressing the partial lipodystrophy associated LMNA R482W mutation, loss of suppressive chromatin environment (H3K27 trimethylation) in the anti-adipogenic *MIR335* locus has been demonstrated during the induction of adipogenesis (Oldenburg, et al., 2017).

The intact nuclear matrix is required for the radial positions of chromosome territories (CTs) (Ma, et al., 1999) and is also associated with the formation of chromatin loops (Vogelstein, et al., 1980). The gene-rich CTs are usually closer toward the centre of the nucleus, whereas the gene-poor CTs are commonly positioned in the periphery near the nuclear lamina (Croft, et al., 1999). The chromatin looping events can activate or repress gene transcription by creating physical proximity of regions otherwise located far apart along the linear chromosome (Jin, et al., 2013). Studies on the nuclear architecture during adipocyte differentiation have shown dynamic changes of CTs (Charo, et al., 2016). Nuclear lamina is fragmented at the early stages of adipogenesis, which enhances plasticity of nuclear components (Verstraeten, et al., 2011). CTs are de-condensed in adipose-differentiated mesenchymal stem cells (Szczerbal, et al., 2009) and relative positions of the CTs of human chromosomes 12 and 16 were changed during differentiation of preadipocytes (Kuroda, et al., 2004). Also, via chromatin looping or moving of CTs, the nuclear locations of several adipogenesis-required genes significantly changed during adipocyte differentiation (Szczerbal, et al., 2009; Tong, et al., 2000). It appears that the dynamic organization of nuclear architecture during differentiation is crucial for the cell fate and also opens a new territory for the epigenome regulation. How the dynamic organization of the nuclear architecture is initiated and regulated during adipogenesis is still largely unknown.

1.4.2 DNA methylation and histone modification

DNA methylation and histone modification are well known epigenetic mechanisms that play roles in regulating the temporal and tissue-specific gene transcription during embryogenesis (Rivera and Ross, 2013), adult tissue homeostasis and also in

tumorigenesis (Avgustinova and Benitah, 2016). When specifically evaluating human adipogenesis, dynamic changes of genome-wide DNA methylation and chromatin remodelling have been demonstrated during *in vitro* adipocyte differentiation of human adipose-derived stem cells (hASCs) (Broholm, et al., 2016; Mikkelsen, et al., 2010). Also, the histone markers and transcription factor localization near the *PPARG* locus were shown to present temporal modifications, which is consistent with the up-regulation of *PPARG* expression during hASC adipogenesis (Mikkelsen, et al., 2010).

1.4.3 Long non-coding RNA

Long non-coding RNA (lncRNA) is defined as a transcript that has more than 200 nucleotides without the ability of encoding proteins (Ma, et al., 2013). The genes in this group usually have relatively low gene expression, but are expressed with high tissue specificity (Cabili, et al., 2011). LncRNAs also display a high-order RNA structure and can potentially function as the scaffold between genomic DNA, RNA and proteins (Li, et al., 2016). Therefore, it is not surprising that lncRNAs can possess multiple functional roles in different levels of cellular or molecular components. For example, lncRNAs have been implicated in carcinogenesis (Fang and Fullwood, 2016), biological processes of various organ systems, such as cardiovascular system (Liu, et al., 2017), immune system, nervous system, endocrine system (Sun and Kraus, 2015) and also adipogenesis (Sun, et al., 2013).

Accumulating evidence has shown that several lncRNAs are involved in epigenetic regulation, such as DNA methylation, histone modification and gene imprinting (Wang, et al., 2017). Numerous lncRNAs are present in the nucleus and can control chromatin structures including nucleosome positioning and chromosome looping (Bohmdorfer and Wierzbicki, 2015). Moreover, lncRNAs are also found to interact with heterogeneous nuclear ribonucleoproteins (hnRNPs) (Sun, et al., 2017). HnRNPs are important for nucleic acid metabolism and are mainly expressed in the nucleus as a major component of the nuclear matrix (Geuens, et al., 2016; Verheijen, et al., 1988). Therefore, lncRNAs can participate in the regulation of nuclear architecture via

interacting with hnRNPs to modulate the chromosome organization, such as the example that hnRNP U is necessary for Xist RNA localization on the inactive X-chromosome (Hasegawa, et al., 2010). Although our current understanding about each individual lncRNAs is very limited, investigations of their function in a tissue-specific manner, such as *HOTAIR* gene in the human gluteofemoral adipose tissue, could potentially provide insight to novel molecular mechanisms governing the cell-specific transcriptome with direct implications for regional adipocyte function and whole body fat distribution.

1.4.4 *HOTAIR* (*HOX* transcript antisense RNA)

HOTAIR is a long non-coding RNA residing in the *HOXC* cluster on chromosome 12 and preferentially expressed in posterior and distal body sites. *HOTAIR* was initially characterized in 2007 when investigating the non-coding RNAs that co-express with the HOX gene clusters in human fibroblasts from distinct positions along the proximal-distal and anterior-posterior body axis. These ncRNAs were thought to regulate the HOX genes by cis-action, but unexpectedly the *HOTAIR* gene was shown to repress the *HOXD* locus on chromosome 2 *in trans* (Rinn, et al., 2007). *HOTAIR* was further recognized to act as a scaffold for interacting with Polycomb Repressive Complex 2 (PRC2) on the 5' end and Lysine-Specific Histone Demethylase 1 (LSD1) on the 3' end to modulate H3K27 tri-methylation and H3K4 demethylation, respectively (Tsai, et al., 2010). It might also be that *HOTAIR* functions beyond epigenetic modification since Fluorescence In Situ Hybridization (FISH) analysis has shown that *HOTAIR* locates in both the nucleus and the cytoplasm (Yoon, et al., 2013). Indeed, studies have shown that *HOTAIR* can act as a sponge to bind with microRNAs (Fu, et al., 2015; Li, et al., 2014; Ma, et al., 2014) and as a platform for protein ubiquitination (Yoon, et al., 2013).

Although *HOTAIR* expression in the normal tissues is relatively low compared with coding genes, it can increase hundreds to thousands of times in cancers, such as in breast cancer cells (Gupta, et al., 2010). *HOTAIR* has been identified as an oncogene

involved in various cancers and its expression was correlated with poor prognosis, risk of metastasis and in this context it has been proposed as a biomarker (Bhan and Mandal, 2015). However, its physiological functions in the normal *HOTAIR*-expressing tissues are still largely unknown. Recently, *HOTAIR* was found as the most differentially expressed gene between gluteal and abdominal subcutaneous adipose tissue (Pinnick, et al., 2014). Considering that these two fat depots possess distinct expression patterns for several developmental HOX genes, it is very possible that the normal presence of *HOTAIR* in the gluteal fat and its absence in the abdominal fat is an essential feature to maintain the tissue-specific epigenetic memory and transcriptome pattern.

My overriding hypothesis for this thesis is that *HOTAIR* plays a key role in shaping fat depot-specific functional characteristics and helps determine a heritable component of body fat distribution.

1.5 Aims

Body fat distribution has been well established as a risk factor for cardiovascular and metabolic disorders independent of body weight. Huge efforts have been put in to evaluate the potential determinants of fat distribution. Due to its high heritability, genetic factors are determinants but they will interact with the hormonal and nutritional influences to shape fat depot expansions during puberty and in response to weight gain. To date, GWAS have identified many genetic loci associated with body fat distribution, but the precise functional mechanisms are poorly understood. I will use a tissue-specific approach based on the divergence between the gluteofemoral and abdominal subcutaneous adipose tissues to demonstrate that these two depots have distinct biological functions and expression patterns of developmental genes, which are tightly controlled by epigenetics and intrinsically maintained in the *in vitro* culture system with a focus on *HOTAIR*. The *HOTAIR* gene is located right under the GWAS peak for the human fat distribution *HOXC13* locus and is coincidentally expressed exclusively in one specific fat depot: the gluteofemoral one. Adding to its unique molecular functions on histone modification as a long non-coding RNA and potentially

regulated by hormonal systems, such as oestradiol (Bhan, et al., 2013), we believe functional investigations of the *HOTAIR* will unlock questions on the regulation of body fat distribution.

Therefore, the aims of this project will include:

1) By using a human genetic approach, I will ascertain the candidacy of the *HOTAIR* as a gene important for human fat distribution.

2) I will use *in vitro* systems to explore the phenotypic consequences of *HOTAIR* knock-down and overexpression in regional-specific adipocyte precursors.

3) I will investigate the potential *HOTAIR* target genes and their epigenetic regulation by *HOTAIR*.

Chapter 2
Methods

2.1 The Oxford Biobank

The Oxford Biobank (OBB; http://www.oxfordbiobank.org.uk/) is a collection of middle-aged (30 to 50 year old) healthy men and women resident in the Oxfordshire. All participants have undergone a detailed examination at a screening visit and signed informed consent to be re-approached. Anthropometric parameters such as height, weight, waist and hip circumference were measured for calculation of BMI and WHR. A fasting blood sample was collected from each individual for numerous biochemical parameters e.g. fasting glucose, insulin, triglyceride and cholesterol.

The regional body fat distribution of each participant was precisely estimated by a DXA scan in addition to basic anthropometric measurements. A blood sample was also collected for isolation of DNA, which was prepared for high-throughput genotyping using the Illumina Human Core Exome and Affymetrix Axiom arrays. Custom genotyping using the kompetitive allele specific PCR (KASP^{TM}) platform (LGC Genomics) or standard TaqMan chemistry can also be performed. The OBB database with its detailed genetic and phenotypic information allowed me to analyse the genotype-phenotype association for gene variants in the *HOTAIR* region.

Based on existing baseline data within the OBB and the specific genotype and/or phenotype of interest, participants can be contacted for recall studies. Recruitment to such studies usually involves the collection of plasma samples, subcutaneous adipose tissue biopsies and a DXA scan with variations in scale and complexity depending on the research question. Adipose tissue biopsies can be used for cell culture, histology, quantitative polymerase chain reaction (qPCR), genomic DNA extraction, Western blotting and/or biochemical analysis of lipid components. In this thesis I made use of this recall function in a number of different ways as described later.

A complementary adipose tissue transcriptome panel for quantitative real-time PCR analysis has been generated by taking paired abdominal and gluteal adipose tissue samples from 213 men and women (mean age 44.3 years; range 33 - 53 years) within

the OBB across a range of BMI (mean BMI 27.4 kg/m^2; range 18.8 – 46.2 kg/m^2). Subcutaneous abdominal and gluteal adipose tissues were taken as described in section 2.2.2. RNA was extracted from adipose tissue biopsies as outlined in section 2.2.4; cDNA synthesis was performed as outlined in section 2.4.2; qPCR analysis was performed as outlined in section 2.4.3. This panel was applied for the measurement of the *HOTAIR* gene expression in paired human subcutaneous adipose tissues.

2.2 Handling of human abdominal and gluteal subcutaneous adipose tissues

2.2.1 Core needle biopsy for adipose tissue histology

Core adipose tissues were obtained by using the gun biopsy under local anaesthetic (1% lidocaine) to preserve the tissue structures for measuring adipocyte cell size. Biopsy samples were fixed and preserved in 10% formaldehyde, embedded in paraffin wax block, cut into 5μm sections and stained with haematoxylin and eosin on the glass slides. Slides were viewed and photographed under microscope at x 20 magnification and adipocyte cross-sectional area was measured by Adobe Photoshop 5.0.1 (Adobe Systems) and Image Processing Tool Kit (Reindeer Games) as previously described (Marinou, et al., 2014).

2.2.2 Needle aspiration biopsy to recover whole adipose tissue

Needle aspiration biopsy was performed under infiltration of the tissue with local anaesthetic (1% lidocaine), then a mini liposuction technique was used by inserting the 12-gauge needle through the skin and aspirating tissue. The needle aspiration biopsy was performed after core needle biopsy. Usually, around 3-500 mg adipose tissue was recovered into the syringe prefilled with 0.9% sodium chloride. Abdominal subcutaneous adipose tissue was taken from the periumbilical area and gluteal subcutaneous adipose tissue was taken from the upper buttock area. The syringe containing the sample was put in the ice immediately. Then, the biopsy samples were poured onto a fine nylon mesh and rapidly and gently rinsed with saline to remove any remaining blood. Aliquots of ~200 mg were snap frozen in liquid N_2 or put directly

into TRIzol as described in section 2.2.4. Samples destined for isolation of live cells (section 2.2.5) were not washed and instead transferred to 10 ml Hanks' Balanced salt solution (HBSS) in a 50 ml Falcon tube.

2.2.3 Extraction of genomic DNA from human adipose tissue or cells

Around 100-200 mg adipose tissue or cells up to 5 x 10^6 were processed for genomic DNA extraction by using the GenEluteTM Mammalian Genomic DNA Miniprep Kit (Sigma). The procedure was performed by following the kit instruction. Adipose tissue was completely digested at 55°C in the Lysis Solution T with Proteinase K for about 2 hrs, incubated in RNase A Solution for 2 mins, then Lysis Solution C was added and samples were further incubated at 70°C for 10 mins. Pelleted cells were resuspended in the Resuspension Solution, incubated in RNase A Solution for 2 mins, then Lysis Solution C with Proteinase K were added and samples were further incubated at 70°C for 10 mins. Genomic DNA was isolated through several steps including column preparation, binding preparation, lysate loading, first and second wash and DNA elution. The eluted genomic DNA was frozen at -20°C for long-term storage.

2.2.4 Homogenizing human adipose tissue with TRIzol for RNA extraction

A total of 200-300 mg of whole adipose tissue was homogenised (Retsch MM301) in ice-cold Tri-reagent (Thermo Scientific). After homogenisation, the sample was spun (12,000 x *g* for 5 mins at 4°C) to separate off the fat layer, which floated on the top. The infranatant was transferred to a clean 1.5ml Eppendorf tube. The sample was stored in -80°C and RNA extraction was performed as outlined in section 2.4.1.

2.2.5 Isolation of stromal vascular fraction cells from human adipose tissue

Stromal vascular fraction cells were isolated from subcutaneous adipose tissue as previously described (Collins, et al., 2010; Hauner, et al., 2001). Adipose tissue from the needle aspiration biopsy was broken up with scissors and then transferred to a new 50 ml Falcon tube containing 1 mg/ml collagenase (Roche) in HBSS for enzymatic

digestion in a shaking water bath (90 rpm) at 37°C for 45 mins. Digested adipose tissue was filtered through 250 μm nylon mesh (SEFAR) into a 15 ml Falcon tube to remove undigested tissue debris, then centrifuged at 600 rpm for 5 mins at 19°C to float the mature adipocytes which were removed. The infranatant was spun again at 1,200 rpm for 5 mins at 19°C and the remaining supernatant was removed. The pellet containing stromal vascular fraction cells was re-suspended in HBSS and filtered again through 100 μm mesh to a new 15 ml Falcon tube. The filtrate was centrifuged again with 1,200 rpm for 5 mins at 19°C and the supernatant was removed. The remaining pellet was then re-suspended in growth medium (the components of growth medium are as section 2.3.1). Cells were plated in a T25 tissue culture flask (Sarstedt) and maintained in a humidified atmosphere 5% CO_2, 37°C incubator. After 1 day, any contaminating red blood cells were washed off with phosphate-buffered saline (PBS), and new growth medium was added in the tissue culture flask.

2.2.6 Immortalised human subcutaneous abdominal and gluteal preadipocytes

Beyond the primary stromovascular cells I also used human immortalized abdominal and gluteal preadipocytes (Darimont and Mace, 2003; Todorcevic, et al., 2017). They originated from a healthy 50-year-old male with BMI 24.4 kg/m^2. The immortalisation was achieved by stable co-expression of HPV16-E7 and hTERT in the primary cells. Immortalised preadipocytes were maintained under the same conditions as primary cells (see section 2.3.1). The term "preadipocytes" used in this thesis refer to the mixed cellular population of the stromal vascular fraction cells isolated from adipose tissue.

2.3 Cell culture of human primary or immortalised preadipocytes

2.3.1 Maintenance of human primary or immortalised preadipocytes

The human primary or immortalised preadipocytes were cultured in the growth medium made with Dulbecco's modified Eagle's medium/nutrient mixture F-12 Ham's (v/v, 1: 1; Sigma) containing high glucose concentration (17.5 mM) supplemented with 10% foetal bovine serum (Labtech); 0.25 ng/ml fibroblast growth

factor (Sigma); 2 mM L-glutamine (Invitrogen); and 100 units/ml penicillin and 100 µg/ml streptomycin (Invitrogen). The growth medium was replaced every 2-3 days and the cells are maintained in the humidified atmosphere, 37°C, 5%CO_2 incubator.

2.3.2 Adipogenic differentiation of human primary or immortalised preadipocytes

Preadipocytes were seeded onto 6-well plates (2 x 10^5 cells/well) and cultured with growth medium to full confluence which normally took 2 days. Cells were further cultured for 2 days after full confluence to reach contact inhibition of proliferation. I then started the stimulation with adipogenic differentiation medium for 14 days. The adipogenic differentiation medium contained Dulbecco's modified Eagle's medium/Nutrient F-12 Ham (v/v, 1:1; Sigma), 17.5 mM glucose supplemented with 2 mM L-glutamine (Invitrogen); 100 units/ml penicillin and 100 µg/ml streptomycin (Invitrogen); 17 µM pantothenate (Sigma); 100 nM human insulin (Invitrogen); 1 nM tri-iodo-L-thyronine (Sigma); 33 µM biotin (Sigma); 10 µg/ml transferrin (Sigma); and 1 µM dexamethasone (Sigma). The adipogenic differentiation medium was further supplemented with 2 µM troglitazone (Sigma) and 250 µM 3-isobutyl-1-methylxanthine (Sigma) for the initial 4 days, and then replaced with the described adipogenic differentiation medium for days 4 to 14. The adipogenic differentiation medium was replaced every 2-3 days and cells were grown in the humidified atmosphere, 37°C, 5%CO_2 incubator.

2.3.3 Estimating cell proliferation

The cell number was calculated by Cellometer Auto T4 Cell Counter (Nexcelom Biosience) and cell doubling time was measured during the exponential phase of cell growth. Four sets of T25 tissue culture flasks (Sarstedt) were seeded with 1 x 10^5 cells per flask for 4 days. Then the cells were trypsinised and cell number was calculated in each T25 flask and seeded at 2 x 10^5 cell density in T75 flasks in quadruplicate. Cells were grown for another 4 days. Finally, cell number in each T75 flask was calculated and cell doubling time was measured with the following formula: $DT = T\ \ln 2/\ln(Xe/$

Xb); T is the incubation time in any units, Xb is the cell number at the beginning of the incubation time, Xe is the cell number at the end of the incubation time.

2.4 Gene expression analysis

2.4.1 RNA extraction

RNA was extracted as the previously described protocol (Collins, et al., 2010). Cells or tissue were homogenised in Tri-reagent (Thermo Scientific) and collected to a 2 ml PhaseLock gel tube (Eppendorf). Chloroform (100 µl) was then added to 500 µl Tri-reagent. The samples were mixed and centrifuged (12,000 x *g* for 30 mins at 4°C). The aqueous supernatant containing the RNA and was collected into a new 1.5 ml Eppendorf tube. An equal amount of isopropanol plus 1 µl glycoblue (Invitrogen) was added and samples were mixed thoroughly and stored at -30°C overnight to precipitate.

Next day the samples were centrifuged (12,000 x *g* for 30 mins at 4°C) and the isopropranol was poured off without disturbing the RNA pellets. The RNA pellets were washed twice with 800 µl 80% ethanol and pelleted by centrifugation (12,000 x *g* for 20 mins at 4°C). The ethanol was aspirated completely without disrupting the RNA pellets and the pellets were air-dried at room temperature. The RNA pellets were re-suspended in nuclease-free H_2O and dissolved at 4°C for 3-5 hrs. The concentration of RNA was measured by the NanoDrop spectrophotometer (Thermo Scientific).

2.4.2 Complementary DNA synthesis

The High Capacity cDNA Reverse Transcription Kit (Life Technologies) was used to synthesise double-stranded complementary (c)DNA from total RNA (1000 ng). Nuclease-free dH_2O was added to the 1000 ng RNA extract to reach total volume of 10 µl. Then, 10 µl of the reverse-transcription reagents was added to each reaction vial. The composition of the reverse transcription reaction mixture is outlined in Table 2.1.

Table 2-1: Reverse-transcription reaction volumes for cDNA synthesis

Reagent	Volume per reaction (µl)
10 x RT buffer	2.0
25 x dNTP mix (100 mM)	0.8
10 x RT Random primers	2.0
Multiscribe^{TM} Reverse transcriptase (50 U/µl)	1.0
Nuclease-free dH_2O	4.2
Total volume	10.0

A no template control (NTC) was also included for quality control, in which RNA was substituted with nuclease-free dH_2O. The cycling parameters for cDNA synthesis are setting as 25°C for 10 mins; 37°C for 120 mins; 85°C for 5 mins; and 4°C for 10 mins.

2.4.3 Quantitative real-time PCR

The cDNA was diluted in 10mM Tris-HCl (pH 8.0) for running quantitative real-time PCR (qPCR). qPCR was performed using Kapa Probe Fast Mastermix (Kapa Biosystems) and TaqMan Assays-on-Demand (Applied Biosystems). The cDNAs of experimental samples were pooled and serially diluted (1/10; 1/20; 1/40; 1/80; 1/160; and 1/320) to generate a standard curve. Experimental and standard samples plus an NTC and Tri-HCl blank (pH 8.0) were run together in triplicate (2.7 µl/well) at a final 6 µl reaction volume on an ABI Prism 7900HT or in triplicate (3.6 µl/well) of a final 8 µl reaction on a Corbett Rotor-Gene 6000. The cycle parameters are; 95°C for 3 mins followed by 40 cycles of 95°C for 3 secs and 60°C for 20 secs.

The method for relative quantification of RNA content has been described (Pfaffl, 2001). The slope of the standard curve generated from the serially diluted standard cDNAs was used to determine the reaction efficiency for each qPCR assay. The reaction efficiency was used to calculate the ΔCt for each sample with the following formula: $\Delta Ct = \text{reaction efficiency}^{(\text{min Ct} - \text{Sample Ct})}$

The ΔCt values of target genes were normalised to the ΔCt of the reference gene *PPIA* to give the ΔΔCt relative quantification and thus the relative transcript abundance. *PPIA* has been found to be reference transcript in adipose tissue and preadipocytes (Neville, et al., 2011).

2.5 Quantification intracellular total protein and triglyceride contents

The differentiated preadipocytes were harvested in lysis buffer (1% IGEPAL CA-630; 150 mM NaCl; 50 mM Tris-HCl, pH 8.0). Usually, 150 µl lysis buffer was used to harvest the whole cell lysate in each well of 6-well plate. The cell lysate was sonicated (30 secs total sonication in 5 secs bursts for 6 times), and the protein contained in the supernatant was collected after around 10 secs of short spin and its concentration was quantified using the DC protein assay kit (Bio-Rad). The remaining lysate was heated to 95°C for 30 mins. Samples were allowed to cool slightly at room temperature before further mixing and centrifugation (12000 x *g* for 10 mins at 4°C) to pellet the cell debris. The concentration of triglyceride in the clear supernatant was quantified by using the enzymatic triglyceride assay kit (Instrumentation Laboratories) on the ILAB 650 Clinical Chemistry system (Instrumentation Laboratories). Quality controls and a lysis buffer-only blank are run with the experimental samples. Normalised triglyceride (TAG) content was measured by dividing triglyceride concentration to the corresponding cellular protein concentration and presented as nanomoles triglyceride/milligram protein.

2.6 Western blotting

2.6.1 Extraction and quantification of cellular protein

Cell culture plates were placed on ice and cells were washed with ice-cold PBS twice. PBS was then aspirated and ice-cold lysis buffer (1% IGEPAL CA-630; 150 mM NaCl; 50 mM Tris-HCl, pH 8.0) supplemented with phosphatase inhibitors (10 mM sodium fluoride and 1 mM sodium orthovanadate) and an EDTA-free protease inhibitor cocktail (Roche) was used to harvest the whole cell lysate. The whole cell lysate was

transferred to a 1.5 ml Eppendorf tube and was placed on ice for 30 mins. The Eppendorf tube was centrifuged (12,000 x *g* for 15 mins at 4°C) and the protein containing supernatant was aspirated and transferred to a new Eppendorf tube, which was used for running Western blotting and protein concentration was quantified by the DC protein assay kit against BSA standards (Bio-Rad).

2.6.2 Gel electrophoresis and wet transfer

Equal amounts of protein (20 µg) were mixed with 4 x Laemmli sample buffer (Bio-Rad) containing 10% β-mercaptoethanol to make final 1 x concentration for denaturing and loading the protein samples. The 5% stacking and 10% resolving gels for Tris-glycine SDS-Polyacrylamide Gel Electrophoresis were made as the composition outlined in Table 2.2.

Table 2-2: Solutions for Preparing Gels for Tris-glycine SDS-Polyacrylamide Gel Electrophoresis

Solution components	5% stacking gel	10% resolving gel
dH_2O	1.7 ml	4 ml
30% acrylamide mix	500 µl	3.3 ml
0.5 M Tris (pH 6.8)	740 µl	-
1.5 M Tris (pH 8.8)	-	2.5 ml
10% SDS	30 µl	100 µl
10% ammonium persulfate	30 µl	100 µl
TEMED	3 µl	8 µl
Total volume	**3 ml**	**10 ml**

The pre-made gel was submerged in running buffer (25 mM Tris; 190 mM glycine; 0.1% SDS; pH 8.3). Samples were heated at 70°C for 3 mins and then loaded onto the premade gel along with a protein standard (Precision Plus Protein™ dual colour standards; Bio-Rad). Proteins were run and separated on the gel by the electrophoresis and then wet-transferred onto the 0.2 µm polyvinylidene difluoride (PVDF) membrane (Bio-Rad) using the transfer buffer (10 mM 3-(cyclohexylamino)-1-propanesulfonic acid, 10% methanol). After transfer, the PVDF membrane was incubated on a shaker (90 rpm) in the blocking buffer (5% skimmed milk dissolved in Tris-buffered saline

containing 0.1% Tween-20 (TBST)) for 1 hr at room temperature. After blocking, the PVDF membrane was incubated overnight at 4°C with a primary antibody (against the target protein of interest) diluted in blocking buffer.

2.6.3 Enhanced chemiluminescence

After incubating with the primary antibody overnight, the blot membrane was washed with TBST (three times for 5 mins) and blocking buffer (twice for 5 mins). The blot membrane was incubated with an appropriate horseradish peroxidase (HRP)-conjugated secondary antibody diluted in the blocking buffer for 2 hrs at room temperature. The blot membrane was further washed with TBST (five times for 5 mins). After adequate washing, the blot membrane was incubated with a 1:1 mixture of Clarity Western enhanced chemiluminescence (ECL) substrate mixture (Bio-Rad) for 2 mins at room temperature. The membrane was then drained off the excess ECL reagent and the protein of interest was visualised on the ChemiDoc^{TM} XRS+ system (Bio-Rad). The chemiluminescent signal was captured using Image Lab software (Bio-Rad) with the selection of blots → chemi. The protein standards were visualised and captured using the selection of blots → colorimetric on the Image Lab software for the 'stain-free' image.

2.6.4 Densitometric analysis of Western blot images

On the Image Lab software (Bio-Rad), the images of the ECL signal were exported as .tiff files. Images were opened in ImageJ (National Institute of Health, USA). The 'Measure' function with the rectangular selection tool was used to quantify the average density of each band. After importing the densitometry data, the relative density was calculated on both the protein of interest and the corresponding reference protein. Then, the experimental data were presented as the adjusted density by normalising the relative density of the interested protein to the relative density of the corresponding reference protein.

2.7 Statistical analysis

Statistics were performed in SPSS statistics version 22 (IBM Corp. Released 2013. IBM SPSS Statistics for Windows, Version 22.0. Armonk, NY: IBM Corp.) and are presented as means ± SEM. The details of statistical tests used were described in the results section and $P < 0.05$ was considered as statistically significant.

Chapter 3
Intrinsic/dynamic *HOTAIR* expression patterns and its genetic variation for identification of phenotypic eQTLs

3.1 Introduction

Genome-wide transcriptome analysis of human tissues and samples have shown that all tissues contain a new class of regulatory RNA: long non-coding RNAs (lncRNAs), which are defined as RNA containing more than 200 nucleotides without protein-coding potential. LncRNAs usually have low expression levels. They often show highly tissue-specific type of expression. Although their biological functions in human disease are still poorly characterized, many studies on differential expression and cell-type specific expression during differentiation have been applied to identify new lncRNAs and their function.

For example, *Braveheart*, a lncRNA with high expression in the heart relative to other tissues, was found to be necessary for commitment of the mouse nascent mesoderm toward a cardiac lineage. This lncRNA mediates epigenetic regulation during cardiomyocyte differentiation (Klattenhoff, et al., 2013). Likewise, performing RNA-sequence during human keratinocyte differentiation has identified two lncRNAs, *ANCR* and *TINCR*, which can mediate epidermal differentiation. *ANCR* is suppressed during differentiation and is required to maintain the undifferentiated cells state within epidermis (Kretz, et al., 2012), whereas *TINCR* is up-regulated during differentiation and is required for somatic tissue differentiation (Kretz, et al., 2013). Using similar strategies and additional methods to investigate the functionality of lncRNAs, a number of lncRNAs have been characterized in many systems including hormonal signalling, reproduction/development, adipogenesis, metabolism, immune system, nervous system, cardioskeletal system, and various cancers (Sun and Kraus, 2015).

HOTAIR (for HOX transcript antisense RNA) is a 2.2 kb lncRNA located within the *HOXC* gene locus on chromosome 12. It is known to epigenetically repress transcription *in trans* across a 40 kb region of the *HOXD* locus on chromosome 2 (Rinn, et al., 2007). The majority of studies on the *HOTAIR* gene have been conducted in relation to carcinogenesis. Aberrant *HOTAIR* overexpression has been found in various types of cancer, such as breast (Gupta, et al., 2010), hepatocellular (Yang, et al., 2011),

gastric (Endo, et al., 2013), colorectal (Kogo, et al., 2011) and pancreatic (Kim, et al., 2013) et al. Recently, the *HOTAIR* gene has been found to be involved in other disorders such as cardiovascular diseases (Carrion, et al., 2014; Gao, et al., 2017), osteoarthritis (Dou, et al., 2017; Zhang, et al., 2016), rheumatoid arthritis (Zhang, et al., 2017) and preeclampsia (Zou and Sun, 2015). Several transcription factor binding sites have been identified in the *HOTAIR* promotor including multiple oestrogen response elements (EREs), hypoxia response elements (HREs), NF-kb binding site et al (Bhan, et al., 2017; Bhan, et al., 2013; Bhan and Mandal, 2015). These findings imply that *HOTAIR* could play a role in maintaining or modulating the physiological function of *HOTAIR*-expressing tissues and possibly being dynamically regulated by various transcription factors.

My supervisors have performed paired transcriptomic analysis comparing human abdominal (ASAT) and gluteal subcutaneous adipose tissue (GSAT) and *HOTAIR* appeared to be the most differentially expressed gene, with exclusive expression in the gluteal fat depot (Pinnick, et al., 2014). This tissue-specific expression pattern suggests that the *HOTAIR* gene is functionally important in gluteal adipose tissue biology. It is also of particular interest that the *HOTAIR* gene is located within the human fat distribution GWAS *HOXC13* locus. With this in mind I wanted to investigate if the GSAT *HOTAIR* expression correlates with body fat distribution and if the GSAT *HOTAIR* expression is sex-specific. I also wanted to investigate how *HOTAIR* expression relates to adipogenesis using an *in vitro* cellular differentiation model as previously described. The SNPs within the *HOTAIR* region may impact on transcription so I searched for expression quantitative trait loci (eQTL). Moreover, investigations of the associations between eQTL-related SNPs and the fat distribution phenotypes may provide the insights to the fat-depot specific *HOTAIR* function.

3.1.1 Aims

- Quantify the fat depot-specific and sex-specific *HOTAIR* expression *in situ*

- Analyse the correlations between GSAT *HOTAIR* expression and anthropometric or biochemical variables

- Evaluate *HOTAIR* expression during *in vitro* dynamic status (adipogenesis or hormone signals)

- Perform detailed annotation of SNPs in the *HOTAIR* locus for eQTL and phenotype associations

3.2 Methods

3.2.1 Collection of paired abdominal and gluteal subcutaneous adipose tissues

As described in section 2.1, the adipose tissue cDNA panel from OBB participants was used to measure the *HOTAIR* expression in paired adipose tissues. The details for generating adipose tissue cDNA are as described in section 2.2.2, 2.2.4, 2.4.1 and 2.4.2.

3.2.2 Isolation of adipose-derived stromal vascular fraction cells

As described in section 2.2.5 primary stromal vascular fraction cells were isolated from human whole adipose tissue and were used as adipocyte progenitor cells (preadipocytes) for *in vitro* experiments

3.2.3 Maintenance and differentiation of human primary or immortalised preadipocytes

As described in section 2.3.1 and 2.3.2, human primary preadipocytes were grown to generate enough cells for the adipogenic differentiation time-course experiment. The experiments using primary cells were performed in the early passages (< passage 7) to avoid the changes of cellular phenotypes. The experiments using immortalised cells were performed within 30 passages.

3.2.4 Administration of dexamethasone or oestradiol

For the administration of dexamethasone, cells were seeded with 1.5 x 10^5 cells per well in the 6-well plates and cultured overnight. Growth medium was then replaced with growth medium containing dexamethasone (Sigma) and/or mifepristone (Sigma) for 48 hrs before cells were harvested. For the experiment of oestradiol administration, 'phenol red free' Dulbecco's modified Eagle's medium/nutrient mixture F-12 (Cambridge Bioscience) and charcoal tripped foetal bovine serum (Sigma) were used for making growth medium. 1.5 x 10^5 cells were plated in each well of the 6-well plate, and cultured overnight. Growth medium was then replaced with growth medium containing oestradiol (Sigma) for 24 hrs or 48 hrs, then cells were harvested.

3.2.5 Measurement of *HOTAIR* gene expression

RNA extraction was performed as described in section 2.4.1. cDNA synthesis was performed as described in section 2.4.2 and real-time qPCR was done as outlined in section 2.4.3. The following TaqMan Assays-on-Demand were used: *HOTAIR* (Hs03296631_m1); *PPIA* (Hs99999904_m1)

3.2.6 Selection of predominant SNPs in *HOTAIR* locus (Haplotype map/1000 Genome data)

Linkage disequilibrium (LD) maps and common haplotypes (> 1%) in the *HOTAIR* locus were generated based on Haplotype map (HAPMAP) (International HapMap, 2003) and 1000 Genome data (Genomes Project, et al., 2012) as the Figure 3-1.

In HAPMAP data, there were a total of 19 SNPs located within the 3000 bps upstream and 1000 bps downstream of human *HOTAIR* transcript variant 1 (NR_047517). rs1899663 and rs12826786 were selected as predominant SNPs as they are independent on LD maps and could represent several alleles (Figure 3-1A & B). rs17840857 (Figure 3-1B, C & F) tagged common haplotypes and could not be captured by either rs1899663 or rs12826786. Therefore, rs17840857 was also selected as a predominant SNP. rs4759314 was not considered as a predominant SNP since it is a rare allele and doesn't tag on any of the common haplotypes.

In 1000 Genome data, there were 41 SNPs located within the 3000 bps upstream and 1000 bps downstream of human *HOTAIR* transcript variant 1 (NR_047517). Based on the LD blocks, rs17720428 represented other 16 SNPs in 1000 Genome data (Figure 3-1D & E) and could also be captured by rs1899663. Since I had already selected rs1899663 as a predominant SNP for genotyping, there was no need to add rs17720428 to the list of predominant SNPs. However, there were still 24 SNPs with low level of LD within the LD map that could not be captured by rs1899663. To further select

predominant SNPs, I evaluated the SNP-tagging patterns across all common haplotypes in both HAPMAP data and 1000 Genome data.

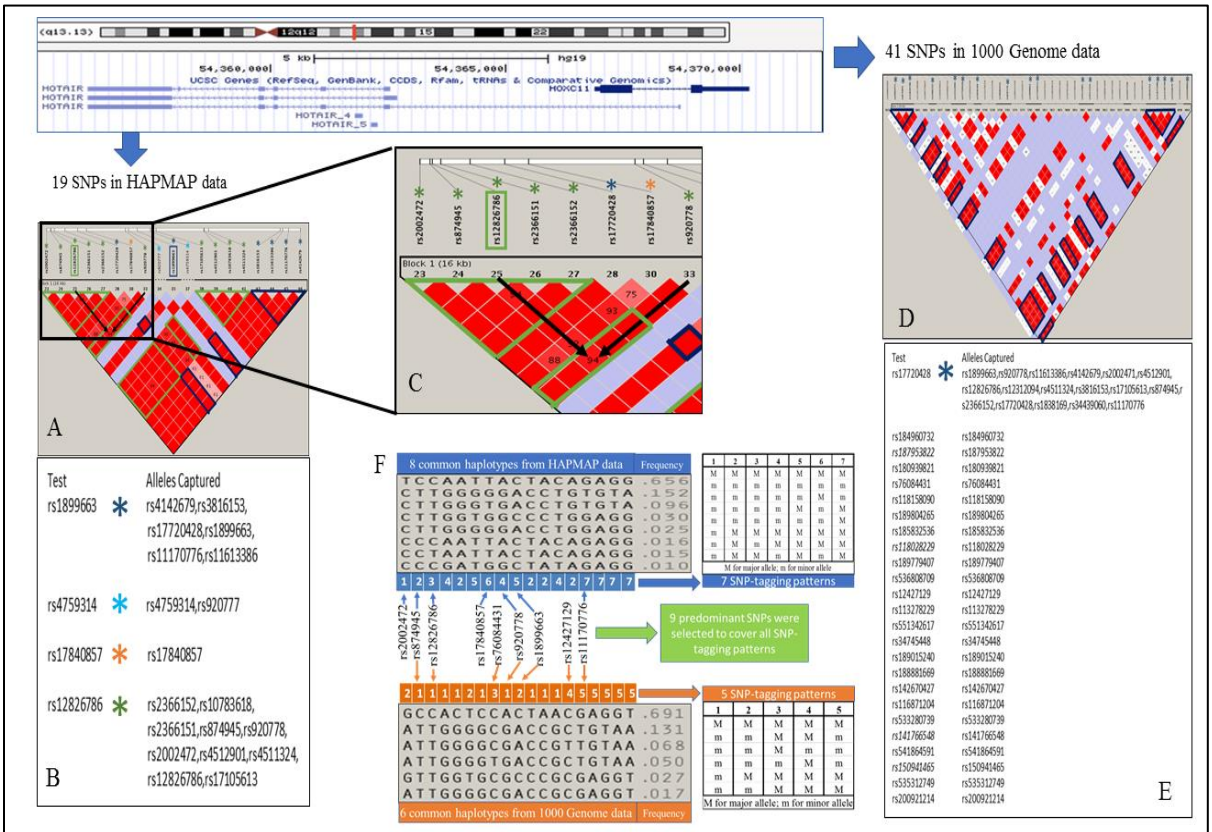


Figure 3-1: Selection of predominant SNPs based on LD maps and common haplotypes (<1%) in the *HOTAIR* locus constructed from HAPMAP and 1000 Genome data

Upstream 3000 bps and downstream 1000 bps of human *HOTAIR* transcript variant 1 (NR_047517) was surveyed (chr12: 54,355,092-54,371,740) (**browser view**). The red colour blocks in the LD maps (**A & D**) represent SNPs that are in high LD with each other and thus are highly inherited together. In the HAPMAP data, there are 19 SNPs located in this region and, more specifically, rs1899663 is in high LD (**A-blue frame area**) with other 5 SNPs labeled as blue asterisks (**A & B**) and rs12826786 is in high LD (**A-green frame area**) with other 9 SNPs labelled as green asterisks (**A & B**). In the 1000 Genome data, there are 41 SNPs located in this region and rs17720428 is in high LD (**D-blue frame area**) with other 16 SNPs labelled as blue asterisks (**D & E**). Higher values of the numbers in the blocks presented higher heritability between two SNPs as shown in the zoom-in view (**C**): rs12826786 is highly correlated (r^2 = 0.94) with rs920778. Haplotypes were further constructed from HAPMAP data (**F-top**) and 1000 Genome data (**F-bottom**). Based on the 8 common haplotypes from HAPMAP data and 6 common haplotypes from 1000 Genome data, SNP-tagging patterns across all haplotypes were evaluated. "M" is used to present the major allele, whereas "m" refers to the minor allele in different SNPs. In total, 7 different SNP-tagging patterns in HAPMAP data and 5 different patterns in 1000 Genome data could be recognized. To cover all SNP-tagging haplotype patterns, total 9 predominant SNPs were chosen.

According to the SNP-tagging pattern for the common haplotypes (Figure 3-1F), the previously selected SNP: rs1899663 refers to the SNP-tagging allele 5 in HAPMAP data and allele 2 in 1000 Genome data; rs12826786 represents haplotype 3 in the HAPMAP data and haplotype 1 in 1000 Genome data. rs17840857 tags haplotype 6 in HAPMAP data. Based on this strategy, an additional 6 predominant SNPs (rs2002472, rs874945, rs76084431, rs920778, rs12427129 and rs11170776) were selected to represent haplotype-tagging alleles. In summary, these 9 predominant SNPs were likely to capture all common haplotypes across the *HOTAIR* gene.

3.2.7 KASP^{TM} genotyping of *HOTAIR* SNPs

Genomic DNA from 7,287 OBB subjects were used and the 9 predominant SNPs in the *HOTAIR* locus were genotyped using the custom-designed KASP^{TM} genotyping assays and the KASP^{TM} Master mix from LGC genomics were run on the Tetrad PTC-225 Thermo Cycle system (Pendragon Scientific; Chinnor, UK) with a total reaction volume of 4 µl for each sample. The wells contained 2 µl of KASP^{TM} Master mix; 1.95 µl of RNase free dH2O; and 0.05 µl of the specific custom-designed KASP^{TM} genotyping assay. The DNA was already dried down in the well in plates prepared for genotyping.

The KASP^{TM} thermal cycling conditions were 94°C for 15 mins, following by 10 cycles of 94°C for 20 secs and 61 to 55°C (drop by -0.6°C/per cycle) for 45 secs, then repeated 34 times at 94°C for 10 secs and 55°C for 45 secs. Experimental samples and NTC were all plated in each 384-well plate with a unique pattern.

The genotyping data were obtained on the 7900HT PCR machine (Applied Biosystems; Warrington, UK) with SDS 2.3 software. All automatically called samples were checked again manually and data points that located outside cluster areas were referred to as undetermined.

3.2.8 Estimation of *HOTAIR* haplotypes by using PHASE program

After obtaining the OBB genotyping data for the 9 predominant SNPs across *HOTAIR*, I reconstructed the haplotypes in the entire OBB sample using the PHylogenetics And Sequence Evolution (PHASE) program (Stephens and Donnelly, 2003).

3.2.9 Chromatin immunoprecipitation for exploring the histone marks

Cells (3 x 10^6 /ChIP) were cross-linked with 1% formaldehyde for 10 mins and cross-linking was stopped with 125 mM glycine. Cells were lysed for 10 mins in ChIP lysis buffer (1% SDS, 10 mM EDTA, 50 mM Tris-HCl, pH 8.0, proteinase inhibitors, 1 mM PMSF, 20 mM Na Butyrate) and sonicated 30 secs ON/OFF for 10 mins in a Bioruptor®Pico (Diagenode) to generate 200-500 bps DNA fragments. After sedimentation at 10,000 g for 10 mins, the supernatant was collected and diluted 6 times in RIPA buffer (140 mM NaCl, 10 mM Tris-HCl pH 8.0, 1 mM EDTA, 0.5 mM EGTA, 1% Triton X-100, 0.1% SDS, 0.1% sodium deoxycholate, protease inhibitors, 1 mM PMSF, 20 mM Na Butyrate).

Table 3-1: ChIP primers for exploring histone marks in the *HOTAIR/HOXC* locus

Amplicons	Forward primer	Reverse primer
R0	TGCTCCCCTCCCCATAGT	CCTAGTGGCCTTGGACTGAG
RS76	GCCGTGGCATTTCTGGTCTT	TAAAGGAAGGAGGGGCGTCT
R1	CACAAGTACACGCACCGGAA	GAGTGTTCACGAGTGGAGGC
R2	ACCCAGGCATCTGATCGCTA	TGATCAAAGTGAGCTCGCGG
R3	CTGCGAAGTGCTCCGAACTG	GGATGGAGGTTTTGGACCCG
R4	CTTTTTCCAAGCAGTGCCCC	CCTCCACCACCCCAATCTTC
R5	CAAGTGGCCTGATTGGAAG	GCGAATGTGGGTAGCTGAAT
R6	CCGCCCCCTTAGACCAAAAA	GGGGAGGAAAGTTAGGGGGA
R7	CAAAGCCCCGGAAGAATAGC	GGGCCTGCGCCTTATCATTT
R8	CTTTGTCCGTCCCCGAAAGA	CTCCAAATCTCGCTGTGGGT
R9	ACCAGTGGCAACTCTAAGCC	GGGCTGACAAAGCCCCTTAT
R10	ATGAAAGGAGGGCAGGAAC	CAAGAACTCGGTATTATGACATCAC
R11	GGAAACTGAGCTCTCGCCTG	CCGGCTGGAGCTGTAATGAA

After a 100 µl sample was taken out (input), diluted chromatin was incubated for 2 hrs with antibodies (2.5 µg/100µl) to H3K4me3 (Diagenode C15410003), H3K27me3

(Diagenode C15410069), H3K27ac (Diagenode C15410174) and H3K4me1 (Diagenode C15410037) coupled to magnetic Dynabeads Protein A (Invitrogen). ChIP samples were washed 4 times in ice-cold RIPA buffer, crosslinks were reversed and DNA was eluted for 2 hrs at 68°C in 50 mM NaCl, 20 mM Tris-HCl pH 7.5, 5 mM EDTA, 1% SDS and 50 ng/µl Proteinase K. DNA was purified and dissolved in H2O. ChIP DNA was used as template for quantitative (q)PCR using SYBR® Green (BioRad), with 95°C denaturation for 3 mins and 40 cycles of 95°C for 30 secs, 60°C for 30 secs, and 72°C for 30 secs. Primers used for ChIP are listed in Table 3-1.

3.2.10 Bisulfite conversion and pyrosequencing of genomic DNA

Genomic DNA was extracted from tissue or cells as described in section 2.2.3. Around 400 ng genomic DNA was collected for each bisulfite conversion reaction. Bisulfite conversion was processed using EZ DNA Methylation -Gold™ Kit (Zymo Research) through a one-step DNA denaturation and a CT-conversion reaction followed by desulphonation and DNA clean-up.

Table 3-2: Composition for bisulfite PCR reactions

Reagent	Volume per reaction (µl)
Bisulfite converted DNA	1
2 x Reaction buffer	12.5
dNTP mix (25 mM each dNTP)	0.25
Zymo Taq™ polymerase (5 U/µl)	0.2
Forward Primer (10 µM)	1.5
(5'-biotinylated) Reverse Primer (10	1.5
dH2O	8.05
Total reaction volume	25

Bisulfite PCR primers were designed using the freely available MethylPrimer program (Applied Biosystems; Warrington, UK). Primers were used to amplify 200-400 bps PCR products in high CpG density sites of genes of interest. "Hot start" ZymoTaq™ DNA polymerase (Zymo Research) was applied for the bisulfite PCR reaction with the composition as Table 3.2. The thermal cycling parameters were: 95°C

for 10 mins followed by 48 cycles of 94°C for 30 secs, annealing temperature for 30 secs and 72°C for 1 min, then 72°C for 7 mins and incubate at 4°C. The annealing temperature was estimated and tested based on the primer sequence and a PCR additive with betaine was used as needed. Once the optimal bisulfite PCR reaction has been deduced, a 5'-biotinylated reverse primer (Sigma) was used to make bisulfite PCR products, which were confirmed by agarose gel electrophoresis. The reverse-strand was captured by Sepharose beads for subsequent pyrosequencing.

In each bisulfite PCR product (200-400 bps), three single-strand sequencing primers (10-25 bps) were designed to anneal the reverse strand for pyrosequencing in three divided segments (usually 50~80 nucleotides in each segment). The sequencing primer was not placed across any CpG dinucleotides.

Pyrosequencing was run on the PyroMark Q96 ID system using PyroMark Gold Q96 reagents (Qiagen). Streptavidin Sepharose High Performance (Sigma) and PyroMark binding buffer/denaturation solution/wash buffer/annealing buffer (Qiagen) were used to capture 5'-biotinylated reverse-strand for preparation of pyrosequencing on the PyroMark Q96 Vacuum Workstation (Qiagen) according to the PyroMark Q96 ID user manual. Q-CpG program (Qiagen) was operated for running the bisulfite pyrosequencing and the methylation status was calculated using the formula: %

Table 3-3: Bisulfite PCR primers and their optimal conditions

Amplicon	Bisulfite Primers	Annealing temp (°C)
*HOTAIR*_A	Forward: GTTTTTATTAGTTGATTTTTTTGTT	53
	Reverse: AAAAAAACAAAAACAAAAATC	
*HOTAIR*_B	Forward: GAGTTGAGTTTGTTTATTGTTTAT	53
	Reverse: ATTTCTTTCTCAAATCCAAA	
*HOTAIR*_C	Forward: GGGTAGATAGAGGTTGGAGG	53
	Reverse: ACCTAAAAAAAAACCCCTCCTAC	
*HOTAIR*_D	Forward: AGAGGGGGGAGAGAGATA	53
	Reverse: CCCAAACCCTATCAACC	

methylation = C peak height x 100/ (C peak height + T peak height).

In this Chapter, four amplicons near the *HOTAIR* gene were pyrosequenced and details of bisulfite primers/sequencing primers are listed in Table 3.3 and Table 3.4.

Table 3-4: Sequencing primers for bisulfite pyrosequencing

Amplicon	Sequencing primer 1	Sequencing primer 2	Sequencing primer 3
*HOTAIR*_	TTAGTTGATTTTTTTGTT	ATAAGATTAGAAATGTTA	ATTTTTATTTTGTTATGG
*HOTAIR*_B	AGTTTGTTTATTGTTTAT	TTAATATATTTGTTTTTT	TTTTGTTTTTAGTTTTAT
*HOTAIR*_C	GTAGATAGAGGTTGGAG	GAAGTTGTTTAGGTTGAT	GGGGAAAATTTGGGAAGG
*HOTAIR*_	GGGGGAGAGAGATA	GGTTTTTTTTTTAGTTTAT	GATTTTTTGTTAGGTTTAG

3.2.11 Statistical analysis

SPSS (IBM Corp. Released 2013. IBM SPSS Statistics for Windows, Version 22.0. Armonk, NY: IBM Corp.) was used to perform statistical analyses and a P value < 0.05 was considered statistically significant. Non-normal distributional data such as GSAT *HOTAIR* expression were assessed with non-parametric tests: Mann-Whitney U-test was used to evaluate the gender and genotype differences of GSAT *HOTAIR* expression and Spearman Rank correlation was used to analyse the correlation between GSAT *HOTAIR* expression and other variables. DXA defined body fat components were obtained in total 4,627 of 7,287 OBB individuals and regional fat mass data were normalised by log transformation. The associations between body fat components according to genotypic groups were analysed by two-tailed independent t-test.

3.3 Results

3.3.1 *HOTAIR* expression presents gluteal depot-specific pattern with gender difference

HOTAIR expression has been found as the most differentially expressed gene between abdominal and gluteal subcutaneous adipose tissues by performing microarray in samples collected from 31 men and 18 women (Pinnick, et al., 2014), but further validation with real-time qPCR in a larger cohort study is needed to understand sex and genotypic relationships. Therefore, *HOTAIR* expression was measured by real-time qPCR in paired adipose tissues from total 204 Oxford Biobank subjects (female BMI range: 18.8-43.3 kg/m^2; male BMI range: 20.6-46.2 kg/m^2; female age range: 33-53 years; male age range: 34-53 years).

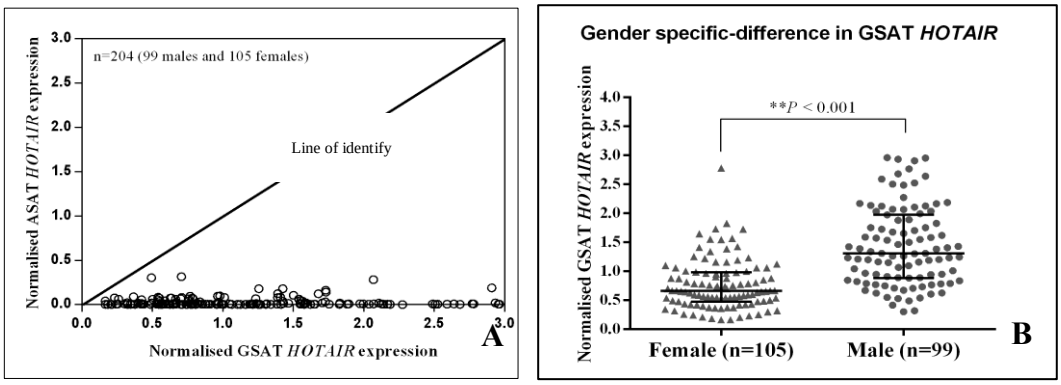


Figure 3-2: Fat depot-specific and gender-specific differences in *HOTAIR* expression

A: Paired adipose tissues from 204 Oxford Biobank subjects (105 females and 99 males) were collected. The paired GSAT and ASAT *HOTAIR* levels for each participant were plotted to display the depot difference. **B:** GSAT *HOTAIR* levels in 105 females were compared with the levels in 99 males. Gene expression was normalised to the reference gene *PPIA* to give the relative transcript abundance. Data were assessed with nonparametric Mann-Whitney U-test and presented as medians [quartiles]. $^{**}P < 0.001$. ASAT: abdominal subcutaneous adipose tissue; GSAT: gluteal subcutaneous adipose tissue

These results (Figure 3-2A) confirm that *HOTAIR* expression is higher in GSAT compared to ASAT in all subjects. More precisely, the *HOTAIR* gene was specifically expressed in the gluteal fat depot with high variation between individuals, but very few individuals showed any significant expression in ASAT. Furthermore, comparing the GSAT *HOTAIR* levels between 105 females and 99 males, women had ~50% lower

HOTAIR expression compared with men (Figure 3-2B). The gender-specific difference in the GSAT *HOTAIR* levels might be influenced by the gender-differential composition of gluteal adipose tissue (e.g., ratio between mature adipocytes and stromal vascular fraction cells) and further investigation will be required to clarify it.

3.3.2 *HOTAIR* expression is negatively correlated with age in males

As GSAT *HOTAIR* expression showed high variation between individuals, I evaluated if the *HOTAIR* expression correlated with basic anthropometric parameters and biochemistry data. Due to intrinsic differences in fat distribution between sexes I performed this analysis separately for men and women. (Table 3-5). GSAT *HOTAIR* expression didn't correlate with BMI, waist to hip ratio, lean mass, fat mass and lipid profiling in either of the sexes, but negatively correlated with age in males (r = -0.246; P = 0.014). Although there was a trend towards a correlation between GSAT *HOTAIR*

Table 3-5: Spearman correlation coefficients between GSAT *HOTAIR* expression and anthropometric or biochemical variables in OBB subjects (105 females and 99 males)

	Female GSAT *HOTAIR*		Male GSAT *HOTAIR*			
	r	*P*	*r*	*P*	*r* (Age adjusted)	*P* (Age adjusted)
Age (years)	-0.055	0.578	-0.246	0.014*		
BMI (kg/m^2)	-0.061	0.536	-0.047	0.647	-0.067	0.509
Waist to hip ratio	-0.098	0.320	0.001	0.993	0.047	0.649
Lean mass (kg)	-0.145	0.144	-0.040	0.697	-0.047	0.648
Fat mass (kg)	-0.108	0.279	-0.036	0.720	-0.075	0.463
Glucose (mM)	0.095	0.333	0.160	0.113	0.134	0.189
Insulin (mUI)	0.066	0.503	0.194	0.054	0.080	0.431
HOMA-IR	0.086	0.385	0.189	0.061	0.086	0.401
Triglyceride (mM)	0.036	0.716	0.062	0.544	0.091	0.374
NEFA (μM)	-0.056	0.573	-0.074	0.469	-0.022	0.832
Total Chol (mM)	0.053	0.589	-0.081	0.427	0.066	0.520
HDL Chol (mM)	-0.005	0.956	-0.011	0.911	-0.025	0.809

Data were assessed with Spearman correlation and presented with coefficients (r). *P < 0.05. Age adjustment was performed with partial correlation. BMI: body mass index; HOMA-IR: homeostatic model assessment of insulin resistance; NEFA: non-esterified fatty acids; Chol: cholesterol; HDL: high density lipoprotein.

expression and glucose homeostasis (Insulin, HOMA-IR) this disappeared after adjusting for age.

3.3.3 *In vitro* gluteal preadipocytes maintain the intrinsic *HOTAIR* expression, which changes during adipogenic differentiation

In order to examine if the gluteal fat depot-specific *HOTAIR* expression is maintained in preadipocytes cultured *in vitro*, I measured the dynamic *HOTAIR* expression pattern during adipogenesis. Primary preadipocytes were isolated from paired subcutaneous adipose tissues from 8 OBB subjects (4 males and 4 females) and cultured in the *in vitro* cellular system for 14 days during adipogenic differentiation. The primary preadipocytes exhibited an intrinsic memory of *HOTAIR* expression in relation to the tissue of origin: the expression was higher in the gluteal adipocytes but nearly undetectable in the abdominal adipocytes (Figure 3-3). During adipogenic differentiation, the *HOTAIR* expression in the gluteal cells showed a dynamic fluctuation which was significantly elevated during differentiation day 6-9 (Figure 3-3), with no induction of expression observed in the abdominal cells.

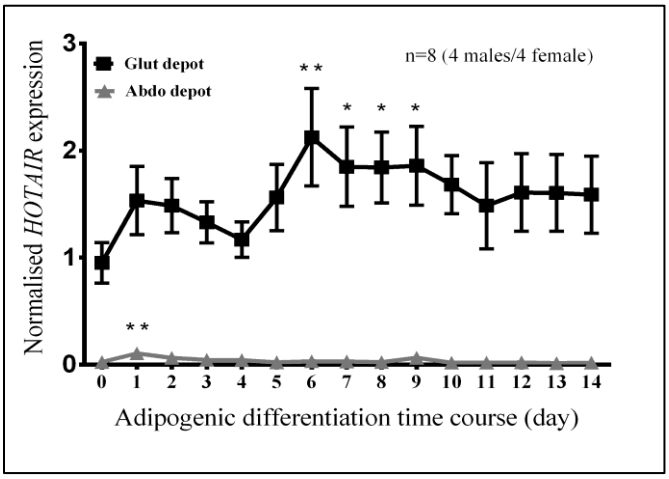


Figure 3-3: *In vitro* dynamic *HOTAIR* expression during adipogenic differentiation

Paired isolated primary preadipocytes from 4 males and 4 females were cultured with adipogenic differentiation medium for 14 days and cells were harvested for measuring *HOTAIR* expression at each time point. Data were analysed with ANOVA LSD pairwise comparison to compare with day 0 in the same fat depot and presented with means ± SEM. **P* < 0.05; ***P* < 0.01.

3.3.4 *HOTAIR* expression was enhanced by dexamethasone, but not by oestradiol in the *in vitro* cellular model

To test the dynamic response toward hormone signals, the glucocorticoid dexamethasone and a glucocorticoid receptor antagonist (mifepristone) were used to evaluate the glucocorticoid effects on *HOTAIR* expression. Oestrogen effects on *HOTAIR* expression were examined by using oestradiol. Male immortalised gluteal/abdominal preadipocyte cell lines and primary female gluteal/abdominal preadipocytes (isolated from 3 females) were used to test the glucocorticoid and oestrogen effects in the *in vitro* cellular model, respectively. After administration of dexamethasone, the *HOTAIR* expression was significantly enhanced in the gluteal preadipocytes, but this was suppressed by co-administration of the glucocorticoid receptor (GR) antagonist, mifepristone. Adding mifepristone alone didn't influence the *HOTAIR* expression in the gluteal preadipocytes (Figure 3-4A). Mifepristone blocked the dexamethasone effect showing that the observed effects are likely to be mediated by the GR.

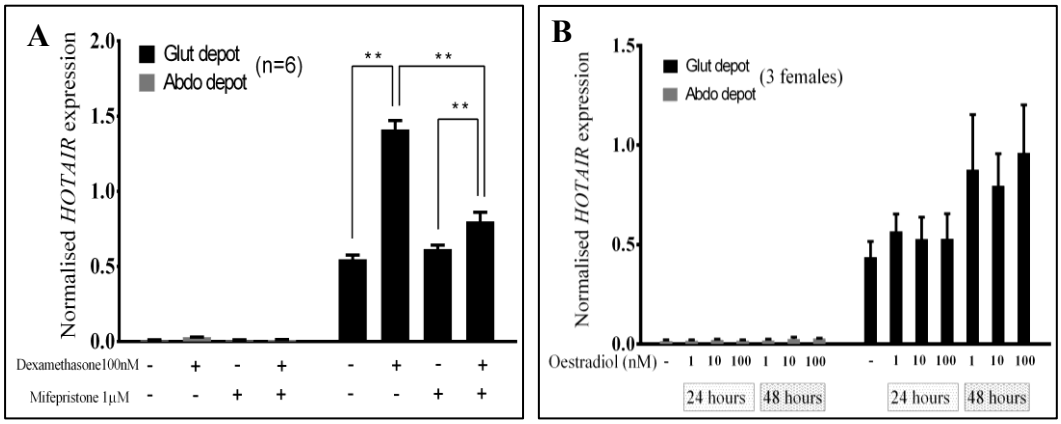


Figure 3-4: *HOTAIR* expression in the gluteal preadipocytes was enhanced by dexamethasone, but not oestradiol in the *in vitro* cellular model

A: Paired immortalised preadipocytes were cultured with growth medium and treated with dexamethasone 100 nM or Mifepristone 1 μM (a glucocorticoid receptor antagonist) for 48 hrs. **B:** Primary preadipocytes were isolated from 3 female individuals and cultured with 'phenol red free' growth medium and charcoal tripped foetal bovine serum. Oestradiol (1, 10 or 100 nM) was added for 24 or 48 hrs. Data were analysed with ANOVA LSD pairwise comparison and presented with means ± SEM. $^{**}P < 0.001$.

When treating the female preadipocytes with a broad range of oestradiol concentration from 1 nM to 100 nM for 24 or 48 hrs, there was no clear dose or time-dependent effect on the *HOTAIR* transcription. The three female gluteal cells showed high variation in the *HOTAIR* expression after the 48 hrs oestradiol treatment (Figure 3-4B). However, it is still possible that oestrogen might have effects on *HOTAIR* expression during adipogenic differentiation, which didn't be examined in my experiments. The abdominal preadipocytes didn't response toward either dexamethasone or oestradiol administration and kept a persistent low *HOTAIR* expression.

3.3.5 Two haplotype-tagging SNPs have eQTLs with opposite directional effects

Using the HAPMAP and 1000 Genome databases, the linkage disequilibrium (LD) maps and common haplotypes (>1%) at *HOTAIR* locus were generated. Then, predominant SNPs were systemically selected by two complementary approaches: 1) choosing SNPs that are independent with each other on the LD maps and 2) evaluating the SNP-tagging haplotype patterns to cover all common haplotypes as described in section 3.2.6. In total, 9 predominant SNPs were selected and genotyped in more than 7,000 OBB subjects. To evaluate if these SNPs contribute to variation in tissue *HOTAIR* mRNA abundance (suggesting an expression quantitative locus (eQTL)), the tissue samples from the 204 OBB subjects were analysed in a sex-specific manner (Table 3-6). The haplotypes generated by genotyping the OBB for the selected predominant SNPs seemed to generate haplotypes frequencies and structures similar to the 1000 Genome data (Figure 3-5). Amongst the rarer haplotypes, two haplotypes appeared to have an association with *HOTAIR* expression. The tagging SNPs were rs76084431 and rs12427129 which showed minor allele frequency (MAF) of 6.39% and 8.92% in the OBB database, respectively. So, the SNPs representing these haplotypes were used to divide the OBB into heterozygous and common homozygous carriers and the haplotype carrying status which was then related to the GSAT *HOTAIR* mRNA abundance.

Table 3-6: GSAT *HOTAIR* levels among rare versus other genotype groups of *HOTAIR* 9 tagging SNPs

rs11170776	N (rare versus others)	TT	TG+GG	*P* value
Females	9 versus 83	0.664 [0.367; 0.921]	0.665 [0.501; 1.004]	0.550
Males	10 versus 85	0.915 [0.816; 1.802]	1.384 [0.930; 2.016]	0.275
rs1899663		TT	TG+GG	*P* value
Females	11 versus 87	0.775 [0.478; 0.989]	0.654 [0.485; 0.967]	0.731
Males	12 versus 84	0.915 [0.800; 1.567]	1.388 [0.949; 2.026]	0.203
rs12826786		TT	CT+CC	*P* value
Female	11 versus 87	0.775 [0.478; 0.989]	0.654 [0.485; 0.967]	0.731
Males	14 versus 82	1.068 [0.816; 1.714]	1.366 [0.939; 2.006]	0.395
rs17840857		GG	GT+TT	*P* value
Females	7 versus 91	0.989 [0.634; 1.004]	0.654 [0.480; 0.909]	0.102
Males	5 versus 91	1.384 [0.691; 2.065]	1.311 [0.893; 1.997]	0.711
rs874945		AA	GA+GG	*P* value
Females	12 versus 84	0.827 [0.516; 0.997]	0.654 [0.488; 0.964]	0.438
Males	13 versus 82	0.944 [0.808; 1.558]	1.400 [0.951; 2.036]	0.166
rs920778		CC	CT+TT	*P* value
Females	13 versus 84	0.775 [0.553; 0.994]	0.654 [0.481; 0.944]	0.421
Males	14 versus 82	1.068 [0.816; 1.714]	1.366 [0.939; 2.006]	0.395
rs2002472		GG	GA+AA	*P* value
Females	13 versus 87	0.775 [0.553; 0.994]	0.654 [0.485; 0.967]	0.489
Males	14 verses 82	1.068 [0.816; 1.714]	1.366 [0.939; 2.006]	0.400
rs76084431		TC	CC	*P* value
Females	16 versus 83	0.463 [0.335; 0.738]	0.702 [0.548; 0.990]	0.017*
Males	9 versus 88	1.098 [0.862; 1.937]	1.388 [0.898; 1.991]	0.494
rs12427129		TC	CC	*P* value
Females	14 versus 83	0.877 [0.657; 1.419]	0.650 [0.439; 0.909]	0.018*
Males	16 versus 77	1.348 [0.850; 1.756]	1.342 [0.902; 2.070]	0.722

Data were analysed with Mann-Whitney U-test and presented as medians [quartiles]. *P <0.05

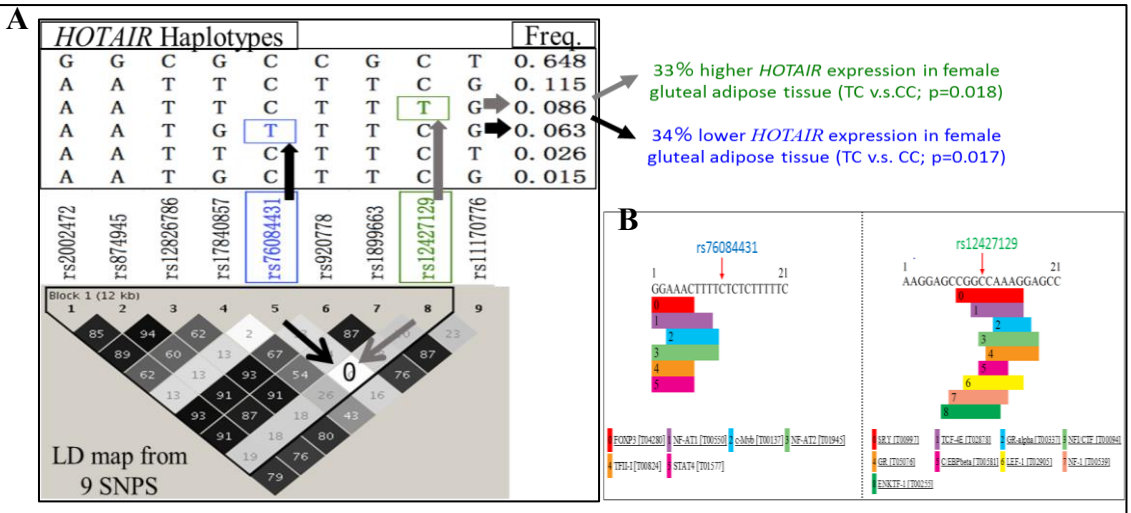


Figure 3-5: Two haplotype-tagging SNPs have eQTLs with opposite directional

A: Genotyping of 9 *HOTAIR* SNPs was performed in Oxford Biobank subjects (n = 7287). *HOTAIR* haplotypes were estimated by PHASE program and linkage disequilibrium (LD) map of r^2 value was drawn from the genotyping results. Two independent SNPs (rs76084431 and rs12427129) tag two common haplotypes and have eQTLs with opposite directional effects on *HOTAIR* expression. **B:** Transcription factor binding sites were predicted in the DNA sequences (flanked by 10 bps) with rs76084431 or rs12427129 in the middle.

The results (Table 3-6) show that females carrying the TC genotype of rs76084431 had 34% lower *HOTAIR* mRNA compared to females carrying the CC genotype. Also, females carrying the TC genotype of rs12427129 have significantly 33% higher *HOTAIR* mRNA transcription compared to females carrying the CC genotype. This suggests that these haplotypes correspond to two eQTLs with opposite directional effects (Figure 3-5A). The transcription factor bindings (Figure 3-5B) on the DNA sequences (flanked by 10 bps) with rs76084431 or rs12427129 in the middle were predicted via using the PROMO (prediction of transcription factor binding sites) program (Messeguer, et al., 2002).

Within the GWAS identified fat distribution *HOXC13* locus, there are three independent lead SNPs (rs1443512, rs10783615 and rs2071449, also denoted A, B and C locus in (Shungin, et al., 2015)) associated with WHR after adjustment for BMI. The A locus for which the lead SNP: rs1443512 links to other SNPs right across the *HOTAIR* gene with linkage disequilibrium (r^2) ranging between 0.2-0.8. This raises the possibility that rs1443512 also influences *HOTAIR* transcription. Therefore, I compared GSAT *HOTAIR* mRNA levels between rs1443512 genotypes. As shown in Table 3-7, the A allele of rs1443512 is associated with decreased GSAT *HOTAIR* mRNA abundance in males (P = 0.043*, β = -0.207), which represents the same directional effect as the already described GSAT *HOTAIR* eQTL: rs76084431 (P =

Table 3-7: GSAT *HOTAIR* levels among genotype groups of rs1443512, rs76084431 and rs12427129

rs1443512	N	AA	AC	CC	*P* value (β coefficient)
Males	6 vs 32 vs 58	0.916	1.211	1.387	**0.043* (-0.207)**
All	10 vs 75 vs 108	0.744	0.871	0.964	0.138
rs76084431	N	TC	CC		*P* value (β coefficient)
Females	16 vs 83	0.499	0.703		**0.026* (-0.224)**
All	25 vs 171	0.692	0.963		**0.014* (-0.175)**
rs12427129	N	TC	CC		*P* value (β coefficient)
Female	14 vs 83	0.950	0.632		**0.01* (0.259)**
All	30 vs 160	1.117	0.898		0.08

Data were log-transformed, analysed with linear regression and presented with geometric means. *$P < 0.05$

0.026*, β = -0.224). This result suggests that a) the one of the lead SNPs from the *HOXC13* locus in the GWAS of WHRadjBMI is a *HOTAIR* eQTL and b) the expression of *HOTAIR* gene is likely to be under control of several independent loci.

3.3.6 Females carrying the *HOTAIR* transcript-lowering SNP have significantly higher android to gynoid fat ratio

Using a precise method, DXA scan, to define fat distribution, the associations between the eQTL SNP genotypes and regional body fat mass were further explored. The phenotypic associations of the two eQTL SNPs (rs76084431 and rs12427129) were analysed with a dominant genetic model assuming the minor allele possessing the phenotypic effect. Comparing rs76084431 TT+TC genotype after adjustment for BMI with the CC genotypes, females carrying the *HOTAIR* mRNA lowering variant

Table 3-8: Body fat distribution among TT+TC versus CC genotype of *HOTAIR* transcript-lowering variant (rs76084431) in females

Variables	rs76084431 TT+TC (n=310)	rs76084431 CC (n=2310)	*P* value	BMI adjusted *P* value (beta value)
Age (years)	41.66 (6.01)	41.22 (5.91)	0.226	
BMI (kg/m²)	25.50 (4.77)	25.35 (5.05)	0.630	
WHR	0.820 (0.076)	0.812 (0.075)	0.098	
Android fat (g)	1648.630	1548.899	0.107	0.026* (0.024)
SubAnd fat (g)	1306.882	1225.004	0.070	0.042* (0.024)
Gynoid fat (g)	4371.231	4312.184	0.492	0.606
Leg fat (g)	8677.597	8609.314	0.694	0.984
Total fat (g)	23498.691	22946.025	0.304	0.185
Android/total fat	0.0701	0.0675	0.030*	0.013* (0.036)
SubAnd/total fat	0.0556	0.0536	0.024*	0.029* (0.037)
Gynoid/total fat	0.1860	0.1879	0.190	0.210
Leg/total fat	0.3692	0.3751	0.103	0.111
Android/gynoid fat	0.3771	0.3591	0.043*	0.022* (0.033)
Android/leg fat	0.1899	0.1799	0.039*	0.024* (0.034)
SubAnd/gynoid fat	0.2993	0.2850	0.022*	0.022* (0.036)
SubAnd/leg fat	0.1508	0.1427	0.021*	0.023* (0.037)

Variables are assessed by independent t-test. Age, BMI, WHR were presented as means (standard deviation). Data of fat components were normalised by log transformation and presented with geometric means. Adjusting was performed by multivariable linear regression. *P < 0.05. BMI: body mass index; WHR: waist to hip ratio; SubAnd: subcutaneous android.

(TT+TC) had significantly higher android fat mass and higher subcutaneous android fat mass. For the regional fat mass ratio, the TT+TC genotype carrying females had higher android fat/total fat ratio, higher subcutaneous android fat/total fat ratio, higher

android fat/gynoid fat ratio, higher android fat/leg fat ratio, higher subcutaneous android fat/gynoid fat ratio and higher subcutaneous android fat/leg fat ratio (Table 3-8).

The same statistic method was applied to assess the phenotypic associations in the *HOTAIR* transcript-elevating variant (rs12427129). The minor T allele of rs12427129 was associated with increased GSAT *HOTAIR* expression in females. However, females carrying the minor allele (TT+TC genotypes) of rs12427129 didn't have any difference in any regional fat mass or fat mass ratio compared to females with CC genotype (Table 3-9).

Table 3-9: Body fat distribution among TT+TC versus CC genotype of *HOTAIR* transcript-elevating variant (rs12427129) in females

Variables	rs12427129 TT+TC (n=476)	rs12427129 CC (n=2142)	*P* value	BMI adjusted *P* value (beta value)
Age (years)	41.48 (6.03)	41.22 (5.90)	0.378	
BMI (kg/m^2)	25.07 (4.43)	25.44 (5.13)	0.105	
WHR	0.817 (0.074)	0.812 (0.075)	0.254	
Android fat (g)	1510.959	1571.993	0.222	0.971
SubAnd fat (g)	1200.027	1242.896	0.238	0.663
Gynoid fat (g)	4257.766	4334.666	0.280	0.795
Leg fat (g)	8502.368	8649.008	0.311	0.790
Total fat (g)	22656.453	23097.969	0.322	0.464
Android/total fat	0.0666	0.0680	0.170	0.603
SubAnd/total fat	0.0530	0.0541	0.135	0.285
Gynoid/total fat	0.1879	0.1876	0.838	0.463
Leg/total fat	0.3753	0.3744	0.793	0.607
Android/gynoid fat	0.3548	0.3626	0.281	0.905
Android/leg fat	0.1777	0.1818	0.308	0.903
SubAnd/gynoid fat	0.2818	0.2879	0.235	0.522
SubAnd/leg fat	0.1411	0.1443	0.266	0.560

Variables are assessed by independent t-test. Age, BMI, WHR were presented as means (standard deviation). Data of fat components were normalised by log transformation and presented with geometric means. Adjusting was performed by multivariable linear regression. *$P < 0.05$. BMI: body mass index; WHR: waist to hip ratio; SubAnd: subcutaneous android.

3.3.7 Recruiting rs76084431 TT genotype females to validate the eQTL effects and exploring the histone modifications/DNA methylation around rs760844431

The minor allele frequency of rs76084431 in OBB database is around 6% and there were only 16 available females carrying the homozygous rare alleles (TT) of rs76084431 in the OBB biobanks. Up until now I had not had access to homozygous carriers of the *HOTAIR* lowering rs76084431 variant, but I postulated that this might have a stronger phenotypic readout. Therefore, I conducted a genotype-based recruitment to recall as many female carriers with the rare rs76084431 TT genotype as possible from the OBB. The recruitment was performed with 1:1 of TT and CC genotype subjects after adequately matching for age and BMI. In total, there were 4 TT and 4 CC female carriers that could be successfully recruited. Paired adipose tissue biopsies were taken from these women and GSAT *HOTAIR* expression were measured with real-time qPCR as described in section 3.2.5. This result (Figure 3-6) shows females carrying rs760844431 TT genotype had significantly lower (44%) GSAT *HOTAIR* expression than CC genotype carriers, which further supports the putative eQTL effect of rs76084431.

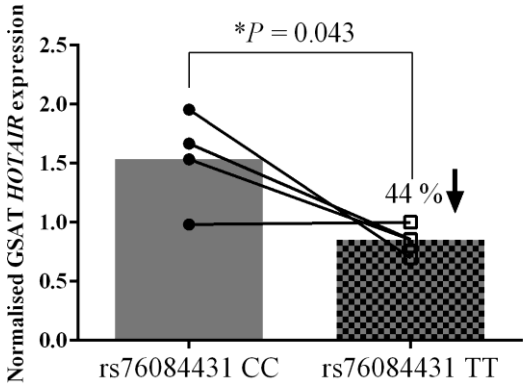


Figure 3-6: Females carrying rs76084431 TT genotype have significant lower *HOTAIR* expression in gluteal adipose tissue than females with CC genotype

Females carrying rs76084431 TT genotype (n = 4) and CC genotype (n = 4) were recruited for measuring *HOTAIR* expression in gluteal subcutaneous adipose tissue (GSAT). Data were analysed with independent t-test (one-tailed) and presented with means ± SEM *$P < 0.05$.

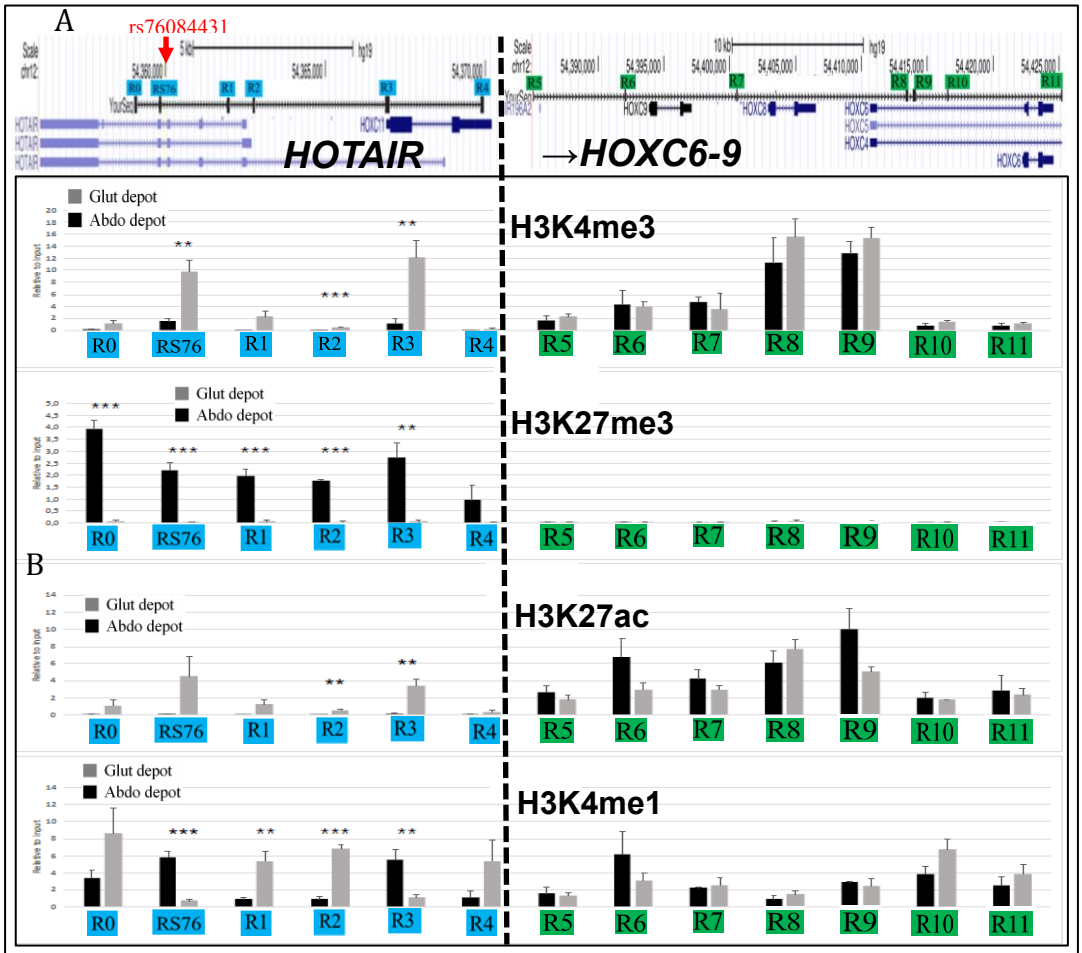


Figure 3-7: Patterns of histone modification across the *HOTAIR/HOXC* locus in gluteal and abdominal preadipocytes

Immortalised gluteal and abdominal cell lines under proliferation were used for performing chromatin immunoprecipitation (ChIP) with technical replications (n = 4). **A:** ChIP primers were designed to target on *HOTAIR* putative promotor/enhancer regions across *HOTAIR/HOXC* locus. R0-R4 regions were labelled as blue colour and R5-R11 were labelled as green colour. R1-R4 were located in the promotor region of *HOTAIR* isoforms. R5-R11 are *HOTAIR* putative enhancers. R0 and RS76 were designed to evaluate the histone marks around rs76084431. **B:** ChIP experiments of histone marks (H3K4me3, H3K27me3, H3K27ac and H3K4me1) were conducted. Data were presented with % of input and analysed with Wilcoxon test. **P* < 0.05; ***P* < 0.01; ****P* < 0.001.

HOTAIR has three transcript variants including two short isoforms (NR_003716 and NR_047518) and one long isoform (NR_047517). rs76084431 is an intronic SNP located in the intron 3 of NR_003716, intron 2 of NR_047518 and intron 4 of NR_047517. However, how this intronic SNP influences the *HOTAIR* expression and how the marked differential *HOTAIR* expression is controlled between abdominal and

gluteal fat depots is still unknown. To address this issue, I used chromatin immunoprecipitation (ChIP) to investigate the state of regulatory histone modifications in the immortalised gluteal and abdominal preadipocyte cell lines under proliferation conditions to search for tissue-specific differences in chromatin state across the *HOTAIR/HOXC* locus. Together with Prof Philippe Collas, University of Oslo, I specifically assessed relative enrichments in H3K4me3, a promoter modification often associated with active genes, H3K4me1, a mark of enhancers, H3K27me3, a promoter/enhancer modification associate with repressed genes, and H3K27ac, associated with active enhancers (together with H3K4me1). Table 3-10 describes the functional interpretation of the histone marks based on the review by Shlyueva et al. (Shlyueva, et al., 2014)

Table 3-10: The interpretation of the histone marks for recognising promoter/enhancer

H3K4me3 represents an active promoter
H3K27me3 represents a repressive chromatin (antagonist to H3K27ac)
H3K27ac represents an active enhancer (antagonist to H3K27me3)
H3K4me1 with H3K27ac represents an active enhancer
H3K4me1 devoid of H3K27ac and H3K27me3 represents a primed enhancer
H3K4me1 with H3K27me3 represents a poised (closed) enhancer
H3K27ac, but low of H3K4me1 might represent an active enhancer mark and H3K4me1 may function to fine-tune gene expression (Rada-Iglesias, 2018; Yan, et al., 2018)

ChIP primers were designed to target the promoter and putative enhancer regions of the *HOTAIR/HOXC* locus (Figure 3-7A). The details of regions (designated R) are as below: the *HOTAIR/HOXC11* promoters (R2: promoter of the *HOTAIR* short isoform, R4: promoter of the *HOTAIR* long isoform and R3: promoter of the *HOXC11* gene). R3 is also in intron 1 of the *HOTAIR* long isoform. R1 region is highly occupied by H3K4me3 in the ENCODE (ENCyclopedia Of DNA Elements) database. R5-R11 are defined as *HOTAIR* putative enhancers in the FANTOM (Functional ANnoTation Of

the Mammalian genome) database.

ChIP results (Figure 3-7B) were interpreted as below

Enrichment profiles of the R1 and R2 regions suggest that R1 and R2 represent active enhancers (H3K27ac+, H3K4me1+) or promoter sites (H3K4me3+) for the short *HOTAIR* isoforms in gluteal cells. In contrast, these sites in abdominal cells are consistent with the repressed state of the locus (H3K27me3+, H3K4me3-).

The data further suggest that R3 may be an active enhancer for *HOTAIR* (and/or *HOXC*) expression in gluteal cells, but its activity might be regulated by H3K4me1 (H3K27ac+, but low H3K4me1). R3 may also be the promoter site (H3K4me3+) for the long *HOTAIR* isoform in gluteal cells. In abdominal cells, however, R3 may be considered as a poised enhancer (H3K4me1+, H3K27me+) for *HOTAIR* expression.

Histone marks on R4 suggest it is a primed enhancer (H3K4me1+, H3K27ac-, H3K27me-) for *HOTAIR* expression in gluteal cells, but in contrast, represents a repressive chromatin region (H3K27me3+) for *HOTAIR* expression in abdominal cells.

R5-R11 regions display similar histone modification profiles not only between them, but also between gluteal and abdominal cells suggesting they do not take part in determining the tissue-specific expression of *HOTAIR*. R5-R11 represent permissive chromatin regions (H3K27me3-, H3K27ac+) with overall similar enrichment of H3K4me1, H3K4me3 and H3K27ac in cells of both origins.

To identify histone modification patterns in closer proximity to rs76084431, ChIP primers were also designed on around 70 bps downstream of rs76084431 and 900 bps downstream of rs76084431 (R0) (Figure 3-7A). Strikingly, regions proximal to rs76084431 shows the same pattern as the R3 site (around 7 k bps upstream) for all histone marks examined. These results suggest that the region surrounding rs76084431 is also an active *HOTAIR* enhancer in gluteal cells. These findings also raise the

possibility that the rs76084431 site interacts with the R3 region. Overall, this ChIP experiment provides evidence that the *HOTAIR* eQTL rs76084431 is localized within a regulatory region putatively enhancing *HOTAIR* expression in a depot-specific (abdominal/gluteal) manner.

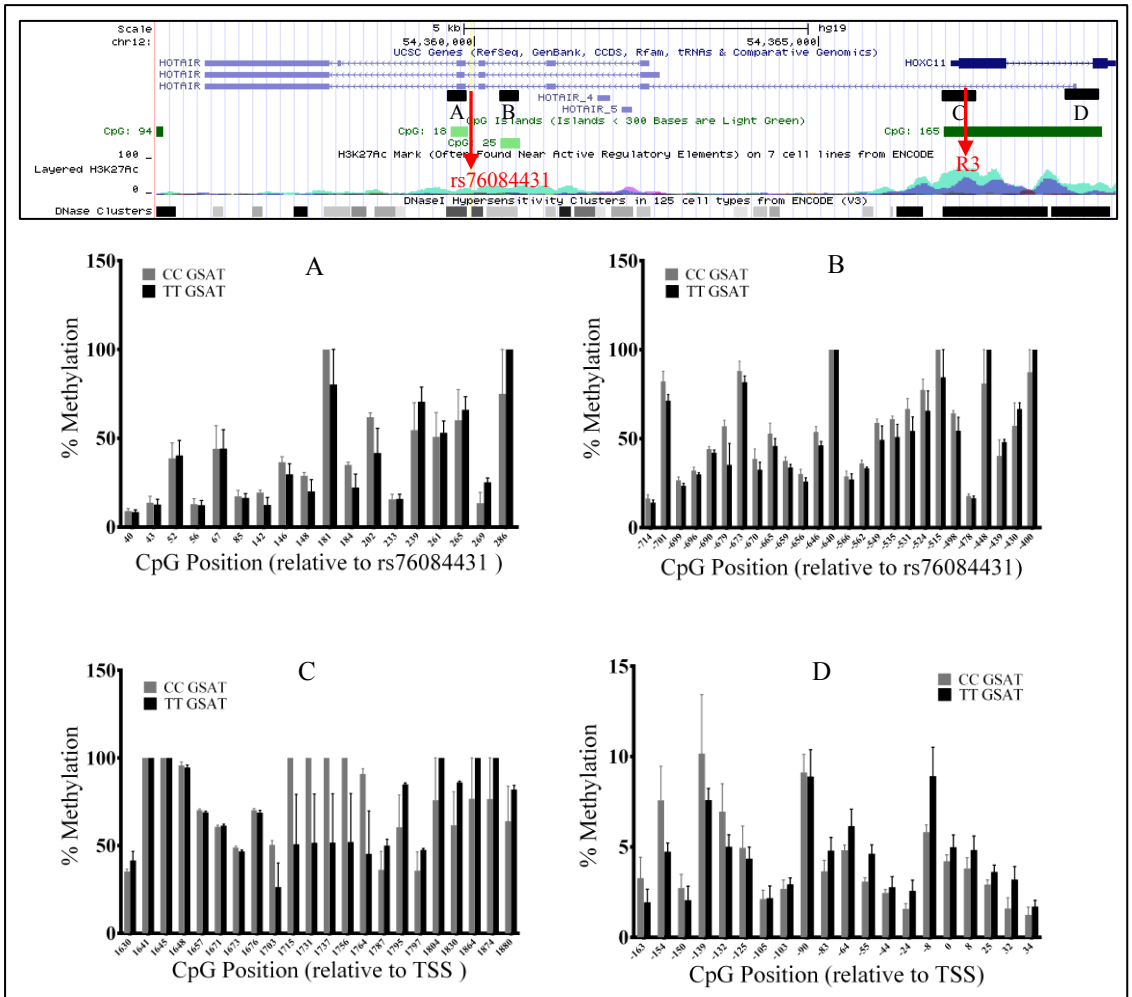


Figure 3-8: Evaluation of the *in vivo HOTAIR* DNA methylation status in genotype-recruited gluteal subcutaneous adipose tissue

Regions around R3 and rs76084431 also enriched for H3K27ac in the human skeletal muscle myoblast and normal human epidermal keratinocyte based on the UCSC genomeic browser view. Pyrosequencing was performed in rs76084431 genotype-recruited females (4 TT versus 4 CC) by using genomic DNA from gluteal adipose tissue. The bisulphite primers were designed on two short CpG islands (A and B) that flank rs76084431 and two ends (C and D) of the long CpG island. Data were presented with % methylation in each CpG position which is relative to rs76084431 in A and B and relative to transcription start site (TSS) of long *HOTAIR* isoform in C and D.

Low DNA methylation in promoter regions has been associated with raised gene

transcription (Ball, et al., 2009), which also related to the histone modifications (Yan, et al., 2015). Therefore, I quantified the DNA methylation status in the putative *HOTAIR* enhancers/promoters of rs76084431 and R3 regions as described on Figure 3-7. Gluteal adipose tissues were obtained from females carrying the rs76084431 TT genotype (n = 4) and CC genotype (n = 4) and genomic DNA was extracted from adipose tissue as described in section 2.2.3. Bisulfite conversion of genomic DNA and pyrosequencing on the CpG sites were performed as described in section 3.2.10.

The A and B regions (Figure 3-8 Browser view) refer to two short CpG islands flanking rs76084431, the C region corresponds to ChIP R3 region and the D region is the promoter region of long *HOTAIR* isoform, which previously has been known to harbour differential DNA methylation status comparing abdominal and gluteal immortalised preadipocyte cell lines (Pinnick, et al., 2014). However, comparing the methylation status in gluteal adipose tissues (Figure 3-8), neither of these CpG regions had any differential methylation in females homozygous for the rs76084431 genotype. This suggests that the rs76084431 has a function other than through affecting or being associated with DNA methylation to influence *HOTAIR* expression in gluteal adipose tissue.

3.4 Discussion

The results provided in this Chapter show that *HOTAIR* expression in gluteal adipose tissue is highly variable between individuals. Isolated gluteal adipocyte precursors retain intrinsic memory of *HOTAIR* expression, which is enhanced by glucocorticoids and dynamically regulated during adipogenic differentiation. Also, genotyping of haplotype-tagging SNPs reveals that *HOTAIR* expression could be influenced by genetic variants and the transcript-lowering T-variant of rs76084431 is additionally associated with the fat distribution phenotypes in females. Furthermore, the histone marks and DNA methylation status at *HOTAIR* locus were explored and identifies rs76084431 located in the open chromatin region with distinct histone marks compared to its surroundings, which further supports rs76084431 as a functional eQTL SNP. Overall, these results point to a functional role of *HOTAIR* transcription determining regional adipose tissue, but some questions remain to be answered.

3.4.1 rs76084431 is not in the same LD with the lead SNPs of the GWAS identified *HOXC13* fat distribution locus

In the genome-wide association studies of fat distribution (Shungin, et al., 2015), three independent signals (rs1443512, rs10783615 and rs2071449) in the *HOXC13* locus have been identified. However, in my study, rs76084431 is not in linkage disequilibrium with any of these three lead SNPs for these signals. In term of genomic positions relative to rs76084431, rs1443512 is about 17 k bps downstream, rs10783615 is about 10 k bps downstream and rs2071449 is about 68 k bps upstream of rs76084431. The *HOTAIR* gene is within the *HOXC13* GWAS peak specifically enriched for the SNPs in LD with rs1443512. In my eQTL studies of the relationship between SNPs and *HOTAIR* expression, the rs1443512 locus also seemed to represent an independent eQTL for *HOTAIR* (Table 3-7) which is directionally consistent with another *HOTAIR* eQTL (rs76084431) identified through the haplotype structures across the *HOTAIR* gene described in this chapter. This finding suggests that the expression of *HOTAIR* is under multiple influences from independent loci. In this study,

I approached the functional SNPs based on the influence of *HOTAIR* transcription, but it is still possible other SNPs might be functional through affecting the *HOTAIR* RNA structure, which couldn't be identified in my experiment. Therefore, it is very likely that in the *HOXC13-HOXC12-HOTAIR* genomic region might have multiple functional loci associated with fat distribution and deserved further investigation.

3.4.2 The potential mechanisms for regulating *HOTAIR* gene expression by intronic SNPs

In the section 3.3.5, two intronic SNPs (rs76084431 and rs12427129) present opposite directional eQTL effect on GSAT *HOTAIR* expression. This result appears to imply there are dynamic and flexible mechanisms harboured in the *HOTAIR* locus for gene regulation. In the section 3.3.7, four histone marks across *HOTAIR/HOXC* locus were investigated. Intriguingly, rs76084431 possesses the same histone modification as the 7 k bps upstream R3 region across all examined histone marks, which represent active enhancer or promotor sites. Moreover, rs76084431 shows inverted H3K4me1 enrichment comparing with its proximal downstream and upstream enhancer regions. The functional roles of H3K4me1 on the enhancers are still uncertain as to whether it directly regulates enhancer activity or only correlates with enhancer activity (Rada-Iglesias, 2018). Recently, H3K4me1 was found to serve as a recruitment site for chromatin remodelling factors with the consequence of maintaining the gene expression (Local, et al., 2018). Other studies (Dorighi, et al., 2017; Rickels, et al., 2017; Yan, et al., 2018) show that H3K4me1 may function to fine-tune enhancer activity and dynamically regulate gene expression during cell differentiation. Therefore, considering these enhancers at the *HOTAIR* locus and the potential fine-tuning function of H3K4me1 in the gene expression, it is tempting to speculate that they might jointly regulate *HOTAIR* expression in the gluteal adipose tissue.

The rs76084431 region had the same histone marks as the R3 site, which could mean these two sites might have physical interaction. Clearly, this speculation cannot be answered in my data, but (Visser, et al., 2012) has demonstrated this possibility. In

human melanocytes carrying the intronic rs12913832 T-allele, a long-range chromatin loop between rs12913832 enhancer and the OCA2 promoter (21 k bps away) was detected that leads to elevated OCA2 expression.

Sequences regulating intronic splicing may be located as far as 200 nucleotides away from the junctions (Majewski and Ott, 2002). Therefore, rs76084431 located only 74 nucleotides away from the intron-exon junction might affect splicing regulation, which will also need further investigation.

3.4.3 Hypothesizing *HOTAIR* function in gluteal adipose tissue based on the genotype-phenotype associations

In the result section 3.3.6, using the DXA scan precisely estimated regional fat mass to analyse the genotype-phenotype association, the GSAT *HOTAIR* transcript-lowering genotype (minor allele of rs76084431) in females showed an association with fat distribution corresponding to 100 g increase of android fat per allele and higher android to gynoid fat ratio. Based on this genotype-phenotype analysis, it is appealing to hypothesize that reduced *HOTAIR* expression in gluteal adipose tissue might impair the adipose tissue expandability in the gluteal depot, with a consequence of shifting fat storage to the android region. This hypothesis will be further examined in the Chapter 4, section 4.3.2 by evaluating the functional consequences after knocking down *HOTAIR* gene in the immortalised gluteal preadipocytes.

3.4.4 Concluding statements

In summary, these data confirm the exclusive gluteal *HOTAIR* gene expression. Results further point out the high individual variability in GSAT *HOTAIR* expression and its multifaceted control and dynamic regulation during different physiological conditions (aging, adipogenesis and hormone signals). The histone modifications at the *HOTAIR* locus may play important roles controlling the depot-specific *HOTAIR* expression. There appears to be genetic control of GSAT *HOTAIR* expression in several eQTL SNPs and rs76084431 is positioned within an active enhancer region.

Chapter 4
Phenotypic effect of modulating *HOTAIR* expression *in vitro* and *in vivo*

4.1 Introduction

Aberrant elevation of *HOTAIR* expression has been observed in several solid cancers and appears to correlate with cancer metastasis and lower survival rate. *HOTAIR* overexpression was showed to increase proliferation, inhibit apoptosis and promote cancer invasion (Ono, et al., 2014; Zhang, et al., 2014; Zhou, et al., 2014). The potential molecular mechanisms linking *HOTAIR* gene expression are still under exploration, but it is known that *HOTAIR* can regulate histone modifications through recruiting polycomb repressive complex 2 (PRC2) and this mechanism has been proposed to suppress hundreds of genes (Gupta, et al., 2010).

According to the online available RNA-sequence data of 53 human tissues within the Genotype-Tissue Expression (GTEx) Project (Consortium, 2013), the *HOTAIR* gene is highly overexpressed in the tibial artery, sun exposed skin (lower leg) and testis. Other tissues in the lower-body region such as bladder, uterus, suprapubic skin and subcutaneous (lower leg) adipose also present higher *HOTAIR* expression than tissues in the upper-body area such as the aorta, visceral (omentum) adipose tissue, brain, heart, lung and liver etc. This expression pattern follows the anterior-posterior axis as its neighbouring developmental genes, *HOXC11-13*. It is still uncertain if the presence of *HOTAIR* in the human tissues is functional or just a developmental relic companying other *HOXC* genes.

Some evidence has suggested that the *HOTAIR* gene is important for bone development. Targeted deletion of mouse *Hotair* lncRNA can cause homeotic transformation of the spine and malformation of metacarpal-carpal bone (Li, et al., 2013). In *in vitro* experiments, *HOTAIR* was found to regulate osteogenic differentiation and proliferation in human mesenchymal stem cells from bone marrow (Wei, et al., 2017). A 50 k bps microdeletion containing *HOXC13*, *HOXC12* and part of the *HOTAIR* was linked to congenital vertical talus in nine affected individuals from 2 different families (Alvarado, et al., 2016). These patients had recurrent deformity of their talus bone, hip dysplasia, hip muscle weakness in childhood and severe arthritis

of hip and knee in older individuals. Based on these findings, it seems very possible that *HOTAIR* is important for bone development in the lower extremity. Hence, it is also possible that *HOTAIR* could be functionally important for other *HOTAIR*-expressing tissue of mesenchymal origin such as gluteofemoral subcutaneous adipose tissue.

Knowledge of the roles of *HOTAIR* gene expression in regional human adipose tissue is very limited. Currently, only one publication suggests that the *HOTAIR* gene possesses a positive effect on in *vitro* adipogenesis in human primary abdominal preadipocytes (Divoux, et al., 2014). There is some evidence from animal models that *HOTAIR* is relevant for adipose tissue deposition and maintenance in distal body parts. In the fat-tailed sheep, the tail fat is an important source of energy, in particular for ewes and serve as a survival buffer during food scarcity (Kang, et al., 2017). RNA-sequencing comparing the transcriptome between subcutaneous abdominal, visceral abdominal and the tail adipose tissues in the fat-tailed sheep have shown that *HOXC11-13* and *HOTAIR_2, HOTAIR_3* genes were specifically enriched in the tail adipose depot which may suggest an association with tail fat development (Kang, et al., 2017). Also, in mice, deletion of *Hotair* in adipose tissue results in significant adipogenic deficiency in the gluteal-femoral fat but didn't cause any obvious skeletal deformity (Lu, et al., 2017). In line with these studies and recognising the site-specific *HOTAIR* expression (Pinnick, et al., 2014), it will be of particular interest to observe the phenotypic effect of suppressing *HOTAIR* expression in human gluteal preadipocytes. It is equally intriguing to observe the effect of overexpressing *HOTAIR* gene in human subcutaneous abdominal preadipocytes. This bidirectional intervention will illustrate the functional roles of *HOTAIR* gene in regional human adipose tissue and provide evidence for a causal relationship between *HOTAIR* gene expression and body fat distribution. A similar experiment can also be done by making use of the *HOTAIR* eQTL (rs76084431) in studying the phenotypic effect in tissue samples from OBB subjects recruited by genotype and by previously quantified GSAT *HOTAIR* mRNA

abundance in tissues. DXA scans and paired adipose tissue biopsies were taken to quantify regional fat components and measure adipocyte size.

4.1.1 Aims

- Assess functional effects of *HOTAIR* knockdown in human immortalised gluteal preadipocytes

- Assess functional effects of *HOTAIR* overexpression in human immortalised abdominal preadipocytes

- Explore interactions between *HOTAIR* and two potential antiadipogenic target genes (*CEBPD* and *PTEN*)

- Recruit OBB subjects based on the *HOTAIR* eQTL rs76084431 as a model for *in vivo* regulation of *HOTAIR* gene expression

- Recruit people in whom tissue *HOTAIR* mRNA abundance has already been quantified: comparing phenotypic differences between high vs low-expressing tissues/individuals

4.2 Methods

4.2.1 Generation of stable *HOTAIR* knockdown in immortalised human gluteal preadipocytes

Pooled *HOTAIR* shRNA lentivirus (ABM, catalogue number: iv009919) and scrambled shRNA lentivirus (ABM, catalogue number: LVP015-G) were used to generate *HOTAIR* stable knockdown and scramble control preadipocytes.

The immortalised human gluteal preadipocytes were revived for 2 passages as described in section 2.3.1. Cells (3 x 10^4 cells per well) were seeded in the 24-well plate and maintained in the humidified atmosphere, 37°C, 5% CO_2 incubator overnight, and left to reach around 70% cell confluence. Two wells were prepared for viral transduction by *HOTAIR* shRNA lentivirus and scrambled shRNA lentivirus, respectively. One extra well was prepared as a control well. Lentiviral particles were added to an estimated 40 infectious units per cell in the growth medium containing hexadimethrine bromide (Sigma) with final concentration of 8 µg/ml. In the control well, the growth medium (8 µg/ml hexadimethrine bromide) without lentivirus was used. Cells were maintained in the humidified atmosphere, 37°C, 5% CO_2 incubator overnight (around 20 hrs). The viral supernatant was removed and cells were further cultured in normal growth medium for 24-48 hrs. Subsequently, puromycin (1-2 µg/ml) containing growth medium was used for selecting the viral transduced cells. The virus transduced cells expressed green fluorescent protein (GFP) and could be observed with fluorescent microscopy. Cells in the control well needed to show complete cell death to indicate adequate puromycin selection.

4.2.2 Cloning of *HOTAIR* construct into pEGFP-Lv105 vector

LZRS-*HOTAIR* (Addgene plasmid #26110) as a gift from Howard Chang (Gupta, et al., 2010) was used for cloning the *HOTAIR* construct and it has been shown could induce genome-wide re-targeting of PRC2 and H3K27me3. The *HOTAIR* sequence matched with the *HOTAIR* short isoform (NR_003716) without including the 5'

untranslated region and is more than 4000 bps distant from the leader sequence of *HOXC11* gene. The LZRS-*HOTAIR* plasmid was isolated via using QIAprep spin Miniprep kit (Qiagen) after streaking/isolation LZRS-*HOTAIR* bacteria on an ampicillin lysogeny broth (LB) agar plate and inoculating in a liquid ampicillin LB overnight.

Two paired primers with added enzyme restriction sites (capital letter) were designed for PCR amplification in two segments of *HOTAIR* sequence from LZRS-*HOTAIR* plasmid as listed in Table 4-1. The sequence overlapped between these two segments contained another enzyme restriction site (CCATGG). The thermal cycling parameters are: 95°C for 3 mins followed by 18 cycles of 95°C for 30 secs, 58°C for 30 secs and 72°C for 90 secs, then 72°C for 6 mins and incubate at 4°C.

Table 4-1: Primers designed for cloning *HOTAIR* construct

Amplicon	Forward primer	Reverse primer	Size (bps)
*HOTAIR*_construct-A	GCTAGCgactcgcctgtgctctggag	ccagaaccctctgacatttg	1150
*HOTAIR*_construct-B	ggcttgttaacaagaccagag	TTCGAAgaaaatgcatccagatattaatat	1227

The PCR products of the *HOTAIR* constructs were run on agarose gel electrophoresis to confirm the size. DNA was isolated from the gel using the QIAquick gel extraction kit (Qiagen). The *HOTAIR*_construct-A and B were ligated to pGEM-T vectors (Promega) and bacterial transformation was performed with ultracompetent XL10 Gold cells (Agilent Technologies). PGEMT-*HOTAIR*_construct-A and PGEMT-*HOTAIR*_construct-B were isolated by inoculating the transformed bacteria in the liquid ampicillin LB and then using QIAprep spin Miniprep kit. These two PGEMT-*HOTAIR* plasmids were then sequenced to confirm the absence of mutated nucleotides in the *HOTAIR* construct. Then, two PGEMT-*HOTAIR* plasmids were digested by matched enzymes that targeted the restriction sites. The digest was run on an agarose gel electrophoresis and the non-mutated clones of the *HOTAIR*_construct-A and *HOTAIR*_construct-B were further purified using QIAquick gel extraction kit.

The non-mutated *HOTAIR*_construct-A and *HOTAIR*_construct-B were ligated with an pEGFP-Lv105 vector (Capital Biosciences) and bacterial transformation was performed with ultracompetent XL10 Gold cells. The transformed bacterial colony was inoculated in the liquid ampicillin LB and the pEGFP-Lv105 vector containing the full non-mutated *HOTAIR* construct was isolated via using QIAprep spin Miniprep kit.

4.2.3 Generation of lentivirus particles containing pEGFP-Lv105-*HOTAIR* vector and pEGFP-Lv105 empty vector

Human embryonic kidney cells (HEK293 cells) were used to generate the lentivirus particles. In the medium for culturing HEK293 cells, the ViraPower^{TM} lentiviral packaging mix (Invitrogen) was added to pEGFP-Lv105 empty vector and pEGFP-Lv105-*HOTAIR* vector, respectively, to generate the pEGFP-Lv105-empty lentivirus and pEGFP-Lv105-*HOTAIR* lentivirus. The lentiviral particles were collected from the supernatant after transfection of HEK293 cells for 48-72 hrs. The viral supernatant was filtered through a Millex-HV 0.45 μm syringe filter and frozen at -80°C for long-term storage.

4.2.4 Generation of constitutive *HOTAIR* overexpression in immortalised human gluteal and abdominal preadipocytes

pEGFP-Lv105-*HOTAIR* lentivirus and pEGFP-Lv105-empty lentivirus were used to generate the constitutive *HOTAIR* overexpression and vector control cells in both immortalised gluteal and abdominal preadipocyte cell lines. The steps of lentiviral transduction are the same as described in section 4.2.1, except for the transduction which was performed in the T25 flasks by the initial seeding of 8 x 10^4 cells per T25 flask.

4.2.5 Separation of nuclear and cytoplasmic total RNA

The SurePrep^{TM} nuclear or cytoplasmic RNA purification kit (Fisher BioReagents) was used to separate the nuclear and cytoplasmic RNA directly from the harvested

cells. In order to have enough nuclear total RNA, cells were cultured to reach high confluence in the T75 flask, then washed with PBS and harvested with the ice-cold lysis solution. The lysate was centrifuged to separate cell fractions. The supernatant fraction contained cytoplasmic RNA and the pellet fraction contained nuclear RNA. The supernatant was carefully collected and transferred to a new RNase-free tube without dislodging the pellet. The separated fraction (the supernatant fraction is used for cytoplasmic RNA extraction and the pellet fraction is used for nuclear RNA extraction) was mixed with binding solution and ethanol, then applied to a spin column for RNA binding via centrifugation. The column was washed three times and RNA was eluted with elution solution. The concentration of RNA was quantified by the NanoDrop spectrophotometer and frozen at -80°C.

4.2.6 Custom TaqMan assay design

Primer Express Software version 3.0 (Applied Biosystems) was used for automatically designing primers and probes of TaqMan assays. The selected primers/probes were ordered online using Custom TaqMan Assay Design Tool (ThermoFisher Scientific).

To evaluate the *HOTAIR* mRNA knockdown efficiency the custom TaqMan assay was designed to target the *HOTAIR* shRNA binding sites. The selected primers/probes are as follows: forward primer: ACAGAGAGAATAATCCGGGTCCTA, probe: CGCCACATGAACGC and reverse primer: CCCGCTCAGGTTTTTCCA. The forward primer overlaps with the sequence of one *HOTAIR* shRNA (801: GAACGGGAGTACAGAGAGA) and the probe overlaps with the sequence of another *HOTAIR* shRNA (840: CCACATGAACGCCCAGAGA).

4.2.7 Anti-H3K27me3 and anti- suppressor of zeste 12 (SUZ12) chromatin immunoprecipitation

The EZ-Zyme^{TM} Chromatin Prep kit (Upstate) was used for the enzymatic digestion of DNA and the EZ-ChIP^{TM} Chromatin Immunoprecipitation kit (Upstate) was used

to perform chromatin immunoprecipitation. Immunoprecipitation of crosslinked protein/DNA was conducted by using a ChIP grade H3K27me3 antibody (Abcam, ab6002) and a ChIP grade SUZ12 antibody (Abcam, ab12073). Mouse IgG antibody (Upstate, 12-371B) was used as the negative control. All steps followed the protocols of these two kits. Briefly, gluteal sh*HOTAIR* and shControl cells were treated with 1% formaldehyde for 10 mins. The cross-linked chromatin was then prepared and 2U of EZ-Zyme^{TM} enzymatic cocktail per 4 x 10^6 cells was used for the enzymatic digestion to cleave DNA to 180-360 bps. Cleaved chromatin (3.3 x 10^6 cell equivalents) was aliquoted for each immunoprecipitation (IP). One % of the chromatin supernatant was collected as the input before adding the immunoprecipitating antibody. Then, protein G Agarose was used to bind the antibody/antigen/DNA complex. The Protein G Agarose-antibody/chromatin complex was pelleted, washed several times and eluted

Table 4-2: Custom TaqMan assays designed for the promoter regions of genes

Custom TaqMan	Primers/Probe	Sequence
ChIP-*HOXD8*	Forward primer	CGGGCAGAGGGTGTTTTTT
	Reverse primer	CACTCTGGCCTCGGTTTACAA
	Probe	CCCTCCAGAGCCGG
ChIP-*HOXD10*	Forward primer	CACCCCCTGGTCTCTTTGC
	Reverse primer	TGGTATAGGGACAGCGCTTTTT
	Probe	TTGCAGTTGCCCCCCAG
ChIP-*CEBPD*	Forward primer	AGGAGCGAGGAGGTTCCAA
	Reverse primer	AGCACTCCAGGGCCTTCTC
	Probe	CCCACAAACAGGAAGA
ChIP-*PTEN*	Forward primer	TCCTACCGTTCCGTACTTTCCA
	Reverse primer	CCGGACCGTGCACGTT
	Probe	TCAACCCGGTAACCC

in the Elution buffer as per protocol. The input tube was added in the same elution buffer. All IP and input tubes were progressed together to reverse the protein-DNA crosslinking to free DNA. The free DNA was further purified and isolated using a spin

column.

All ChIP experiments were performed in triplicate. The purified free DNA was run on a real-time quantitative PCR with custom designed TaqMan assays (as described in section 4.2.6). For designing the TaqMan assays to target the promoter region, Ensembl genome browser (http://www.ensembl.org/index.html) was used to retrieve putative promoter sequences. ChIP-qPCR data were analysed and presented with % input after normalising for both background levels and quantity of input chromatin. In the ChIP experiments within this Chapter, custom TaqMan assays were designed to target the promoter sequences of *HOXD8*, *HOXD10, CEBPD* and *PTEN* genes (Table 4-2).

4.2.8 Western blotting for phosphorylated Akt (pAkt) and total Akt (tAkt) proteins

Cells were cultured with normal differentiation medium (as described in section 2.3.2) till day 7. Then, differentiation medium was removed, cells were washed with PBS twice and basal medium without insulin (Dulbecco's modified Eagle's medium/nutrient mixture F-12 Ham's, 17.5 mM glucose supplemented with 2 mM L-glutamine, 100 units/ml penicillin and 100 µg/ml streptomycin) was added. Cells were maintained in the humidified atmosphere, 37°C, 5% CO_2 incubator for 24 hrs, then treated with insulin at four different final concentrations (0 nM, 25 nM, 50 nM, 100 nM) for 10 mins. Cells were harvested immediately for western blotting as described in section 2.6. Antibodies against phosphorylated Akt (Cell Signalling #4060) and total Akt (Cell Signalling #4685) were used for the blotting. The image was captured and the relative density was calculated as described in section 2.6.3 and 2.6.4.

4.2.9 Transfecting with siRNA oligos

In this Chapter, human siRNA oligo duplexes were used to transiently suppress *CEBPD* (Trilencer-27, Origene, SR300761) or *PTEN* (Trilencer-27, Origene, SR321496) expression. Each kit contains three unique 27 mer siRNA duplexes (2 nmol

each), one scrambled negative control siRNA duplex (2 nmol) and RNase-free siRNA duplex resuspension buffer. The resuspension buffer (100 µl) was added to each duplex to make a stock siRNA solution (20 µM) which was frozen at -80°C for long-term storage. Before commencing the main knockdown experiment two concentrations of each siRNA duplex (10 nM and 20 nM) were tested for knockdown efficiency.

Briefly, cells were plated into 6-well plates and cultured as outlined in section 2.3.1 and 2.3.2. The siRNA stock solutions (20 µM) were diluted to the required concentrations in 125 ul Dulbecco's modified Eagle's medium/nutrient mixture F-12 Ham (v/v, 1: 1; Sigma, antibiotic- and serum-free). In separate tubes, 7.5 ul Lipofectamine 2000 (Invitrogen) were diluted in 125 µl Dulbecco's modified Eagle's medium/nutrient mixture F-12 Ham. The solutions were mixed for 5-10 secs and incubated at room temperature for 15 mins. Diluted siRNA was then added to the diluted Lipofectamine 2000 (1:1 ratio), mixed for 5-10 secs and incubated for a further 15 mins at room temperature. Cells were washed with PBS twice before 750 µl antibiotic-free maintenance medium (differentiation or growth medium depending on the experiment type) was added to each well. The siRNA-Lipofectamine mixture (250 µl) was then added dropwise onto the cells and the plate was gently rocked for adequate mixing. After overnight transfection for around 20 hrs, cells were washed with PBS twice and the maintenance medium was replaced.

For testing the knockdown efficiency of each siRNA duplex, the cells were harvested at 48-72 hrs after transfection and *CEBPD* or *PTEN* knockdown efficiency was assessed by performing real-time qPCR. The unique siRNA duplex (SR300761A) with the best knockdown efficiency (> 70%) was chosen for suppressing *CEBPD* and the concentration (10 nM) was selected as it was shown to have a similar knockdown efficiency. The unique siRNA duplex (SR321496C) with the best knockdown efficiency (> 70%) was selected for suppressing *PTEN* and the concentration (20 nM) was chosen as it was shown to give a more efficient knockdown than the 10nM concentration. The duration of the *CEBPD* or *PTEN* knockdown was tested and found

to be maintained for more than 5 days in the human preadipocytes.

To knockdown *CEBPD* or *PTEN* from differentiation day 4, cells were cultured and differentiated as described in section 2.3.1 and 2.3.2. Then equal concentrations of unique siRNA duplex or scramble siRNA were added on differentiation day 4.

4.2.10 Bisulfite pyrosequencing for measuring DNA methylation status in the *PTEN* promoter region

Table 4-3: Bisulfite PCR primers and their optimal conditions

Amplicon	Bisulfite Primers	Annealing temp (°C)
PTEN	Forward: GGAATTTTTAGGTAAAGGTTGTTATAG	53
	Reverse: CATACCCAATATAACTACCTAAAACTTAC	

Bisulfite pyrosequencing was performed as outlined in section 3.2.10. In this Chapter, one amplicon in the *PTEN* promoter region was pyrosequenced and details of bisulfite primers/sequencing primers are listed in Table 4-3 and Table 4-4. The region selected for pyrosequencing is based on the Li et al paper (Li, et al., 2013).

Table 4-4: Sequencing primers for bisulfite-pyrosequencing

Amplicon	Sequencing primer 1	Sequencing primer 2	Sequencing primer 3
PTEN	TGTTATAGTTAAATTTTTG	GTATAGGTAATTTTAGATT	TGGGTTTTTGGGTAGAGGT

4.2.11 Recruitment of OBB subjects based on genotype and previous GSAT *HOTAIR* levels

Within the entire OBB (n ~ 7,000) only 16 females carried the rs76084431 TT genotype and were contacted for recruitment. Of these, only 4 females were successfully recruited. Age and BMI matched females with rs76084431 CC genotype were recruited with 1:1 ratio. This small scale recruitment was made with the intention of identifying large phenotypic effects, if there were any. Participants underwent a DXA scan for precise quantification of regional fat masses, blood collection for

biochemistry and paired (abdominal and gluteofemoral) adipose tissue biopsies for RNA/DNA isolation as well as for adipose tissue histology.

Based on the GSAT *HOTAIR* expression measured in the previously described adipose tissue cDNA panel (204 OBB subjects), the participants exhibiting the 20 top high and 20 lowest *HOTAIR* expression levels in either sex were invited for a recall study. Overall, 13 subjects (5 males and 8 females) with previous high GSAT *HOTAIR* levels and 13 subjects (4 males and 9 females) with previous low GSAT *HOTAIR* levels were successfully recruited. These participants underwent the same phenotypic pipeline as the genotype-recalled participants.

4.2.12 Gene expression analysis

RNA extraction of adipose tissue or cells was performed as described in section 2.4.1. cDNA synthesis was performed as described in section 2.4.2 and real-time qPCR was done as outlined in section 2.4.3. The TaqMan Assay-on-Demand used in this Chapter include: *PPIA* (Hs99999904_m1); *HOTAIR* (Hs03296631_m1); *HOTAIR* (Hs03296680_s1); *HOTAIR* (Hs03296661_mH); *HOTAIR* (Hs03296630_m1); *CEBPA* (Hs00269972_s1); *CEBPB* (Hs00270923_s1); *CEBPD* (Hs00270931_s1); *PPARG2* (Hs01115510_m1); *HOXD8* (Hs00251905_m1); *HOXD10* (Hs00157974_m1); *PTEN* (Hs02621230_s1). In this project, *HOTAIR* assay (Hs03296631_m1) was selected to measure *HOTAIR* expression as it detects the maximum number of transcripts and best meets the design criteria. Other *HOTAIR* assays were also used in some situations and will be mentioned specifically.

4.2.13 Statistical analysis

SPSS (IBM Corp. Released 2013. IBM SPSS Statistics for Windows, Version 22.0. Armonk, NY: IBM Corp.) was used to perform statistical analyses and a P value < 0.05 was considered statistically significant. Data are presented ad means ± SEM.

4.3 Results

4.3.1 Evaluation of *HOTAIR* knockdown efficiency between stable *HOTAIR* knockdown and scramble control gluteal preadipocytes

Immortalised human gluteal preadipocytes were transduced with *HOTAIR* shRNA lentivirus to generate gluteal sh*HOTAIR* cells as outlined in section 4.2.1. The gluteal shControl cells were generated through the same procedure via using scrambled shRNA lentivirus. After adequate puromycin selection for more than one week and checking the cells with positive GFP expression under fluorescent microscope, the knockdown efficiency was evaluated between gluteal sh*HOTAIR* cells and shControl cells via using TaqMan assay (Hs03296631_m1) for real-time *HOTAIR* expression.

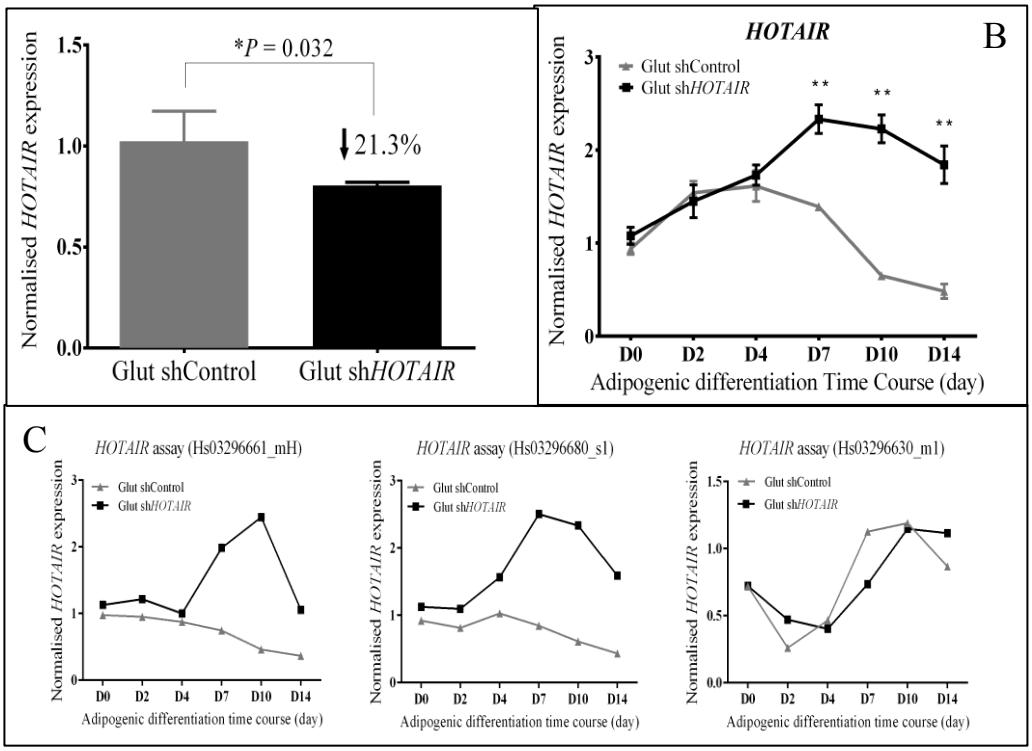


Figure 4-1: Transducing *HOTAIR* shRNA lentivirus in gluteal cells interferes the *HOTAIR* expression with counterintuitively elevated levels during adipogenesis
A: *HOTAIR* expression in gluteal shControl and sh*HOTAIR* preadipocytes was measured with real time qPCR during cell proliferation (n = 3). Data were assessed with independent t-test (one-tailed) and presented with means ± SEM. **P* < 0.05. **B:** Real-time qPCR of *HOTAIR* expression during adipogenesis was evaluated in gluteal shControl and sh*HOTAIR* cells with technical triplicates (n = 3). Data were analysed with ANOVA to compare levels between two cells in each time point and presented with means ± SEM. **P* < 0.05; ***P* < 0.001. **C:** Three different *HOTAIR* TaqMan assays were further applied to measure *HOTAIR* expression during adipogenesis.

Experiments were performed with technical triplicates via seeding cells of the same passage into three different 6-well plates and cultured with the same medium at the same time.

The immortalised preadipocytes were generated by stable co-expression of HPV16-E7 and hTERT, which promote cell proliferation and inhibit cell senescence. It is still uncertain if the immortalisation process would influence the effect of *HOTAIR* knockdown or overexpression. In future, applying *HOTAIR* knockdown or overexpression experiments to primary preadipocytes will be able to answer this question.

During cell proliferation, the gluteal sh*HOTAIR* cell shows about 21% ($P = 0.032$) decrease of *HOTAIR* levels comparing to the control cell (Figure 4-1A). To further assess the *HOTAIR* knockdown efficiency during differentiation, both cells were proceeded to *in vitro* adipogenesis. The *HOTAIR* expression was measured at 6 different time points (Figure 4-1B). Paradoxically, the *HOTAIR* expression showed a significant increase during differentiation time course with the knockdown treatment. At this state I already knew that the sh*HOTAIR* cells had increased expression of *HOXD8* (see later), which would be consistent with alleviation of the expected *HOTAIR* effect on the known target *HOXD8*. I therefore suspected the actual quantification of *HOTAIR* mRNA in the sh*HOTAIR* experiments did not represent available effective *HOTAIR* mRNA. To interrogate this problem, I proceeded with a number of experiments.

The *HOTAIR* gene has three isoforms and the shRNA pools targets the terminal 3' exon in all three transcript variants. To exclude the possibility of false detection of degraded *HOTAIR* fragment and evaluate the expression of individual transcript variants, real-time *HOTAIR* expression was measured with an additional three different TaqMan assays during differentiation (Figure 4-1C). The assay (Hs03296631_m1) that I had used up until now detected transcript variant 1&2; another assay,

Hs03296661_mH detects transcript variant 3; Hs03296680_s1 measures all three transcripts and Hs03296630_m1 targets transcript variant 1 only. However, none of them displayed reduced *HOTAIR* expression in gluteal sh*HOTAIR* cells.

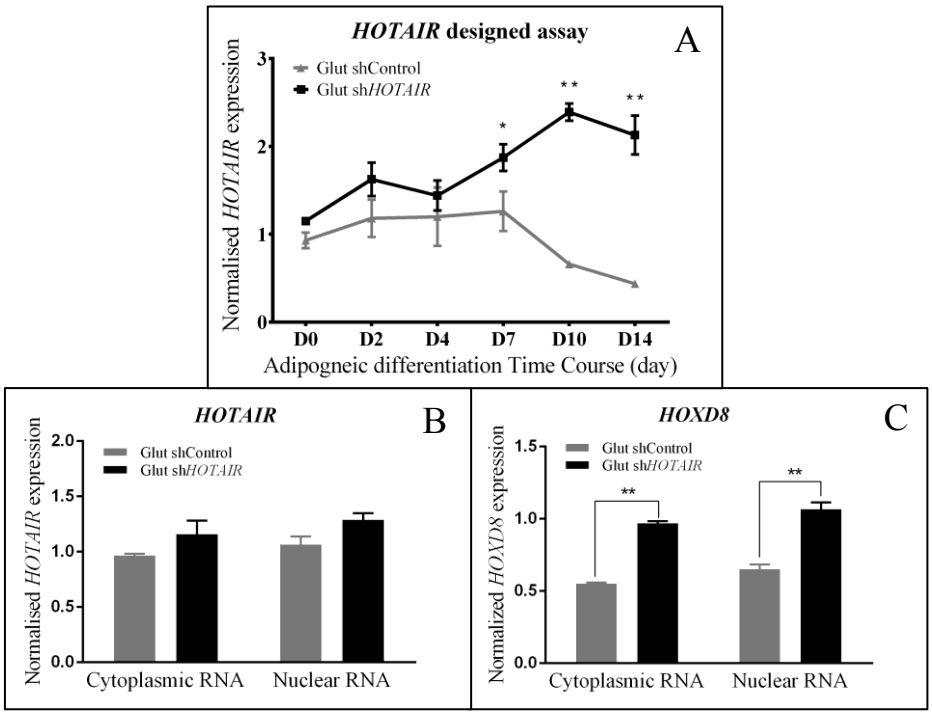


Figure 4-2: Using designed TaqMan assay to assess the cleavage of *HOTAIR* mRNA by shRNAs and evaluate *HOTAIR* knockdown efficiency in cytoplasmic and nuclear components

A: *HOTAIR* designed assay targets on the shRNA binding sites was applied to assess *HOTAIR* knockdown efficiency during differentiation (n = 3). Data were analysed with ANOVA to compare levels between two cells in each time point and presented with means ± SEM. **P* < 0.05; ***P* < 0.001. **B & C:** Cytoplasmic and nuclear RNA was separated to measure real-time *HOTAIR* and *HOXD8* expression in both cells under proliferation (n=3). Data were assessed with independent two-tailed t-test and presented with means ± SEM. **P* < 0.05; ***P* < 0.001.

In order to specifically interrogate if the shRNAs induced *HOTAIR* mRNA cleavage, I designed the custom TaqMan assay in which its forward primer and probe overlapped with the shRNA sequences as described in section 4.2.6. Theoretically, as long as the RNA-induced silencing complex leads to degradation of the *HOTAIR* mRNA, this *HOTAIR* designed assay won't detect the *HOTAIR* transcript. However, abundance of undegraded *HOTAIR* transcripts did not appear to explain the paradoxically high

HOTAIR mRNA content during adipogenesis (Figure 4-2A).

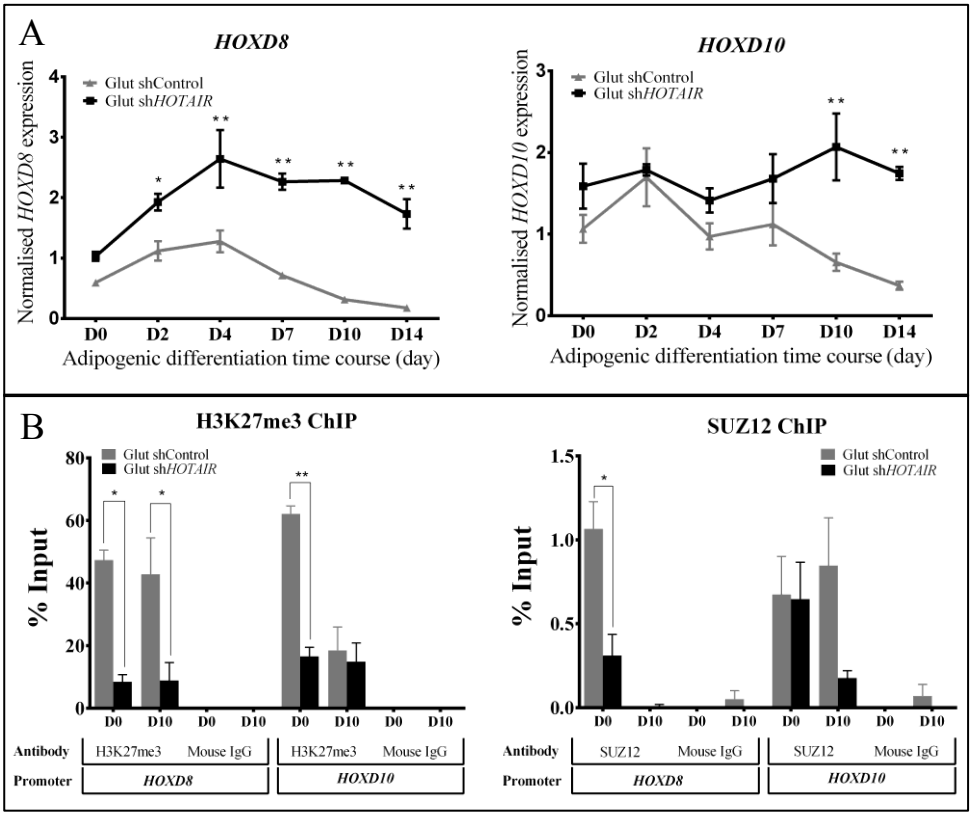


Figure 4-3: *HOXD8* and *HOXD10* genes were de-repressed and *HOTAIR* function was suppressed in the gluteal sh*HOTAIR* cells

A: Real-time qPCR of *HOXD8* and *HOXD10* expression was measured during in vitro adipogenesis of gluteal shControl and sh*HOTAIR* cells (n = 3). Data were analysed with ANOVA to compare levels between two cells in each time point and presented with means ± SEM. **P* < 0.05; ***P* < 0.001. **B:** Anti-H3K27me3 and anti-SUZ12 ChIPs were performed in both cells on differentiation day 0 and day 10 with independent technical triplicates (n = 3). Mouse IgG antibody was used as the negative control. Data were assessed with ANOVA and presented with means ± SEM. **P* < 0.05; **p<0.001.

The *HOTAIR* transcript is localised in both nuclear and cytoplasmic components (Yoon, et al., 2013). Therefore, I separated the cytoplasmic RNA and nuclear RNA (as outlined in section 4.2.5) to measure the abundance of the transcript separately in these two cell compartments. The SurePrepTM nuclear or cytoplasmic RNA purification kit was used to separate the RNA, but how efficiently the kit works will still need to be validated by adequate controls. However, there was no difference of *HOTAIR*

transcript abundance in either of the cell compartments. Since *HOTAIR* is known to epigenetically suppress HOXD locus *in trans*, I measured *HOXD8* expression as a *HOTAIR* downstream gene and both the cytoplasmic and nuclear *HOXD8* expression was significantly enhanced in the gluteal sh*HOTAIR* cells (Figure 4-2B&C). These results suggested that the *HOTAIR* knockdown experiment had worked but for some reason a 'silenced' *HOTAIR* transcript was still abundant. I also tested another downstream target of *HOTAIR* (*HOXD10*) during a full differentiation time course (Figure 4-3), and these results also showed signs of alleviation of repression consistent with a relative absence of *HOTAIR* in the knockdown situation. The expressing levels of *HOXD8* and *HOXD10* were significantly higher than control in the gluteal sh*HOTAIR* cells during adipogenic differentiation (Figure 4-3A).

Since SUZ12 is a component of the PRC2 complex and *HOTAIR* is known to recruit PRC2 to induce H3K27 trimethylation, I used anti-H3K27me3 and anti-SUZ12 chromatin immunoprecipitations (ChIP) to investigate the epigenetic function of *HOTAIR* in the promoter regions of *HOXD8* and *HOXD10*. The method is described in section 4.2.7. The ChIP results showed that presence of H3K27me3 and SUZ12 on the promoter regions of *HOXD8* and *HOXD10* genes were decreased in the gluteal sh*HOTAIR* cells (Figure 4-3B). Based on these results, it seems as if functional *HOTAIR* knockdown was achieved in the gluteal sh*HOTAIR* preadipocyte. I therefore moved on to study the functional impact of *HOTAIR* stable knockdown on the biological properties of gluteal preadipocytes.

4.3.2 Assessing the functional effects of *HOTAIR* stable knockdown in gluteal preadipocytes

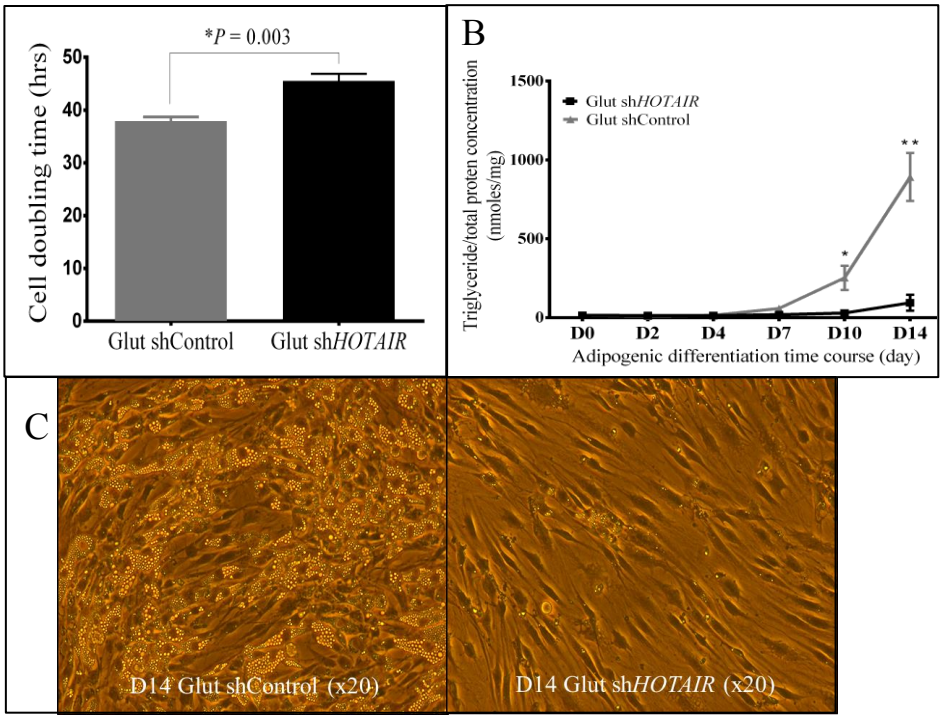


Figure 4-4: Cell proliferation rate and adipogenesis were impaired in the gluteal sh*HOTAIR* preadipocytes

A: Cell doubling time of gluteal shControl and sh*HOTAIR* cells was estimated during proliferation (n = 4). Data were analysed with independent t-test and presented with means ± SEM. **P* < 0.05. **B:** Cellular triglyceride concentration was normalised to total protein levels for quantifying the *in vitro* adipogenesis in both cells (n = 3). Data were assessed with ANOVA to compare levels between two cells in each time point and presented with means ± SEM. **P* < 0.05; ***P* < 0.001. **C:** Photos of day 14 cells were taken with x 20 amplification under microscope.

Gluteal shControl and sh*HOTAIR* cells were cultured in parallel to assess the functional properties of cell proliferation and differentiation. The cell doubling time was estimated as described in section 2.3.3. The gluteal sh*HOTAIR* cell had longer cell doubling time compared to the gluteal shControl cell, which means the cell proliferation rate was decreased in the gluteal sh*HOTAIR* preadipocytes (Figure 4-4A).

Cells underwent adipogenic differentiation as outlined in section 2.3.2 and the cellular triglyceride contents were measured as described in section 2.5. The gluteal sh*HOTAIR* cells showed remarkably lower triglyceride content compared to control cells (Figure 4-4B) and also maintained the spindle shape of preadipocytes rather than

morphing into the circular shape of lipid-laden adipocytes undergoing differentiation day 14 (Figure 4-4C).

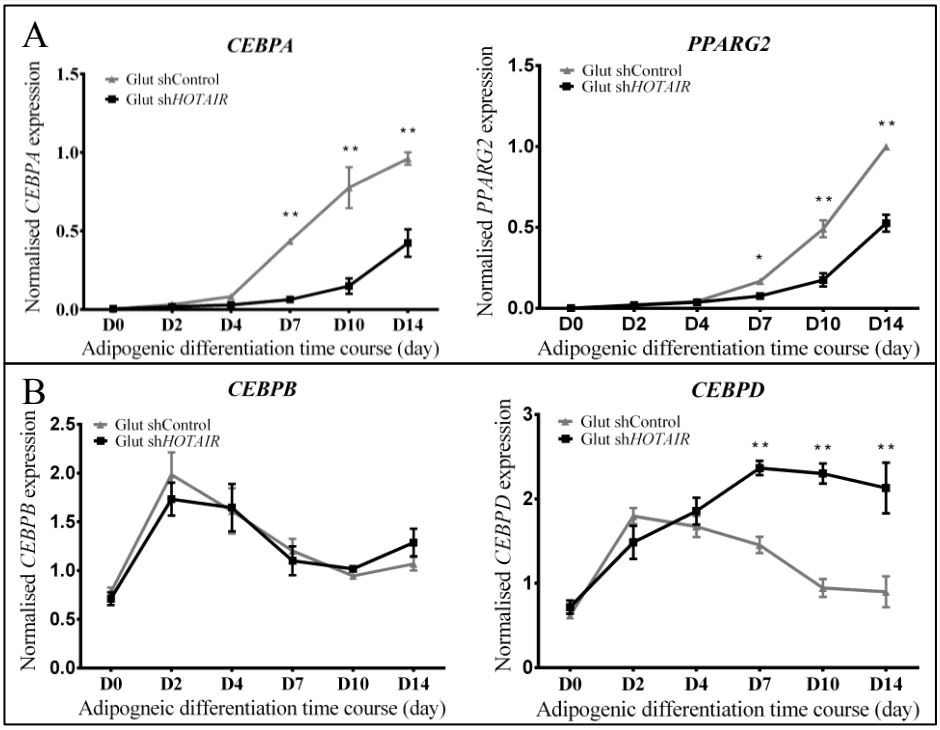


Figure 4-5: Expression of master adipogenic transcription genes and early adipogneic genes were influenced in the gluteal sh*HOTAIR* cell

Master adipogenic transcription genes of *CEBPA* and *PPARG2* (**A**) and early adipogenic genes of *CEBPB* and *CEBPD* (**B**) were measured with real-time qPCR during differentiation time course (n = 3). Data were assessed with ANOVA to compare levels between two cells in each time point and presented with means ± SEM. **P* < 0.05; ***P* < 0.001.

The normal stages of adipogenesis include early stage of mitotic clonal expansion with elevation of *CEBPB* and *CEBPD*, followed by terminal differentiation with increase of master adipogenic transcription factors such as *CEBPA* and *PPARG2*, which are required for forming of mature white adipocyte (Lefterova and Lazar, 2009). During the differentiation time course in the sh*HOTAIR* cells, the master adipogenic transcriptional factors: *CEBPA* and *PPARG2* were repressed. The early adipogenic marker *CEBPB* was unaffected whereas another classic early adipogenic gene, *CEBPD* showed a drastic elevation during late adipogenesis. (Figure 4-5A&B).

As preadipocytes require insulin-stimulated glucose uptake to provide substrate for *de novo* lipogenesis, I postulated that this pathway could be failing in the sh*HOTAIR* cells. To explore this further, I investigated the insulin signalling response by western blotting of phosphorylated Akt on Ser473 (pAkt) and total Akt (tAkt) proteins on differentiation day 8 as outlined in section 4.2.8. The gluteal shControl cells showed full response in the relative pAkt/tAkt ratio after treatment with 25 nM insulin and the gluteal sh*HOTAIR* cells showed a diminished response (Figure 4-6A). In this experiment, gluteal shControl and sh*HOTAIR* cells were both cultured under high glucose concentration (17.5 mM), but only the sh*HOTAIR* cells presented a diminished capacity for insulin signal transduction.

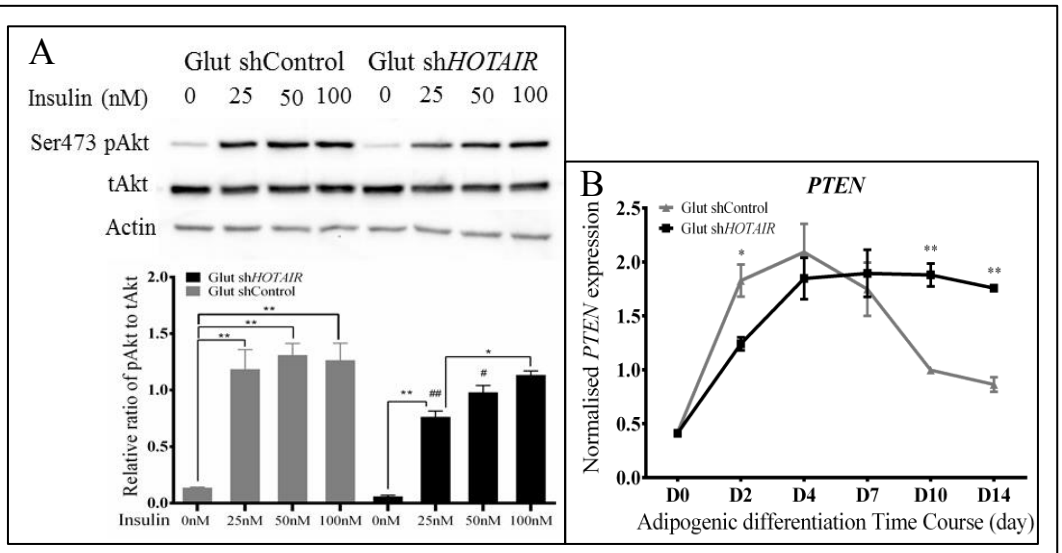


Figure 4-6: The gluteal sh*HOTAIR* cell becomes relatively insulin resistant with increased *PTEN* expression in the late phase of differentiation

A: Western blotting for relative pAkt to tAkt ratio was performed on differentiation day 8 in gluteal sh*HOTAIR* and shControl cells (n = 3). Data were analysed with ANOVA and presented with means ± SEM. **P* < 0.05; ***P* < 0.001 as compared in the same cell; # *P* < 0.05; ## *P* < 0.001 as compared between two cells treated with the same insulin concentration. **B:** *PTEN* expression was measured with real-time qPCR in both cells during differentiation (n = 3). Data were assessed with ANOVA to compare levels between two cells in each time point and presented with means ± SEM. **P* < 0.05; ***P* < 0.001.

A mechanism linking *HOTAIR* and insulin signalling is not well understood, but *HOTAIR* was found to epigenetically regulate Phosphatase and Tensin homolog (*PTEN*) gene in laryngeal squamous cell carcinoma (Li, et al., 2013). As PTEN acts to inhibit

the PIP3/Akt signalling pathway, I went on to study the *PTEN* expression in the gluteal sh*HOTAIR* cell and shControl cells during a differentiation time course (Figure 4-6B). Intriguingly, the gluteal sh*HOTAIR* cell showed a higher *PTEN* expression than control cell in the late stage of differentiation. This result provides a potential explanation for the induction of insulin resistance in the sh*HOTAIR* cells.

4.3.3 Assessing the functional effects of *HOTAIR* constitutive overexpression in abdominal and gluteal preadipocytes

The constitutive *HOTAIR* overexpression in gluteal and abdominal preadipocytes was achieved by transducing with pEGFP-Lv105-*HOTAIR* lentivirus and cells were termed *HOTAIR* preadipocytes. The pEGFP-Lv105-empty lentivirus was used to generate the control cells and were termed Control preadipocytes. The method is described in section 4.2.2, 4.2.3 and 4.2.4. The *HOTAIR* overexpression is confirmed

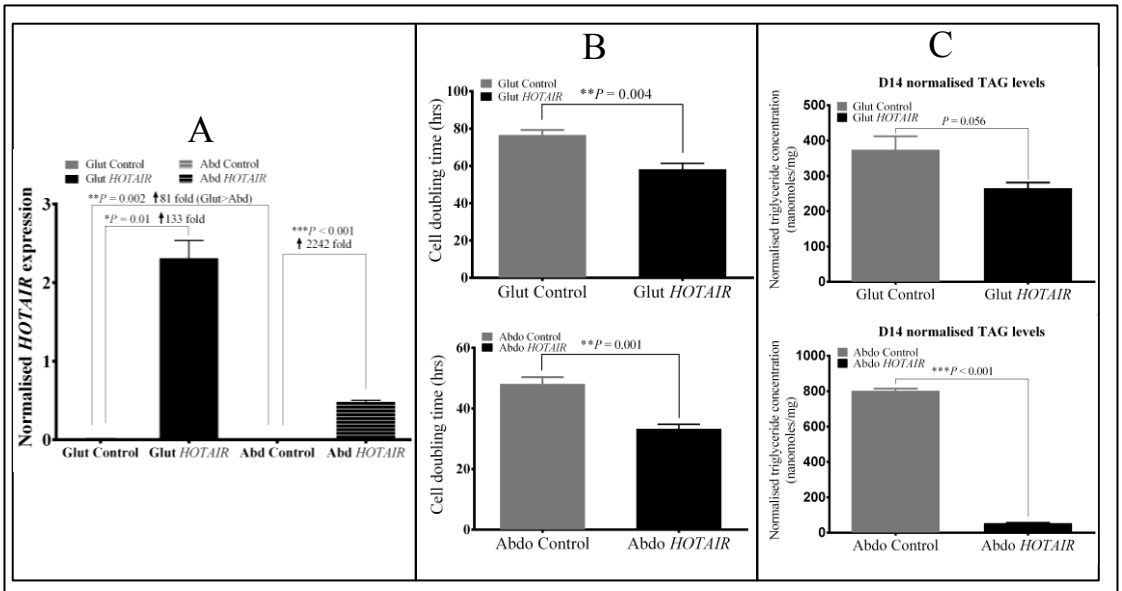


Figure 4-7: Cell proliferation rate was increased in both *HOTAIR* preadipocytes and adipogenesis was suppressed specifically in the abdominal *HOTAIR* cell

A: Real-time qPCR of *HOTAIR* expression was measured in both *HOTAIR* and Control preadipocytes of abdominal and gluteal depots under cell proliferation (n = 3). **B:** Cell doubling time of *HOTAIR* and Control preadipocytes from two depots was estimated during proliferation (n = 4). **C**: Intracellular triglyceride concentration was normalised to total protein levels for quantifying the *in vitro* adipogenesis in both cells from abdominal and gluteal depots (n = 3). Data were analysed with independent t-test and presented with means ± SEM. **P* < 0.05; ***P* < 0.01; ****P* < 0.001.

by measuring real-time qPCR of *HOTAIR* expression between *HOTAIR* and Control preadipocytes (Figure 4-7A). The functional impact of *HOTAIR* overexpression on the biological properties of preadipocytes was evaluated in a depot-specific manner (Figure 4-7B&C). The *HOTAIR* and Control preadipocytes were cultured in parallel to quantify cell doubling time as outline in section 2.3.3. Both cell types underwent adipogenic differentiation as described in section 2.3.2. Cellular triglyceride contents were quantified as mentioned in section 2.5.

The results show that both gluteal and abdominal *HOTAIR* preadipocytes had a shorter cell doubling time than Control cells (Figure 4-7B), which means they proliferated more rapidly. Adipogenic differentiation in the gluteal *HOTAIR* cells shows a non-significant trend towards lower triglyceride content compared with gluteal Control cells (Figure 4-7C). The abdominal *HOTAIR* preadipocytes had a strikingly lower triglyceride content compared with the abdominal Control cells. This result shows that overexpression of *HOTAIR* in preadipocytes has anti-adipogenic effect in abdominal whereas the gluteal cells are largely unaffected.

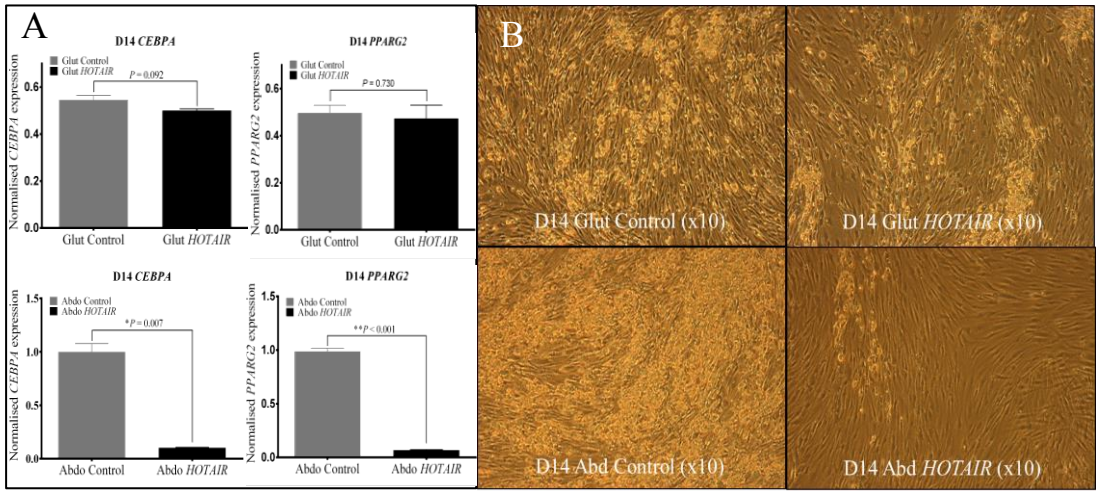


Figure 4-8: Overexpression of *HOTAIR* in the abdominal preadipocytes significantly suppresses the adipogenic differentiation

A: *CEBPA* and *PPARG2* levels were measured in both *HOTAIR* and Control preadipocytes of abdominal and gluteal depots on differentiation day 14 (n = 3). **B:** Photos of day 14 cells were taken with x 10 amplification under microscope. Data were analysed with independent t-test and presented with means ± SEM. **P* < 0.05; ***P* < 0.001.

Expression levels of major adipogenic genes: *CEBPA* and *PPARG2* were also measured by real-time qPCR in the day 14 *HOTAIR* and Control preadipocytes (Figure 4-8A). The abdominal *HOTAIR* cell showed significantly lower levels of *CEBPA* and *PPARG2*, which is compatible with the cell morphology and lower triglyceride content of the cells. The day 14 abdominal *HOTAIR* cells also maintained the spindle shape of preadipocytes rather than the circular shape of lipid-laden adipocytes otherwise seen in successfully differentiating cells (Figure 4-8B). There was no effect in the *HOTAIR* gluteal cells.

4.3.4 Exploring interactions between *HOTAIR* and two potential target genes (*CEBPD* and *PTEN*)

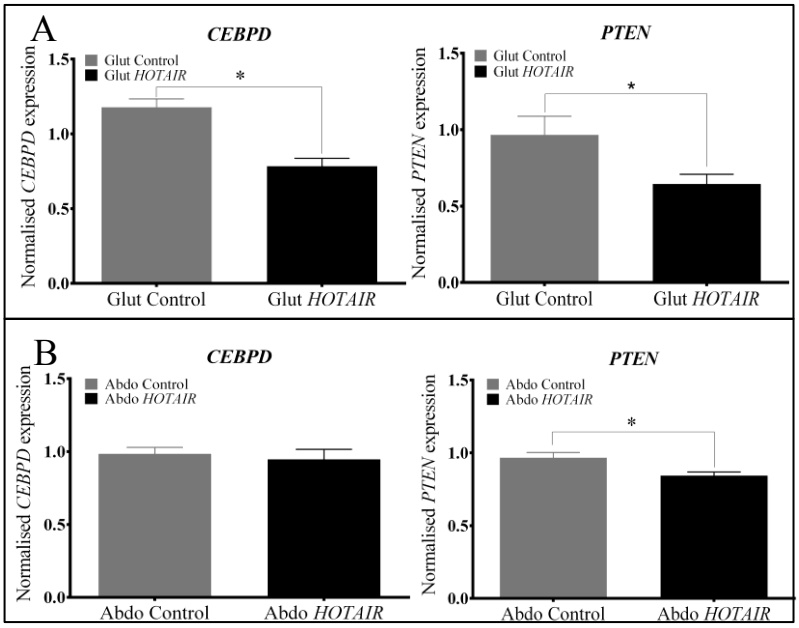


Figure 4-9: Overexpression of *HOTAIR* in human gluteal preadipocytes suppresses *PTEN* and *CEBPD* levels during cell proliferation

mRNA expression of *CEBPD* and *PTEN* was measured in gluteal and abdominal *HOTAIR* preadipocytes and compared to the levels in corresponding vector control cells under proliferation (n = 3). Data were assessed with independent t-test and presented with means ± SEM. **P* < 0.05.

Since the *HOTAIR* knockdown experiments identified *CEBPD* and *PTEN* as potential *HOTAIR* targets, I further evaluated if *CEBPD* and *PTEN* genes were inhibited when overexpressing *HOTAIR* in human preadipocytes. Therefore, I measured mRNA expression of *CEBPD* and *PTEN* in the *HOTAIR* overexpressed

abdominal and gluteal preadipocytes and compared the gene expression with the corresponding vector control cells under the condition of proliferation (Figure 4-9). The results revealed that both *CEBPD* and *PTEN* expression was suppressed after constitutively overexpressing *HOTAIR* in the gluteal preadipocytes and a decrease of *PTEN* transcription was also shown in the abdominal *HOTAIR* preadipocytes.

Furthermore, I investigated if *HOTAIR* mediates transcriptional repression of *CEBPD* and *PTEN* through an interaction with PRC2. To assess the status of repressive histone modifications in the promoter regions of *CEBPD* and *PTEN*, I performed anti-H3K27me3 and anti-SUZ12 ChIP experiments in gluteal sh*HOTAIR* and gluteal shControl cells (Figure 4-10).

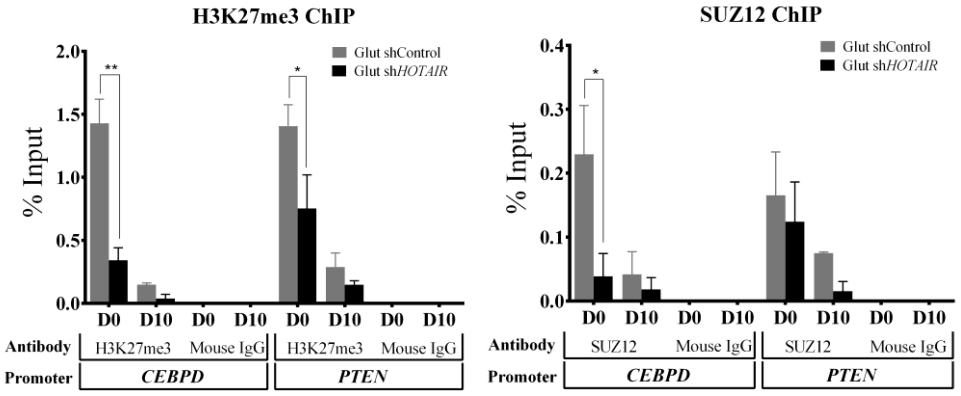


Figure 4-10: The presence of H3K27me3 or SUZ12 in the *CEBPD* and *PTEN* promoter regions were significantly reduced in gluteal sh*HOTAIR* cells

Anti-H3K27me3 and anti-SUZ12 ChIPs were performed in gluteal sh*HOTAIR* and shControl cells on differentiation day 0 and day 10 with independent technical triplicates (n = 3). Mouse IgG antibody was used as the negative control. Data were assessed with ANOVA to compare levels between the two experimental conditions and presented with means ± SEM. **P* < 0.05; ***P* < 0.001.

The results show that there is less presence of the suppressive histone mark (H3K27me3) within the promoter regions of *CEBPD* and *PTEN* in gluteal sh*HOTAIR* cells compared to gluteal shControl cells on differentiation day 0. Presence of the suppressive histone modifier (SUZ12 subunit of PRC2) within the promoter region of *CEBPD* was also lower in gluteal sh*HOTAIR* cells. This experiment indicates that

expression of the *CEBPD* and *PTEN* genes is epigenetically regulated by *HOTAIR* in human gluteal preadipocytes via PRC2 repressive histone modification.

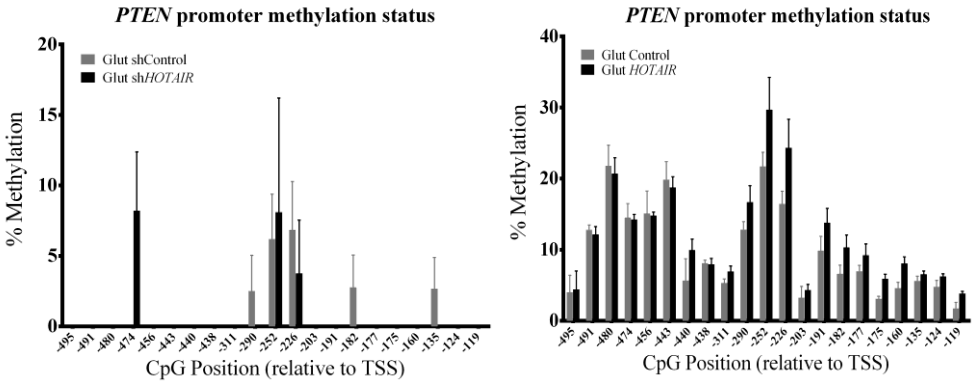


Figure 4-11: Methylation of the *PTEN* promoter is not regulated by *HOTAIR* in proliferating cells condition.

PTEN promoter methylation status was measured via bisulfite pyrosequencing to compare gluteal sh*HOTAIR* to shControl cells and gluteal *HOTAIR* to Control preadipocytes under cell proliferation (n = 3). Data were assessed with ANOVA Bonferroni pairwise comparison and presented with means of % methylation ± SEM in each CpG position relative to the transcription start site (TSS) **P* < 0.05.

Since *HOTAIR* has also been proposed to regulate *PTEN* expression by modulating the DNA methylation status in the promoter region (Li, et al., 2013), I performed bisulfite pyrosequencing to measure the DNA methylation status of the *PTEN* promoter region in the gluteal sh*HOTAIR* and gluteal *HOTAIR* preadipocytes, which was compared with the status in the corresponding control cells. However, neither *HOTAIR* knockdown nor *HOTAIR* overexpression in the gluteal preadipocytes significantly influence the methylation of the sequenced CpG sites in the *PTEN* promoter region (Figure 4-11).

During adipogenic differentiation, the gluteal sh*HOTAIR* cell shows increased *CEBPD* and *PTEN* levels after differentiation day 4. Therefore, I designed a 'rescue' experiment by transfecting the gluteal sh*HOTAIR* cell with the specific siRNA oligos to correct the dysregulated expression pattern of these two genes. I hypothesised that reducing the expression of these two factors in the later part of adipogenesis would

rescue the poor-differentiation phenotype of gluteal sh*HOTAIR* preadipocytes. The procedure of transfecting cells with siRNA oligos is described in section 4.2.9.

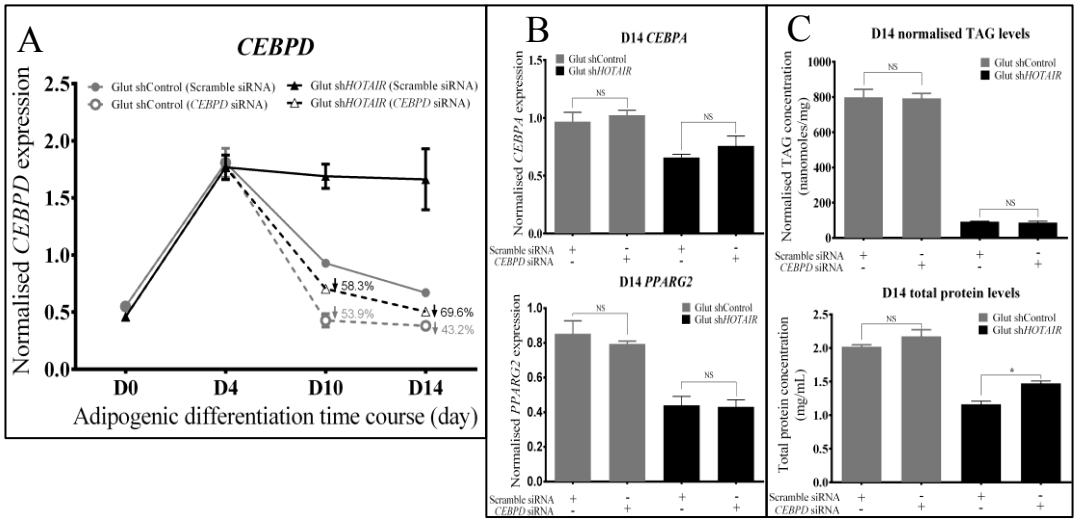


Figure 4-12: Transient suppression of *CEBPD* expression in gluteal sh*HOTAIR* and gluteal shControl cells during *in vitro* adipogenesis

A: The gluteal sh*HOTAIR* and shControl cells were treated with *CEBPD* siRNA and Scramble siRNA on differentiation day 4. **B&C:** *CEBPA*, *PPARG2*, intracellular TAG (triglyceride) and total protein levels were measured on differentiation day 14 (n = 3). Data were assessed with ANOVA and presented with means ± SEM. **P* < 0.05; ***P* < 0.001.

In the experiment of transient *CEBPD* knockdown, *CEBPD* siRNA and scramble negative siRNA were added in the cells on differentiation day4. After treating the gluteal sh*HOTAIR* cell with *CEBPD* siRNA (hollow triangles), the *CEBPD* expression was suppressed to similar levels as the gluteal shControl cell treated with scramble siRNA (solid circles) (Figure 4-12A). Then, *CEBPA*, *PPARG2*, normalised intracellular TAG and total protein levels were measured in the end (day 14) of adipogenesis. As shown in Figure 4-12B&C, transient suppression of *CEBPD* gene in the gluteal sh*HOTAIR* cell from differentiation day4 could not rescue the poor-differentiation phenotype (no increase of day 14 *CEBPA* expression, day 14 *PPARG2* expression and day 14 normalised TAG levels). However, at day 14 total protein concentration was increased in the gluteal sh*HOTAIR* cell that had been treated with *CEBPD* siRNA (Figure 4-12C). As *CEBPD* has been reported to induce growth arrest (Gery, et al., 2005; Ikezoe, et al., 2005), at least this result fits with a biological effect

of *CEBPD* knockdown.

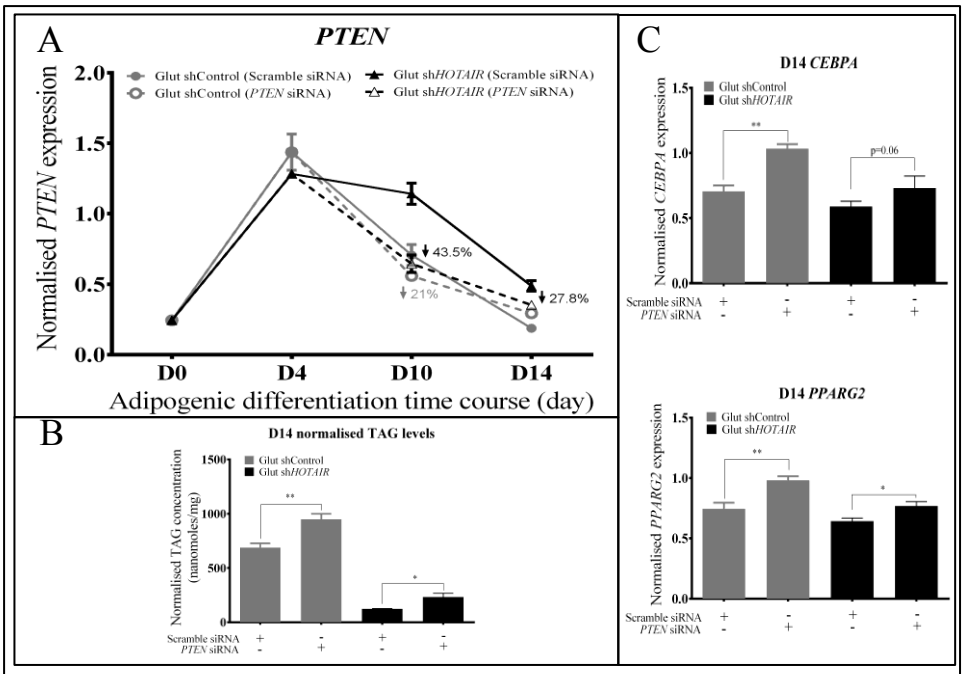


Figure 4-13: Transient suppression of *PTEN* expression in gluteal sh*HOTAIR* and gluteal shControl cells during *in vitro* adipogenesis

A: The gluteal sh*HOTAIR* and shControl cells were treated with *PTEN* siRNA and Scramble siRNA on differentiation day 4. **B&C:** Intracellular normalized TAG (triglyceride), *CEBPA* and *PPARG2* levels were measured on differentiation day 14 (n = 3). Data were assessed with ANOVA and presented with means ± SEM. **P* < 0.05; ***P* < 0.001.

In the experiment of transient *PTEN* knockdown, cells were treated with *PTEN* siRNA and scramble negative siRNA on differentiation day4. After treating the gluteal sh*HOTAIR* cell with *PTEN* siRNA (hollow triangles), the *PTEN* expression was reduced to similar levels as the gluteal shControl cell treated with scramble siRNA (solid circles) (Figure 4-13A). Then, *CEBPA*, *PPARG2* and normalised intracellular TAG were measured in the end (day 14) of adipogenesis. As shown in Figure 4-13B, transient suppression of *PTEN* gene in the gluteal sh*HOTAIR* cell from differentiation day4 could only mildly improve the *in vitro* adipogenesis (the mean of normalised TAG concentration is increased from 123 nmol/mg to 232 nmol/mg). However, it is worth noting that a similar effect was also observed in the gluteal shControl cells (the mean of normalised TAG concentration is increased from 688 nmol/mg to 948 nmol/mg). The major adipogeneic genes: *CEBPA* and *PPARG2* also present

compatible increases of expression on differentiation day 14 (Figure 4-13C). These results indicate that suppression of *PTEN* allows the expected effect of insulin signalling on adipogenesis, but it seems unlikely that raised *PTEN* is the single factor explaining the failing adipogenesis in sh*HOTAIR* gluteal cells.

4.3.5 Comparing the adipocyte sizes between females carrying rs76084431 TT and CC genotype

Genotype-based recall was conducted to recruit females carrying with rs76084431 TT genotype to compare the regional adipocyte size with CC genotype females as described in section 4.2.11. Paired abdominal and gluteal adipose tissues obtained via core needle biopsy were used to measure adipocyte size as outlined in section 2.2.1.

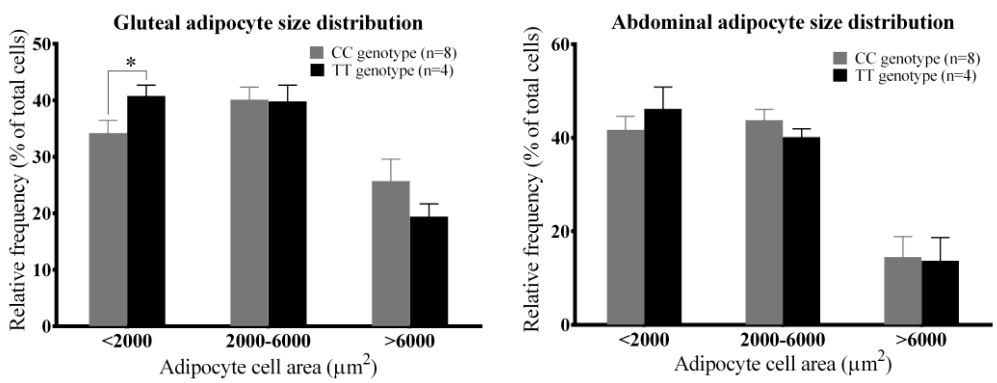


Figure 4-14: Comparison of gluteal and abdominal adipocyte size distribution between rs76084431 TT genotype and CC genotype females

Females carrying rs76084431 TT genotype have an increased proportion of small gluteal adipocytes. > 100 cells were measured for each biopsy. Data were assessed with ANOVA and presented with means ± SEM. **P* < 0.05.

Due to the limitation in numbers of accessible rare genotype carriers (only four TT genotype females and age, BMI matched four CC genotype females were recruited), anything but very large phenotypic differences had the potential of being detected. By using the histological database containing cell size information in our research group, I further obtained adipocyte size data from an additional four age and BMI matched CC genotype females. So, regional adipocyte sizes were compared between four TT genotype females (mean age 48.5 years; mean BMI: 28.27 kg/m^2) and eight CC genotype females (mean age 47.4 years; mean BMI: 27.82 kg/m^2) (Figure 4-14).

With the limitation of small sample numbers in this analysis, the adipocyte size distribution in the rs76084431 TT genotype females showed a trend towards smaller gluteal adipocytes, which will need to increase number of cells counted to be sure there is significant difference.

4.3.6 Recruiting subjects in whom tissue *HOTAIR* abundance has already been quantified to evaluate the *in vivo* functional roles of *HOTAIR* gene

A limited recruitment based on GSAT *HOTAIR* transcript abundance was performed as mentioned in section 4.2.11. Adipose tissue RNA extraction and gene expression analysis was performed as described in section 4.2.12. The 7 recruited males had a mean age increase of about 12 years (from 46.9 to 59.1 years) but a maintained mean BMI of around 30 kg/m^2 (from 30 to 30.4 kg/m^2). The 17 recruited females had a mean age increase from 44.2 years to 58.1 years and a slight increase in mean BMI (from 26.5 to 27.8 kg/m^2). The age difference might be more biologically significant for the women as it essentially meant comparing the same person pre vs postmenopausally. There was a strong positive correlation between GSAT *HOTAIR* in men, but this correlation was not seen in women (Figure 4-15).

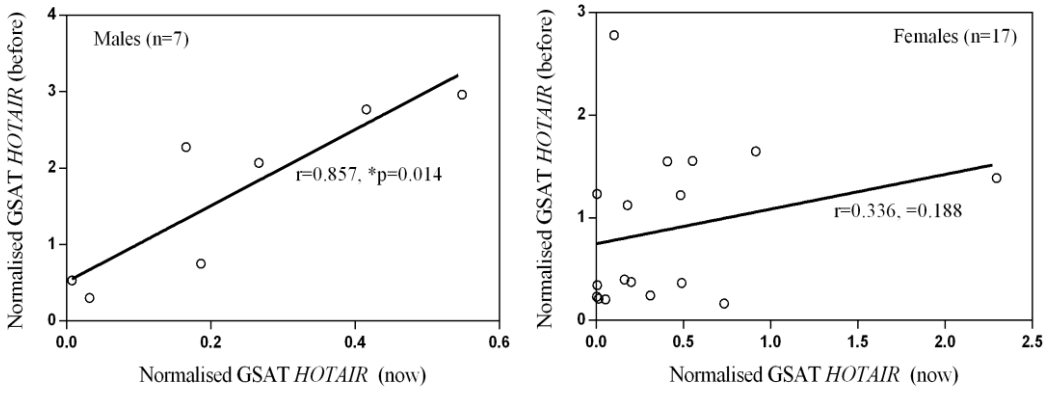


Figure 4-15: Current GSAT *HOTAIR* expression retains positive correlation with previous expression levels only in males, but not in females

Previous and current GSAT *HOTAIR* expression was plotted in the same individuals with gender-specific manner to show the correlation coefficient (*r*). Data were assessed with Spearman's correlation. *$P < 0.05$.

In relation to previous statements on the possible role of oestrogen regulating *HOTAIR* expression, I therefore consulted another small dataset made available to me

consisting of 21 pre vs 27 postmenopausal women (Hodson, et al., 2015) to see if menopause per se had an effect on *HOTAIR* expression. However, there was no difference in gluteal tissue *HOTAIR* expression in this dataset (Figure 4-16). Unfortunately, there was no mRNA left from either the old or the new set to further investigate this.

In this recruitment based on previous GSAT *HOTAIR* levels, the difference of DXA estimated regional body fat mass between subjects with high and low GSAT *HOTAIR* was also analysed in a sex-specific manner, but this analysis was limited by the small sample size and no statistically significant differences were observed (data not shown).

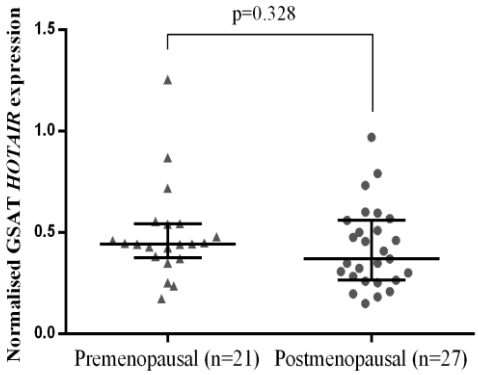


Figure 4-16: GSAT *HOTAIR* expression between premenopausal and postmenopausal women

GSAT *HOTAIR* levels were compared between 21 premenopausal and 27 postmenopausal females. Data were presented as medians [quartiles]. The presented *P* value is further adjusted for age and BMI by multivariable linear regression. **P* < 0.05.

4.3.7 Comparing regional fat distribution in women with differential GSAT *HOTAIR* levels.

As there was no significant difference of GSAT *HOTAIR* levels in females before and after menopause, I combined all the available resources to study a total 63 women having both GSAT *HOTAIR* expression and DXA data. These women were divided into high and low (median) GSAT *HOTAIR* expression levels to test the potential phenotypic effect on fat distribution by GSAT *HOTAIR* expression.

As shown in the Table 4-5, the *HOTAIR* expression is about double higher in the GSAT-high expressing *HOTAIR* group than the low GSAT *HOTAIR* group. However, comparing the DXA scan quantified regional fat masses between two groups, there is no any significant differences could be seen by differential GSAT *HOTAIR* levels.

Table 4-5: Body fat distribution among females with differential GSAT *HOTAIR*

Variables	Low GSAT *HOTAIR* (n=32)	High GSAT *HOTAIR* (n=31)	*P* value	Adjusting Age & BMI *P* value
GSAT *HOTAIR*	0.208 [0.154; 0.298]	0.435 [0.367; 1.205]	<0.001**	
Age (years)	55.0 [42.5; 59.0]	56.0 [43.0; 59.0]	0.601	
BMI (kg/m^2)	25.0 [22.8; 28.3]	25.0 [22.7; 26.9]	0.592	
Total fat (g)	24626 [20246; 28419]	23040 [20006; 29290]	0.837	0.602
Android fat (g)	1987 [1403; 2735]	1958 [1351; 2620]	0.578	0.790
Gynoid fat (g)	5132 [4468; 6240]	4880 [4245; 5901]	0.248	0.240
Leg fat (g)	8628 [7475; 11733]	8911 [7350; 11120]	0.984	0.691
Visceral fat (g	338 [159; 872]	404 [208; 753]	0.509	0.465
SubAnd fat (g)	1478 [1092; 1954]	1450 [1126; 1886]	0.913	0.843

Variables are assessed by nonparametric Mann-Whitney U test and presented as median [quartiles]; adjusting was performed by multivariable linear regression; BMI: body mass index; WHR: waist to hip ratio; SubAnd: subcutaneous android fat; *$P < 0.05$, ** $P < 0.001$

4.4 Discussion

The results generated in this chapter have provided solid support for *HOTAIR* affecting regional human preadipocyte function. With the exclusive expression pattern of *HOTAIR* it was perhaps not unsurprising that inhibition of *HOTAIR* expression in the gluteal preadipocytes was as harmful as the induction of aberrant expression of *HOTAIR* in the abdominal preadipocytes. In both these instances there was a striking suppression of the normal adipogenic differentiation. This was verified demonstrating the relative absence of cellular triglyceride accumulation and suppression of the major adipogenic genes *CEBPA* and *PPARG2*. Although the suppression of *HOTAIR* in gluteal preadipocytes generated some likely targets, such as *CEBPD* which is as an early adipogenic gene and *PTEN* being a suppressor of insulin signalling, but repression of these targets did not adequately alleviate the stalled adipogenesis. The role of *HOTAIR* in regulating site-specific adipogenesis is clearly more complex than being mediated by single factors.

4.4.1 Difficulties quantifying the knockdown effect of *HOTAIR* in gluteal sh*HOTAIR* preadipocytes during adipogenesis

Based on the molecular mechanisms of shRNA mediated mRNA degradation (Carthew and Sontheimer, 2009), there are several possibilities that could explain the difficulties of quantifying the *HOTAIR* abundance whilst knocking it down. First, degraded *HOTAIR* fragments could have been falsely detected by the TaqMan assay. I made several additional efforts to design alternative and independent ways of quantifying the transcripts but this did not resolve the issue. Further analysis could be done by RNA-sequencing, but with all other attempts so robustly negative I find it unlikely to resolve the issue. However, it is still possible that the binding of siRNA to *HOTAIR* could change its secondary structure without inducing degradation. As the secondary structure of *HOTAIR* gene is very crucial to determine its molecular function (Somarowthu, et al., 2015), such an effect could impair its function.

Second, RNA-induced silencing complex (RISC) couldn't cleave the *HOTAIR*

sequence because the binding of siRNA changed its secondary structure. A third option was also ruled out: shRNA might only degrade *HOTAIR* mRNA in the cytoplasmic compartment, but this was not the case as the *HOTAIR* transcripts showed similar levels after measuring them in the respective nuclear and cytoplasmic compartments.

I was therefore left with the option to demonstrate that *HOTAIR* had been attenuated by studying downstream effects. This seemed to show a pattern consistent with truly reduced *HOTAIR* activity. Both *HOXD8* and *HOXD10* were de-repressed through the entire course of differentiation (Figure 4-3A). *HOTAIR* has been known can interact with Polycomb Repressive Complex 2 (PRC2) to trimethylate histone H3 on lysine 27 (H3K27me3) for silencing the transcription on its target genes (Tsai, et al., 2010). As SUZ12 is one of the subunits of PRC2, I performed anti-H3K27me3 and anti-SUZ12 ChIP experiments to evaluate the *HOTAIR* gene mediated epigenetic regulation on the promoter regions of *HOXD8* and *HOXD10* genes. The ChIP data (Figure 4-3B) showed that the presence of H3K27me3 and SUZ12 to the promoter regions of *HOXD8* and *HOXD10* genes were significantly reduced in the gluteal sh*HOTAIR* cell, which indicated that the normal molecular function of *HOTAIR* gene was suppressed.

The *HOTAIR* knockdown experiments were performed using pooled *HOTAIR* shRNA lentiviruses which contain four different shRNAs. Therefore, the knockdown efficiency of individual shRNAs and their potential the off-target effects couldn't be evaluated. Also, I didn't clone the individual viral transduced cells to demonstrate the phenotypic effect could be seen in different cell clones. Future experiments using individual *HOTAIR* shRNA lentiviruses and evaluating if the phenotypic effect could be represented in different shRNAs will be required to exclude the potential off-target effects.

4.4.2 Depot-specific functional roles of *HOTAIR* gene in human preadipocytes

The molecular mechanisms of how *HOTAIR* modulates the cell proliferation is still unclear, but studies in numerous cancer cell lines have found that depletion of *HOTAIR*

gene could increase total apoptotic cell numbers and induce cell cycle arrest through changing the cell cycle distribution between G2/M phase and S phase (Qiu, et al., 2015; Ren, et al., 2016; Yu, et al., 2017). In my studies, modulation of the *HOTAIR* gene expression in human preadipocytes showed directional effects on cell proliferation similar to those observed in cancer cells. Suppression of *HOTAIR* in gluteal preadipocytes resulted in reduced cell proliferation whereas constitutive overexpression of *HOTAIR* increased cell proliferation in both abdominal and gluteal preadipocytes.

Exploration of the role of lncRNAs in adipogenesis has been sparse. Only three studies have been published using human cells: two (Kalwa, et al., 2016; Xiao, et al., 2015) in human mesenchymal stem cells (MSCs) and one (Divoux, et al., 2014) in primary preadipocytes isolated from abdominal subcutaneous adipose tissue. In human mesenchymal stem cells, ADINR (adipogenic differentiation induced noncoding RNA) was found to enhance *CEBPA* transcription *in cis* promoting adipogenesis (Xiao, et al., 2015) and *HOTAIR* was considered as a negative regulator for differentiation of MSCs toward both adipogenic and osteogenic lineages (Kalwa, et al., 2016). However, in the human abdominal preadipocytes, ectopic overexpression of *HOTAIR* has been proposed to promote *in vitro* adipogenesis (Divoux, et al., 2014), which is clearly opposite to my findings. With the striking difference in cell phenotypic effects in response to *HOTAIR* overexpression between abdominal and gluteal pre-adipocytes, these contrary results might be due to differences in cell origin but differences in protocol/medium composition for *in vitro* adipogenesis and the method for quantifying the adipogenesis are also possible. I used cellular triglyceride concentrations normalised to total protein levels to assess the status of adipogenesis, which is likely to give greater precision than observing the number of differentiated cells under the microscope. Clearly, in the normal condition, the abdominal preadipocytes do not express *HOTAIR* gene and can still differentiate well. So, *HOTAIR* is dispensable for abdominal preadipocytes, which makes its pro-adipogenic role suggested by (Divoux,

et al., 2014) questionable.

4.4.3 Limited evidence of phenotypic effect shown in *in vivo* studies of *HOTAIR* gene

The *HOTAIR* genotype-based measurement of adipocyte size distribution showed that the homozygous carriers of the *HOTAIR* transcript-lowering variant (TT of rs76084431) had a higher proportion of small adipocytes in the gluteal fat depot, which seems directionally consistent with the poor differentiation phenotype seen in the gluteal sh*HOTAIR* cells. The absence of a difference of abdominal adipocyte size distribution between CC and TT genotypic carriers serves as a negative control experiment as *HOTAIR* is not expressed in that tissue.

By dividing females GSAT *HOTAIR* levels to two groups, the high GSAT *HOTAIR* females possess around two-fold higher levels than the low GSAT *HOTAIR* women. However, the difference in the GSAT *HOTAIR* expression did not seem to contribute to any measurable difference in body fat distribution. This result suggests that the *in vivo* phenotypic effect mediated by the abundance of *HOTAIR* transcription is small, therefore the difference of regional fat mass could not be revealed in this small-scale comparison.

4.4.4 Concluding statements

Overall, the *in vitro* experiments of *HOTAIR* knockdown and overexpression highlights its depot-specific roles in both gluteal and abdominal preadipocytes and reveals that its presence in gluteal fat depot and its absence in abdominal fat were both crucial for maintaining the normal adipogenesis in the regional adipose tissue. These results emphasize the intrinsic difference between gluteal and abdominal subcutaneous fat depots. Two *HOTAIR* potential target genes (*CEBPD* and *PTEN*) were shown to be negatively regulated by *HOTAIR*/PRC2 mediated histone modifications. When exploring *HOTAIR in vivo* function via genotype or the expression level-based approaches, I only found limited evidence for a strong effect. It seems there is no

extreme fat distribution phenotype related to high vs low *HOTAIR* expression and this probably speaks to the fact that the phenotypic effect is small. Indeed, more than 220,000 people were required to identify a fat distribution effect for the *HOXC13* locus within which *HOTAIR* has an eQTL with a rather substantial effect (~30% altered expression per allele).

Chapter 5
Identifying novel *HOTAIR* targets using an unbiased approach of RNA-sequencing

5.1 Introduction

With the evolution of developmental processes in complex organisms, versatile phenotypes have developed with specialised characteristics, which help organisms to accommodate or even utilise the environment. It has been found that complex epigenetic regulation significantly contributes to the phenotypic variability (Folguera-Blasco, et al., 2018; Julian, 2017), but detailed mechanisms are still largely unclear. Over the past decade, using high-throughput genomic platforms, it has been unveiled that noncoding portions of the genome are pervasively transcribed into tens of thousands of non-coding RNAs (ncRNAs) that could play significant regulatory roles in the developmental processes of complex organisms (Guttman, et al., 2010; Mattick, 2004). LncRNAs (defined as more than 200 nucleotides in size) were further separated from other classes of small ncRNAs, such as miRNA, siRNA and piRNA by the diverse array of mechanisms through which they exert epigenetic regulation on DNA packaging, and RNA and protein expression.

Based on the similarities in molecular mechanisms, the diverse functions of lncRNAs can be grouped into four categories: Signals, Decoys, Guides, and Scaffolds (Wang and Chang, 2011). These four categories are not mutually exclusive for an individual lncRNA. Instead, lncRNAs can actually provide their functional roles through the combined use of these mechanisms. The *HOTAIR* gene, as one of the most well studied lncRNA, is a good example for this.

First, *HOTAIR* serves as a molecular signal with anatomic-specific expression as it is expressed in cells located in distal and posterior positional identities (Rinn, et al., 2007). When comparing abdominal and gluteal subcutaneous adipose tissues, *HOTAIR* presents gluteal depot-specific expression (Pinnick, et al., 2014) and our results in Chapter 3 further illustrated that its transcription was elevated during adipogenesis and enhanced under stimulation by glucocorticoids.

Second, *HOTAIR* also acts as a molecular decoy. *HOTAIR* can function as a

competing endogenous RNA to sequester miRNAs (Cai, et al., 2017; Wei, et al., 2017; Xu and Zhang, 2017; Yao, et al., 2017). miRNAs can interact with target gene transcripts with incomplete complementary sequence, leading to instability at the levels of messenger RNAs and a reduction in the abundance of target proteins (Ambros, 2004). When *HOTAIR* functions through this mechanism, it can indirectly increase the expression levels of miRNA target genes. It is likely that a growing numbers of miRNAs will be identified as being sequestered by *HOTAIR* since the *HOTAIR* gene has more than 2000 nucleotides.

Third, *HOTAIR* behaves as a guide. *HOTAIR* can exert its transcriptional effects *in trans* via targeting of PRC2 in hundreds of genes that have been demonstrated to be crucial for breast tumorigenesis (Gupta, et al., 2010). Therefore, *HOTAIR* can alter and regulate epigenetic states through this occupancy/localization/enzymatic activity of the chromatin-modifying complex. Combining its expression with a temporal and spatial pattern in human gluteal preadipocytes, this epigenetic modulation will be dynamic and tissue-specific, which will be explored in this Chapter.

Fourth, *HOTAIR* is a scaffold to connect the methyltransferase activity fragment: enhancer of zeste homolog 2 (EZH2) of the PRC2 complex in the 5' end and to recruit the lysine-specific histone demethylase 1 (LSD1) in the 3' end. This *HOTAIR*/PRC2/LSD1 complex can collaboratively suppress target gene expression via histone modifications at the same time (Tsai, et al., 2010). Also, the secondary structure of *HOTAIR* is crucial for maintaining its normal scaffold function (Somarowthu, et al., 2015).

In line with these intricate molecular mechanisms operated by *HOTAIR*, investigation of potential *HOTAIR* target genes will need to be considered in a temporally and spatially specific manner. Therefore, I performed RNA-sequencing to compare the global transcriptome profiling between gluteal sh*HOTAIR* and gluteal shControl cells at three consecutive time points (day 0, day 4 and day 14) during

adipogenic differentiation. Using co-expression analysis during adipogenesis, the genes that were significantly and persistently enhanced in the gluteal sh*HOTAIR* cells will be considered as candidates that are suppressed by *HOTAIR*/PRC2/LSD1 complex. Furthermore, I conducted chromatin immunoprecipitation to examine the states of histone modifiers (H3K27me3 and SUZ12) in the promoter regions of the candidate genes. Then, DNA methylation status of the promoter regions was also evaluated by bisulfite pyrosequencing. Moreover, I used siRNAs to transiently repress the expression of *HOTAIR* candidate targets in gluteal sh*HOTAIR*/shControl preadipocytes and evaluate the impact on adipogenesis. The combination of all these experiments could reveal *HOTAIR*/PRC2 complex-mediated molecular mechanisms specifically in the human gluteal adipose tissue.

Aims

- RNA-sequencing for comparing global transcriptome between gluteal sh*HOTAIR* and gluteal shControl cells during adipogenesis
- Performing ChIP and bisulfite pyrosequencing to validate another *HOTAIR* putative target: *PCDH10* gene
- Transiently knocking down the *HOTAIR* candidate target gene (*PCDH10*) in gluteal sh*HOTAIR*/shControl preadipocytes to evaluate its influence on *in vitro* adipogenesis

5.2 Methods

5.2.1 Gene expression analysis

RNA extraction of adipose tissues or cells was performed as described in section 2.4.1. cDNA synthesis was performed as described in section 2.4.2 and real-time qPCR was done as outlined in section 2.4.3. The TaqMan Assays-on-Demand used in this Chapter include: *PPIA* (Hs99999904_m1); *CEBPA* (Hs00269972_s1); *PPARG2* (Hs01115510_m1); *PCDH10* (Hs00252974_s1); *PAX3* (Hs00240950_m1); *HOXD3* (Hs00232506_m1); *HOXD9* (Hs00610725_g1).

5.2.2 RNA-sequencing for global transcriptome comparison

Triplicates of total RNA samples from gluteal sh*HOTAIR* and gluteal shControl preadipoctyes under differentiation day 0, day 4, day 14 were extracted as described in section 2.4.1. RNA samples were DNase treated using DNA-free™ DNA removal kit (Life Technologies) and RNA quality was analysed on a Bio-analyser 2100 (Agilent). All RNA samples prepared for RNA-sequencing had RIN scores > 9. PolyA RNA-sequencing was performed on the HiSeq4000 sequencing system (Illumina) at the Wellcome Trust Centre for Human Genetics, University of Oxford.

The annotation and normalisation of the raw RNA-seq data was kindly performed by Dr. Agata Wesolowska-Andersen at the Wellcome Trust Centre for Human Genetics. False discovery rate (FDR) of 5% was defined as the threshold for reporting of the significantly differentially expressed genes (DEGs) between gluteal sh*HOTAIR* and shControl cells. The gene expression pattern during adipogenesis (day 0, day 4, day 14) was further compared between cells using Weighted Gene Co-expression Network Analysis (WGCNA) (Langfelder and Horvath, 2008). In total 19,555 genes expressed at a minimum threshold of 1 Transcript Per Million (TPM) in at least 3 samples were analysed via WGCNA. 28 co-expressed modules were detected and 897 genes were not assigned to any module. The functional enrichments of grouped genes were analysed using the web-based gene set enrichment software DAVID (Database for

Annotation, Visualization, and Integrated Discovery) (http://david.abcc.ncifcrf.gov) (Huang da, et al., 2009). The results of gene functional enrichments were presented with the term name and FDR adjusted *P* value.

5.2.3 Chromatin immunoprecipitation in the *PCDH10* promoter region

Anti-H3K27me3 ChIP and anti-SUZ12 ChIP were performed as described in section 4.2.7. The purified DNA was used for running real-time quantitative PCR with custom designed TaqMan assays (as described on 4.2.6). When retrieving *PCDH10* promoter sequence and designing the ChIP-*PCDH10* TaqMan assay, I selected the primers/probe as listed in Table 5-1, which is near to the *PCDH10* ChIP primers designed in the Gupta, et al. paper (Gupta, et al., 2010).

Table 5-1: Custom TaqMan assay designed for the promoter regions of *PCDH10* gene

Custom TaqMan	Primers/Probe	Sequence
ChIP-*PCDH10*	Forward primer	GCGAGCTCTCCAAAGCAAAA
	Reverse primer	TCTCCTAGCGGCGAAATCAG
	Probe	TCTCTGGCCTGCCC

5.2.4 Bisulfite pyrosequencing for measuring DNA methylation status

Bisulfite pyrosequencing was performed as outlined in section 3.2.10. Four

Table 5-2: Bisulfite PCR primers and their optimal conditions

Amplicon	Bisulfite Primers	Temp (°C)
*PCDH10*_A	Forward: GGGGTATTTATAGTTGGTTAAG	53
	Reverse: CAATCCTAAAATCAACCC	
*PCDH10*_B	Forward: AGTATGGTGGGTAAAGGGAT	53
	Reverse: CTTACCAAATAAATTAACTCACTC	
*PCDH10*_C	Forward: ATTTTGGGAGGAAAGAAGTA	53
	Reverse: CAATCTAAAAATAAAAAAATCTAAC	
*PCDH10*_D	Forward: GGTTGGGGATTGGGAAT	53
	Reverse: CTAAACTAACAATTTCTAAACTCC	

amplicons in the *PCDH10* promoter regions were pyrosequenced and details of bisulfite primers/sequencing primers are listed in Table 5.2 and Table 5.3. The amplicon of *PCDH10*_A was selected according to the region sequenced in the Lee et al paper (Lee, et al., 2016). In addition, three other amplicons were selected to cover most of the CpG sites in the *PCDH10* promoter region.

Table 5-3: Sequencing primers for bisulfite-pyrosequencing

Amplicon	Sequencing primer 1	Sequencing primer 2	Sequencing primer 3
*PCDH10*_A	TATTTATAGTTGGTTAAG	GAGGATGGATGTAAGTAT	GGGTTTTGTTTATTATTT
*PCDH10*_B	TATGGTGGGTAAAGGGAT	GTAGGGATATTAGAGG	TTTTTAGTTATTGATGAA
*PCDH10*_C	TTTGGGAGGAAAGAAGT	TATTTTTATTTTTTATTT	-
*PCDH10*_D	GGTTGGGGATTGGGAAT	TTATATTTATATTTATTT	GTTAGTTTGGTTAATTAT

5.2.5 Western blotting of PCDH10 protein

Cells were cultured in growth medium to reach high confluence (as described in section 2.3.1) and harvested during cell proliferation for western blotting as described in section 2.6. Antibodies to PCDH10 (ATLAS, HPA011220) and actin (1-19) (Santa Cruz Biotechnology, sc-1616) were used to probe PCDH10 and beta-Actin proteins.

5.2.6 Transfecting with siRNA oligos

In this Chapter, human siRNA oligo duplexes were used to transiently suppress *PCDH10* expression (Trilencer-27, Origene, SR324736). Each kit contains three unique 27 mer siRNA duplexes (2 nmol each), one scrambled negative control siRNA duplex (2 nmol) and RNase-free siRNA duplex resuspension buffer. The resuspension buffer (100 µl) was added to each duplex to make a stock siRNA solution (20 µM) which was frozen at -80°C for long-term storage. Before commencing the main knockdown experiment two concentrations of each siRNA duplex (10n M and 20n M) were tested for knockdown efficiency. The procedure of cell transfection is as described in section 4.2.9.

For testing the knockdown efficiency of each siRNA duplex, the cells were harvested at 48-72 hrs after transfection and *PCDH10* knockdown efficiency was assessed by performing real-time qPCR. The unique siRNA duplex (SR324736A) with the best knockdown efficiency (> 70%) was chosen and the concentration (20 nM) was selected as it showed a better knockdown efficiency than the 10 nM concentration. The duration of the *PCDH10* knockdown was tested and found to be maintained for more than 5 days in the human preadipocytes.

To knockdown *PCDH10* during proliferation, 9 x 10^4 cells were seeded into each well in a 6-well plate and maintained in growth medium overnight (as described in section 2.3.1). Then equal concentrations of the *PCDH10* siRNA duplex or scramble siRNA were added to the cells. For this experiment, the first time of adding the siRNA duplex is 7 days before starting the differentiation. Cells were cultured to reach full confluence, and then subsequently differentiated as described in section 2.3.2. The unique siRNA duplex or scramble siRNA was added again on differentiation day 4.

5.2.7 Statistical analysis

SPSS (IBM Corp. Released 2013. IBM SPSS Statistics for Windows, Version 22.0. Armonk, NY: IBM Corp.) was used to perform statistical analyses and a P value < 0.05 was considered statistically significant. Data are presented ad means ± SEM.

5.3 Results

5.3.1 RNA-sequencing for comparing global transcriptome between gluteal sh*HOTAIR* and gluteal shControl cells during adipogenesis

Taking an unbiased approach to compare the global transcriptome expression during adipogenic differentiation after suppressing *HOTAIR* in the gluteal preadipocytes, RNA-sequencing was performed in both gluteal sh*HOTAIR* and shControl cells at three consecutive time points (day 0, day 4 and day 14) during adipogenesis. The 5% false discovery rate (FDR) was used as the cut-off for analysing the significantly differentially expressed genes between gluteal sh*HOTAIR* and gluteal shControl cells.

A

Day	DEGs at 5% FDR	DEGs up in Glut sh*HOTAIR*	DEGs down in Glut sh*HOTAIR*
Day 0	619	393	226
Day 4	443	242	201
Day 14	7586	3811	3775

B

Top 5 genes up in D0 Glut sh*HOTAIR*

Gene	log2FC	Padj
AJAP1	2.61	6.90e-34
NEFL	1.95	3.53e-23
PCDH10	1.78	4.56e-22
GABBR2	1.65	8.40e-21
DHRS2	1.45	3.05e-20

Top 5 genes down in D0 Glut sh*HOTAIR*

Gene	log2FC	Padj
KRT14	-3.43	1.52e-86
WNT2	-1.69	5.28e-30
RAPGEF6	-1.56	2.70e-24
MEST	-1.33	7.49e-22
PDE10A	-2.07	4.96e-21

C

Day	DEGs at 5% FDR	DEGs up in Glut sh*HOTAIR*	DEGs down in Glut sh*HOTAIR*
Day 0	619	393	226

Term	Padj
GO CC: plasma membrane part	5.93e-10
GO MF: calcium ion binding	3.34e-04
GO BP: response to wounding	4.01e-03
GO BP: cell adhesion	7.58e-03
GO BP: cell motion	1.37e-02
GO CC: extracellular region part	1.05e-02

Term	Padj
GO CC: extracellular matrix	3.05e-07

Figure 5-1: Comparing the transcriptome profiling between gluteal sh*HOTAIR* and shControl cells during adipogenesis

RNA-sequencing was performed in differentiation day 0, day 4 and day 14 gluteal sh*HOTAIR* and shControl cells to compare the global transcriptome (n = 3). **A:** The day 0, day 4 and day 14 differential expressed genes (DEGs) were assessed at 5% false discovery rate (FDR). **B:** The top 5 genes up- and down-regulated in sh*HOTAIR* cells at day 0 are shown with log2FC (fold change) and Padj (adjusted *P* value). **C:** Functional enrichment analysis was performed separately on the up- and down-regulated DEGs at day0 and shown with GO (Gene Ontology) terms. CC: Cellular Component, BP: Biological Process, MF: Molecular Function.

On differentiation day0, 63% (393/619) of total DEGs were significantly higher and ~37% (226/619) of all DEGs were significantly lower expressed in the gluteal sh*HOTAIR* preadipocytes. On differentiation day 4, 242 genes were higher expressed

and 201 genes were lower expressed in the gluteal sh*HOTAIR* cells compared to the gluteal shControl cells. At the end of *in vitro* adipogenesis (day 14), there were more than seven thousand genes differentially expressed between the gluteal sh*HOTAIR* and shControl cells with about half up and half down (Figure 5-1A). As the adipogenesis was significantly impaired in the gluteal sh*HOTAIR* cells, the 7,586 DEGs shown on day 14 are likely to heavily rely on the stark difference in differentiated adipocytes and undifferentiated preadipocytes and are unlikely to be direct targets of *HOTAIR*. Therefore, I focussed on the gene expression changes that were already detectable at differentiation day0, before differentiation. The top 5 genes up- and down-regulated in the gluteal sh*HOTAIR* cells are listed in Figure 5-1B. Then, the functional enrichments of the 393 genes up- and 226 genes down-regulated in gluteal sh*HOTAIR* preadipocytes were further analysed (Figure 5-1C). Interestingly, the up- and down-regulated genes are both functionally enriched for extracellular matrix and the up genes are also enriched for plasma membrane part, calcium ion binding, response to wounding, cell adhesion and cell motion.

To further address the difference in gene expression patterns during adipogenic differentiation after *HOTAIR* knockdown, WGCNA was applied to a total of 19,555 genes expressed at a minimum of 1 Transcript Per Million (TPM) in at least 3 samples. Overall, 28 co-expressed modules were detected (Figure 5-2A). Since the main function of *HOTAIR*/PRC2/LSD1 complex is to silence gene transcription, I hypothesized that *HOTAIR* target genes would be upregulated (de-repressed) in the gluteal sh*HOTAIR* preadipocytes. Therefore, genes that show persistently higher expression throughout differentiation in the gluteal sh*HOTAIR* compared to the gluteal shControl cells are specifically highlighted (Figure 5-2B). In the 28 detected co-expressed modules, the lightgreen module contains 135 genes, which represents consistently higher levels of gene expression in the gluteal sh*HOTAIR* cells. Importantly, three *HOXD* genes (*HOXD3, HOXD8* and *HOXD9*) belong to this module (Figure 5-2C), which demonstrates that this approach can capture genes that are known

to be silenced via *HOTAIR*/PRC2/LSD1 mediated mechanisms (Tsai, et al., 2010). In the group of homeobox genes, asides from the *HOXD* genes, *PAX3* also showed persistently higher levels in the gluteal sh*HOTAIR* cells.

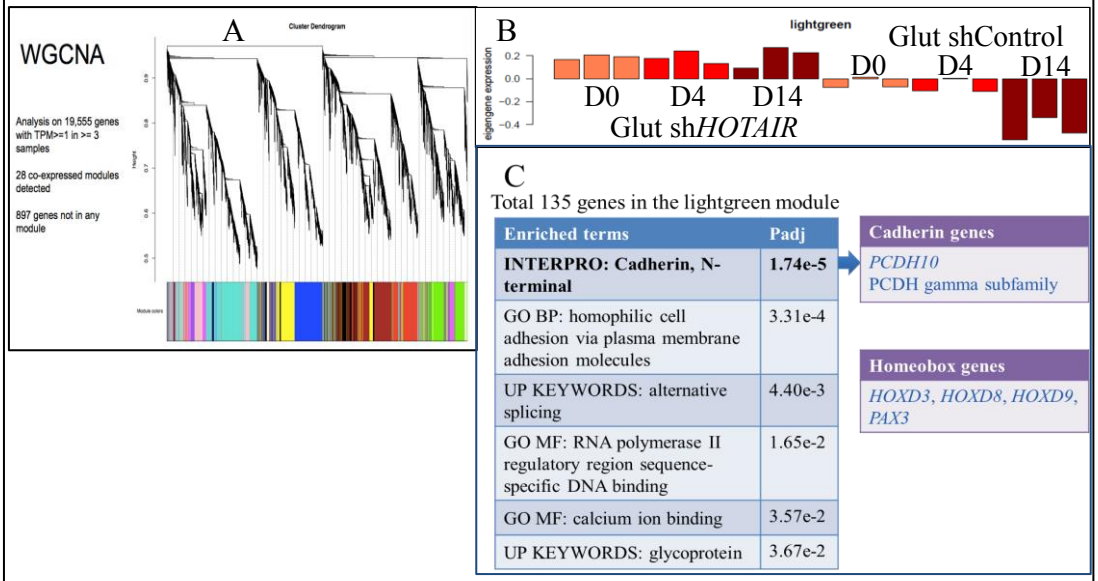


Figure 5-2: Weighted Gene Co-expression Network Analysis (WGCNA) highlights 135 genes maintain significant increased expression in the gluteal sh*HOTAIR* cells

A: 19,555 genes expressed at ≥ 1 TPM in ≥ 3 samples were evaluated for co-expression patterns during adipogenesis and a total of 28 co-expressed modules were detected. **B:** The lightgreen module included 135 genes that maintain elevated expression through adipogenesis in the gluteal sh*HOTAIR* cell. **C:** Functional enrichment analysis was performed in the DAVID bioinformatics database and shown with GO (Gene Ontology) terms. INTERPRO: Protein Interactions, BP: Biological Process, MF: Molecular Function. Padj: *P* value adjusted for false discovery rate (FDR).

Moreover, the functional enrichments of these 135 genes were analysed in the DAVID bioinformatics database (Huang da, et al., 2009) and the INTERPRO term "cadherin, N-terminal" was flagged as showing significant enrichment. The genes belonging to the "cadherin, N- terminal" term include protocadherin 10 (*PCDH10*) and several protocadherin (PCDH) gamma subfamily members (Figure 5-2C). The *PCDH10* gene is listed as the third highest gene that is up-regulated in the day 0 gluteal sh*HOTAIR* preadipocytes (Figure 5-1B).

To validate the RNA-seq data, I measured the expression levels of *HOXD3*, *HOXD9*, *PAX3* and *PCDH10* with real-time qPCR (Figure 5-3). The results demonstrate all four

genes maintain higher levels in the gluteal sh*HOTAIR* preadipocytes during adipogenic differentiation, which is consistent with the findings shown in the co-expression pattern analysis of RNA-seq data.

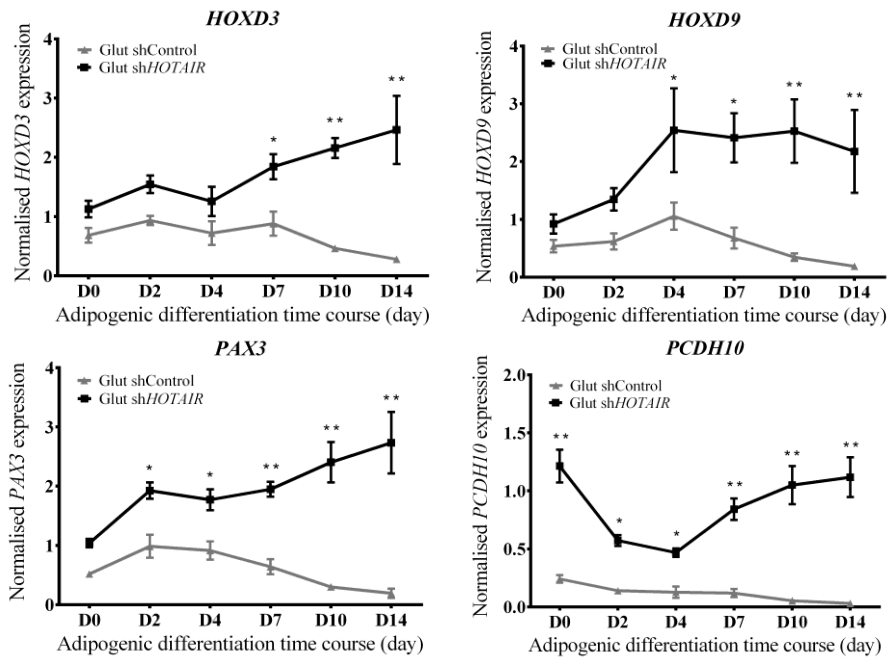


Figure 5-3: Real-time qPCR confirms *HOXD3*, *HOXD9*, *PAX3* and *PCDH10* genes maintain increased expression in the gluteal sh*HOTAIR* cells through adipogenesis

HOXD3, HOXD9, PAX3 and *PCDH10* genes were further measured with real-time qPCR in the gluteal sh*HOTAIR* and gluteal shControl cells during adipogenesis (n = 3). Data were assessed with ANOVA to compare levels between two cells and presented with means ± SEM. **P* < 0.05; ***P* < 0.001.

5.3.2 *PCDH10* gene was epigenetically regulated by *HOTAIR* through both histone modifications and DNA methylation

In order to evaluate if *PCDH10* was suppressed by *HOTAIR* in the human preadipocytes, I also measured mRNA expression of *PCDH10* in the *HOTAIR* overexpressed cells include gluteal *HOTAIR* and abdominal *HOTAIR* preadipocytes under proliferation status (Figure 5-4A). Comparing between gluteal Control and abdominal Control cells, gluteal Control cells present significantly lower *PCDH10* expression than abdominal Control preadipocytes, which is inversely correlated with *HOTAIR* expression, as *HOTAIR* is exclusively expressed in the gluteal depot. Comparing between abdominal *HOTAIR* and abdominal Control cells, the *PCDH10* levels were significantly lower in the abdominal *HOTAIR* preadipocytes, which is

consistent with *PCDH10* being negatively regulated by *HOTAIR*. However, when comparing *PCDH10* expression between gluteal *HOTAIR* and gluteal Control cells, *PCDH10* transcription was significantly enhanced in the gluteal *HOTAIR* cells, this is opposite to the proposed suppressive effect driven by *HOTAIR*. Therefore, I performed Western blotting to quantify the relative abundance of PCDH10 protein to beta-actin protein (Figure 5-4B). This experiment demonstrated that the PCDH10 protein was significantly decreased after overexpressing *HOTAIR* in the gluteal preadipocytes, and the increased *PCDH10* transcription in the gluteal *HOTAIR* cells could represent a compensation mechanism.

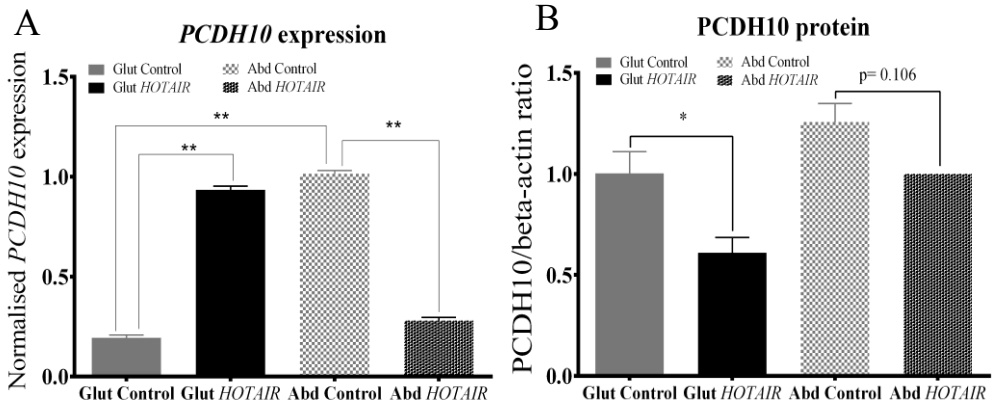


Figure 5-4: Overexpression of *HOTAIR* in the human gluteal preadipocytes reduces the abundance of PCDH10 protein

Real-time qPCR of *PCDH10* expression (**A**) and western blotting of relative PCDH10/beta-actin ratio (**B**) were measured in gluteal *HOTAIR* and abdominal *HOTAIR* preadipocytes under proliferation and compared to the levels in the control vector cells (n = 3). Data were assessed with independent t-test and presented with means ± SEM. **P* < 0.05; ***P* < 0.001.

To further explore the interaction between *PCDH10* and *HOTAIR*, anti-H3K27me3 and anti-SUZ12 ChIP experiments were performed to evaluate *HOTAIR*/PRC2 mediated histone modifications specifically on the *PCDH10* promoter region. On differentiation day0, suppression of *HOTAIR* function in the gluteal preadipocytes significantly decreased the presence of H3K27me3 and SUZ12 on the promoter region of *PCDH10* gene (Figure 5-5). Overall, these results provide supporting evidence that *PCDH10* was epigenetically suppressed by *HOTAIR* in the human gluteal preadipocytes.

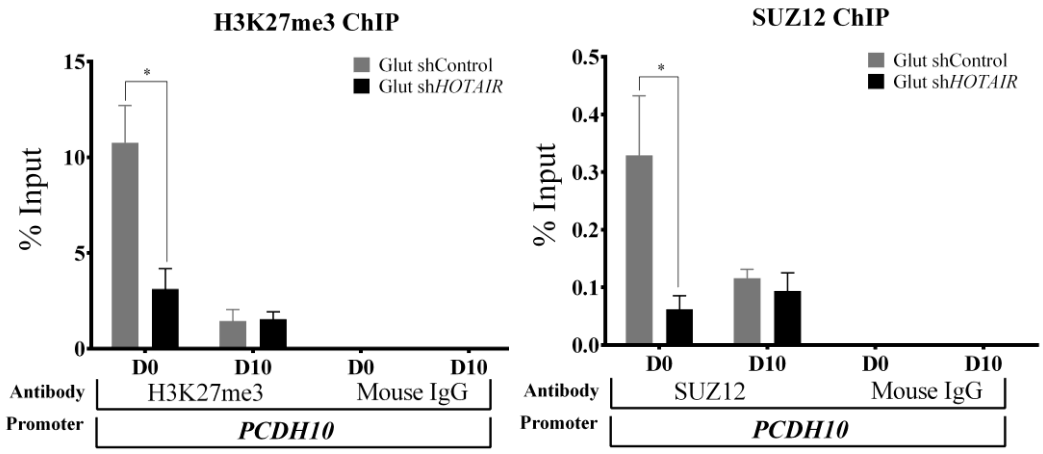


Figure 5-5: The presence of H3K27me3 and SUZ12 on the promoter region of *PCDH10* were significantly reduced in the D0 gluteal sh*HOTAIR* preadipocytes

Anti-H3K27me3 and anti-SUZ12 ChIPs were performed in gluteal sh*HOTAIR* and shControl cells on differentiation day 0 and day 10 with independent technical triplicates (n = 3). Mouse IgG antibody was used as the negative control. Data were assessed with ANOVA to compare levels between two cells and presented with means ± SEM. **P* < 0.05; ***P* < 0.001.

The *HOTAIR* driven histone modifications might link to modulation in DNA methylation. Therefore, I ran bisulfite pyrosequencing to measure DNA methylation status in the *PCDH10* promoter region. This experiment was performed on the gluteal sh*HOTAIR* and gluteal shControl preadipocytes under cell proliferation and in total four amplicons were designed to contain most CpG sites in the *PCDH10* promoter region (Figure 5-6 browser view). The data show very consistent findings that, in multiple CpG sites, the percentage of DNA methylation was significantly reduced in the gluteal sh*HOTAIR* preadipocytes (Figure 5-6 A-D), which is compatible with its significant elevated *PCDH10* expression.

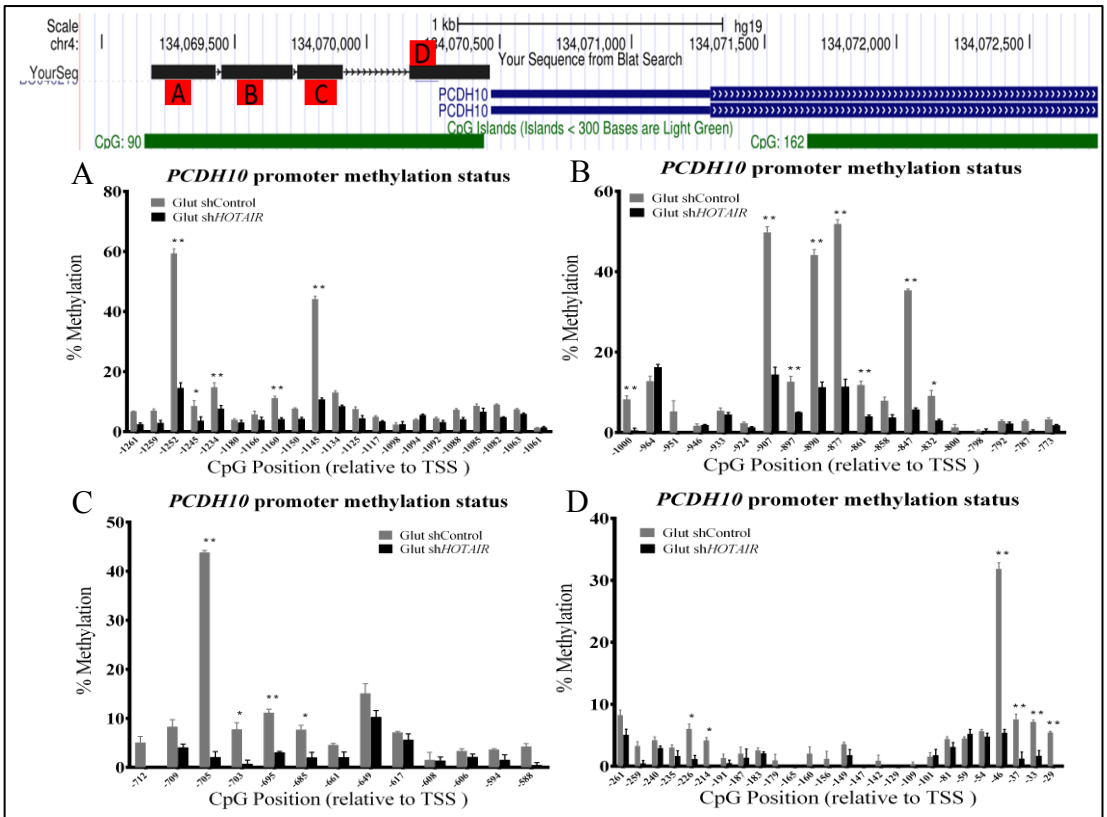


Figure 5-6: Evaluation of the DNA methylation status in the *PCDH10* promoter region between gluteal sh*HOTAIR* and shControl preadipocytes under proliferation

Pyrosequencing was performed in gluteal sh*HOTAIR* and gluteal shControl preadipocytes under proliferation (n = 3). Four paired bisulfite primers (**A-D**) were designed to cover most CpG sites in the *PCDH10* promoter region (**browser view**). Data were assessed with ANOVA Bonferroni pairwise comparison and presented with means of % methylation ± SEM in each CpG position relative to the transcription start site (TSS) **P* < 0.05; ***P* < 0.001.

To extend these findings to *in vivo* condition in gluteal subcutaneous adipose tissue, I measured mRNA expression of *PCDH10* and *HOTAIR* in gluteal subcutaneous adipose tissue obtained from 24 subjects (7 males and 17 females), who were recruited based on previous GSAT *HOTAIR* expression as described in section 4.2.11. Strikingly, GSAT *PCDH10* levels are significantly negatively correlated with GSAT *HOTAIR* expression (Figure 5-7). This result suggests *PCDH10* expression is also negatively controlled by *HOTAIR* gene in the *in situ* gluteal subcutaneous adipose tissue.

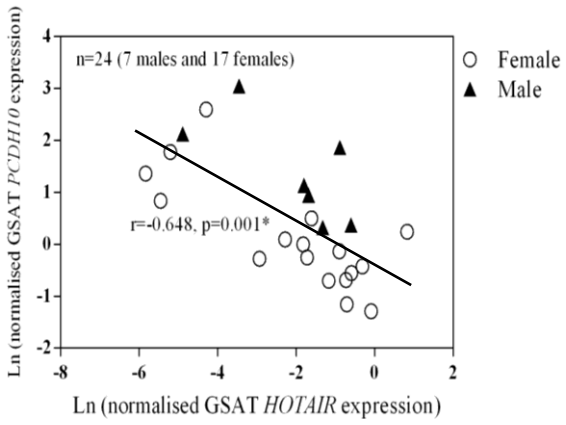


Figure 5-7: GSAT *PCDH10* expression is negatively correlated with GSAT *HOTAIR* expression

HOTAIR and *PCDH10* expression were measured with real-time qPCR in the gluteal subcutaneous adipose tissues obtained from 24 Oxford Biobank subjects (17 females and 7 males). Data were log-transformed and assessed with Pearson correlation. **P* < 0.05 GSAT: gluteal subcutaneous adipose tissue

5.3.3 Transiently knocking down the *HOTAIR* candidate target gene *PCDH10* in gluteal sh*HOTAIR*/shControl preadipocytes to evaluate its influence on *in vitro* adipogenesis

During adipogenic differentiation, *PCDH10* expression was persistently elevated throughout adipogenesis in the gluteal sh*HOTAIR* cell (Figure 5-3). Combining the results shown in this Chapter, it is believed that *PCDH10* is epigenetically regulated

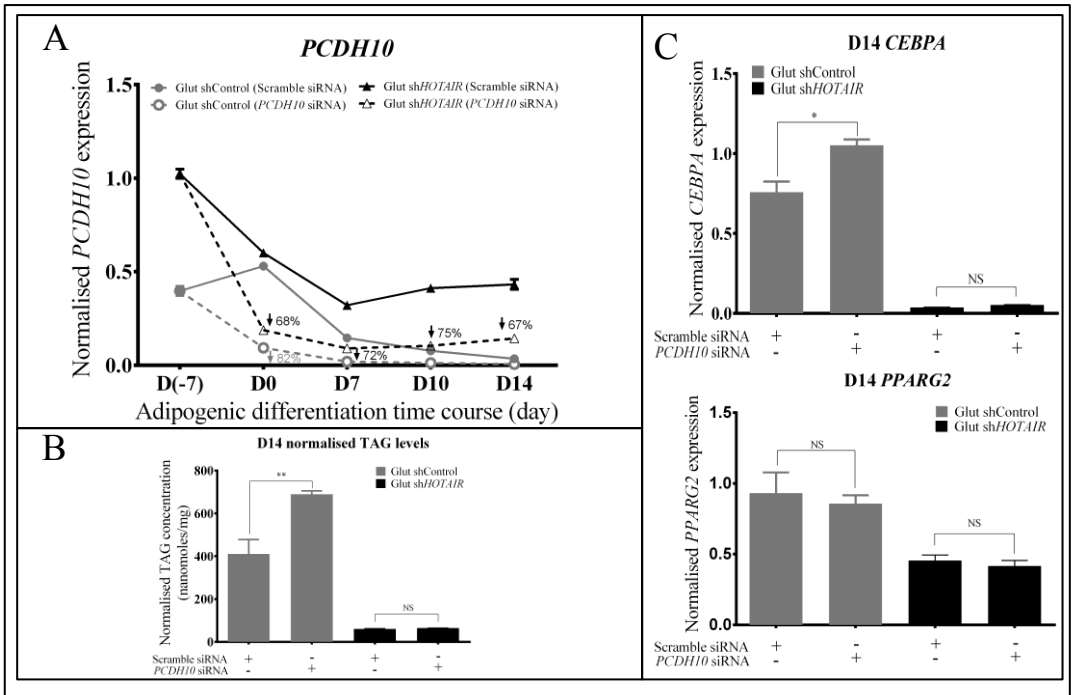


Figure 5-8: Transient suppression of *PCDH10* expression in gluteal sh*HOTAIR* and gluteal shControl cells through adipogenesis

A: The gluteal sh*HOTAIR* and shControl cells were treated with *PCDH10* siRNA and Scramble siRNA on 7 days before and 4 days after differentiation. **B&C:** Intracellular normalized TAG (triglyceride), *CEBPA* and *PPARG2* levels were measured on differentiation day 14 (n = 3). Data were assessed with ANOVA and presented with means ± SEM. **P* < 0.05; ***P* < 0.001.

by *HOTAIR* in human gluteal preadipocytes. The dysregulation of *PCDH10* might in part contribute to the poor differentiated phenotype of the gluteal sh*HOTAIR* preadipocytes. Therefore, I transfected the gluteal sh*HOTAIR* cells with *PCDH10* siRNA oligos to correct the dysregulated expression pattern during *in vitro* adipogenesis and evaluated if this intervention can rescue the impaired adipogenesis of gluteal sh*HOTAIR* preadipocytes. The procedure of transfecting cells with siRNA oligos is described in section 5.2.6.

In the experiment of transient *PCDH10* knockdown, cells were treated with *PCDH10* siRNA and scramble negative siRNA 7 days before differentiation and on differentiation day 4, with the aim to suppress *PCDH10* throughout differentiation (Figure 5-8A). After treating the gluteal sh*HOTAIR* cells with *PCDH10* siRNA (hollow triangles), *PCDH10* expression was reduced by 68% to low levels at differentiation day 0. In the later phase of differentiation, *PCDH10* expression was maintained at a similar level to that seen in the gluteal shControl cells treated with scramble siRNA (solid circles). Then, *CEBPA*, *PPARG2* and normalised intracellular TAG were measured at the end (day 14) of adipogenesis. As shown in Figure 5-8B, suppression of *PCDH10* in the gluteal sh*HOTAIR* cells throughout differentiation did not rescue the poor differentiated phenotype. Whereas, it is interesting that treating the gluteal shControl cells with *PCDH10* siRNA significantly enhances the adipogenic differentiation (the mean normalised TAG concentration is increased from 410 nmol/mg to 689 nmol/mg). There is no difference in day 14 *PPARG2* levels, but day 14 *CEBPA* gene shows higher expression in the gluteal shControl cells that were treated with *PCDH10* siRNA (Figure 5-8C).

5.4 Discussion

Overall, results shown in this Chapter have provided supporting evidence that *PCDH10* is epigenetically regulated by *HOTAIR*/PRC2 mediated histone modifications and promoter DNA methylation in human gluteal preadipocytes. RNA-sequencing co-expression analysis captured several well-recognized *HOXD* genes as *HOTAIR* targets, which provides further validation that *HOTAIR* function was successfully inhibited in the gluteal sh*HOTAIR* preadipocytes as addressed in section 4.3.1. Using functional enrichment analysis of grouped genes, the cellular component of extracellular matrix was highlighted to be largely influenced after repressing *HOTAIR* function in gluteal preadipocytes. Protocadherin (PCDH) genes, plasma membrane adhesion molecules and calcium ion binding were also revealed as potential cellular components and biological processes that might be involved in the poor differentiated phenotype of the gluteal sh*HOTAIR* cells. According to the data presented in this Chapter, I focussed specifically on *PCDH10* and explored its role in determining adipogenesis in the gluteal fat depot, this will be further discussed here.

5.4.1 Impact of transiently knocking down individual *HOTAIR* target genes

In this Chapter, I also used siRNA oligos to suppress *PCDH10* expression throughout adipogenesis to evaluate its potential functional role in the gluteal preadipocytes. Combining siRNA knockdown experiments in Chapter 4, all results show that suppressing *CEBPD*, *PTEN* or *PCDH10* genes individually cannot successfully rescue the poor differentiated phenotype of the gluteal sh*HOTAIR* cells (suppression of *PTEN* only mildly improves adipogenesis). It appears that the intricate molecular mechanisms operated by *HOTAIR* cannot be easily modulated in the gluteal sh*HOTAIR* preadipocytes merely by correcting an individual target gene. Whereas, it is still interesting to find that suppression of *PTEN* or *PCDH10* gene in the control gluteal cells can enhance adipogenesis, which suggests *PTEN* and *PCDH10* might be anti-adipogenic. As *PTEN* is a negative regulator of PI3K/Akt signalling (Hlobilkova, et al., 2003), the observation of its anti-adipogenic effect might not be surprising.

However, on the other hand, the potential anti-adipogenic effect of *PCDH10* is a novel finding which has not previously been reported. The molecular mechanisms underpinning *PCDH10* regulation of adipogenesis remain to be elucidated.

5.4.2 Functional roles of *PCDH10* gene

Our results indicate *PCDH10* expression was epigenetically suppressed by *HOTAIR* in the gluteal preadipocytes by changes in histone mark/modifier (H3K27me3/SUZ12) and DNA methylation in the promoter region. This finding is supported by previous reports that *HOTAIR* overexpression leads to increased occupancy of *PCDH10* by SUZ12 in breast cancer cells (Gupta, et al., 2010) and methylation of *PCDH10* was induced by *HOTAIR* with a SUZ12-dependent manner in the gastrointestinal stromal tumour cells (Lee, et al., 2016). More strikingly, *PCDH10* expression is strongly negatively correlated with *HOTAIR* expression in gluteal subcutaneous adipose tissue. This negative correlation suggests *PCDH10* might have a functional impact on the gluteal fat depot and also indicates that low abundance of *HOTAIR* is sufficient for suppressing *PCDH10* expression *in situ*. As mentioned before, *PCDH10* might be an anti-adipogenic factor for the gluteal fat depot. To discuss the potential molecular mechanisms of *PCDH10* in the adipose tissue, it is necessary to review current knowledge and understanding about *PCDH10*.

PCDH10 is a member of the PCDH subfamily. The protocadherins (PCDHs) are the largest subgroup within the cadherin superfamily. Cadherin is a calcium-dependent adhesion protein and the cell-cell adhesion is mediated by the extracellular calcium-binding domains, whereas the intracellular cytoplasmic tail associates with intracellular signalling proteins (Redies, et al., 2012). PCDH10 has 6 extracellular repeats, a transmembrane domain and a unique cytoplasmic tail, which may activate distinct intracellular signalling (Kim, et al., 2011). Although other PCDH family members are mainly expressed in the nervous system, PCDH10 has been shown to present widespread expression in almost all normal tissue (Wolverton and Lalande, 2001; Ying, et al., 2006). Current understandings about its potential functional roles

are predominantly from studies in the neuropsychiatric and cancer fields.

In the neuropsychiatric field, *PCDH10* has been associated with autism by genome-wide association studies (Morrow, et al., 2008) where it has been implicated in the morphogenesis and functional differentiation of grey matter in the central nervous system (Redies, et al., 2012). PCDH10 protein is also expressed in functional neural circuits such as the olfactory/visual system and nigrostriatal/olivocerebellar projection (Aoki, et al., 2003; Hirano, et al., 1999) and *PCDH10*-deficient mice have selective anomalies in several major axon tracts (Uemura, et al., 2007). These studies indicate *PCDH10* has important functions in the development of the neural system and neural cell migration, especially the striatal axon elongation.

In the cancer field, *PCDH10* is considered as a tumour suppressor gene and has been found to be epigenetically silenced in various cancers including gastrointestinal stromal tumours, nasopharyngeal, esophageal and colorectal carcinomas (Lee, et al., 2016; Ying, et al., 2006; Zhong, et al., 2017). The functional roles of *PCDH10* in cancer include induction of cell apoptosis and suppression of cell growth/migration/metastasis (Zhong, et al., 2017).

Regarding molecular mechanisms associated with PCDH10, PCDH10 has been found to remodel the motility and adhesion machinery in human astrocytoma cells by recruiting Nck-associated protein 1 (Nap1)-WAVE1 complex, which subsequently can promote actin assembly (Nakao, et al., 2008). Also, PCDH10 is considered as a negative regulator for the canonical Wnt/beta-catenin pathway and the WAVE complex mediated by its cytoplasmic domain might be involved in Wnt/PCP signalling for changing cytoskeletal dynamics (Mah and Weiner, 2017; Xu, et al., 2015). Moreover, PCDH10 was shown to inhibit the PI3K/Akt signalling pathway in hepatocellular carcinoma cells (Ye, et al., 2017).

Given that the PI3K/Akt signalling pathway (Nelson, et al., 2014), WNT signalling

pathway (Prestwich and Macdougald, 2007) and actin depolymerization (Chen, et al., 2018) are also involved in the processes of adipogenesis, the functional roles and molecular mechanisms of *PCDH10* in regional adipose tissue should be noticed and worth further investigating.

5.4.3 Extracellular matrix and adipogenesis

Comparing the global transcriptome profiling between gluteal sh*HOTAIR* and shControl preadipocytes on differentiation day 0, the differentially expressed genes are enriched for the extracellular matrix (ECM), which suggests the cellular component of ECM was significantly influenced after knocking down *HOTAIR* and it might contribute to the impaired adipogenesis in the gluteal sh*HOTAIR* cell. This finding is supported by a study that compared ECM related genes and ECM major molecules between subcutaneous adipose tissue and visceral adipose tissue from rats (Mori, et al., 2014). The authors found these two fat depots present site-specific and timing-specific extracellular matrix expression during *in vivo* tissue development and *in vitro* adipocyte differentiation. Also, several studies have described that the inherent stiffness of the ECM has a critical impact on cell morphology, proliferation and cell fate determination (Engler, et al., 2006; Shih, et al., 2011; Ye, et al., 2015). More specifically, culturing adipose-derived stem cells in substrates with varying degrees of stiffness has shown softer matrices that mimic the natural stiffness of adipose tissue can promote *in vitro* adipogenic differentiation (Zhang, et al., 2018). Therefore, all these reports emphasize the importance of ECM for maintaining the bioactivity of regional preadipocytes and further investigation will be warranted to elucidate the detailed molecular mechanisms.

5.4.4 Concluding statements

In summary, there are three main results generated in this Chapter. First, RNA-sequencing provides validation that normal *HOTAIR* function was inhibited in the gluteal sh*HOTAIR* preadipocytes with corresponding elevation of several *HOXD* genes.

Second, *PCDH10* was shown to be negatively regulated by *HOTAIR*/PRC2 mediated histone modifications and promoter DNA methylation. Third, protocadherin genes and extracellular matrix genes are the predominant downstream targets of *HOTAIR* which may contribute to maintaining the distinct biological properties of gluteal preadipocytes.

Chapter 6
General discussion

6.1 From GWAS identification of the fat distribution *HOXC13* locus to functional evaluation of *HOTAIR* in human gluteal fat

Body fat distribution is strongly associated with metabolic disorders with high genetic heritability (Malis, et al., 2005). Therefore, GWAS have been performed and in total 49 fat distribution loci have been found to be associated with WHR adjusted for BMI. By using the enriched genes analysis of these fat distribution loci, subcutaneous adipose tissues have been proposed as the main organ accountable for the fat distribution phenotype (Shungin, et al., 2015). However, the direct connections between the GWAS identified loci and functional signalling pathways or molecular mechanisms in the regional adipose tissues are still elusive. Meanwhile, microarray transcriptome comparison between GSAT and ASAT has disclosed *HOTAIR* as the most differentially expressed gene and only detectable in the gluteal fat depot (Pinnick, et al., 2014). The *HOTAIR* gene is located under the GWAS peak of the *HOXC13* fat distribution locus (Shungin, et al., 2015). This unusual coincidence raises the hypothesis that the *HOTAIR* gene might be functionally important for the gluteal fat depot and might subsequently modulate human body fat distribution.

To address this question, I studied the regulation of *HOTAIR* expression in a number of different ways and used a *HOTAIR* eQTL (rs76084431) to assess the effect on regional fat distribution. This eQTL appeared to be directionally consistent with one (rs1443512) of the established loci in the GWAS WHRadjBMI loci. Paired (abdominal and gluteal) primary and immortalised human preadipocytes were also used as cellular models to evaluate functional consequences (proliferation rate, adipogenic differentiation, gene expression, protein quantification, histone modifications and DNA methylation) under various *in vitro* interventions (hormones/insulin administration, *HOTAIR* stable knockdown, *HOTAIR* constitutive overexpression and siRNA oligos transfection). OBB recall studies based on genotypes and previous GSAT *HOTAIR* expression were also conducted to assess *in vivo HOTAIR* functional effects. In these recruited subjects, DXA scan was performed and paired adipose tissues were collected for gene expression, regional adipocyte sizes and genomic DNA

methylation. This project aimed to use human sourced materials to investigate the *HOTAIR* functional characteristics in a fat-depot specific manner, which is unique and has not been performed before.

6.2 Summary of main findings

This study confirms the exclusive expression of *HOTAIR* in GSAT whereas it is undetectable in ASAT. The GSAT *HOTAIR* expression shows wide variation between individuals with overall lower expression in females. *HOTAIR* transcription in the gluteal preadipocytes was enhanced during *in vitro* adipogenesis by administration of dexamethasone. The *HOTAIR* rs76084431 minor allele was associated with decreased abundance of GSAT *HOTAIR* mRNA and increased DXA defined android to gynoid fat ratio. This locus is located within a DNA region possessing distinct histone marks compared to surroundings, which corresponds to a transcriptional enhancer.

In vitro functional experiments showed that suppression of *HOTAIR* impaired adipogenesis and decreased proliferation rate in gluteal preadipocytes. In contrast, *HOTAIR* constitutive overexpression specifically suppressed adipogenesis in abdominal preadipocytes and increased the proliferation rate in both abdominal and gluteal cells. In the late phase of adipogenesis, de-repression of *CEBPD* and *PTEN* transcription with impaired insulin sensitivity were found in the gluteal sh*HOTAIR* preadipocytes, which might in part contribute to the poor differentiated phenotype.

In the *in vivo* functional evaluation, females carrying the *HOTAIR* transcript-lowering genotype (TT of rs76084431) have an increased proportion of small gluteal adipocytes, which is consistent with the *in vitro* finding that adipogenesis was impaired in the gluteal sh*HOTAIR* preadipocytes. However, comparing 32 versus 31 females with differential GSAT *HOTAIR* expression, there was no significant difference in the DXA estimated regional fat mass. This result might reflect *HOTAIR*-mediated phenotypic effect is mild *in vivo* and a large cohort study is required to reach enough statistical power. Indeed, in our initial assessment of the association between *HOTAIR*

haplotype-tagging SNPs and DXA defined fat masses in 4,627 OBB subjects, females carrying the minor allele of rs76084431 have been identified to have only around 100g increase of android fat per allele, which contributes to increased android to gynoid fat ratio. Since the rs76084431 is not in LD with the lead SNP (rs1443512) for WHRadjBMI reported from the Genetic Investigation of ANthropometric Traits (GIANT) consortium, but represents a directionally consistent eQTL, it is reasonable to observe that the phenotypic effects are similar as for rs1443512. However, very large cohorts would be required to confirm this; the rs76084431 is not represented in the data of the GIANT consortium.

To further investigate the *HOTAIR*/PRC2 mediated epigenetic regulation in the gluteal preadipocytes, H3K27me3/SUZ12 ChIP experiments and bisulfite genomic pyrosequencing were performed in the gluteal sh*HOTAIR*/shControl cells. These experiments provided some support that three *HOTAIR* candidate targets: *CEBPD*, *PTEN* and *PCDH10* were epigenetically regulated by *HOTAIR* via histone modifications and *PCDH10* expression was further controlled by *HOTAIR* via promoter methylation. Comparing RNA-seq analysis between gluteal sh*HOTAIR* and gluteal shControl cells before the start of adipogenesis suggests that extracellular matrix and protocadherin genes might be implicated in the *HOTAIR* mediated downstream signalling pathways maintaining normal biological function in the gluteal preadipocytes.

In summary (Figure 6-1), we determined that *HOTAIR* is undetectable in ASAT and presents a wide range of expression in GSAT. *In vitro HOTAIR* knockdown and overexpression experiments demonstrated depot-differential *HOTAIR* transcription is not just a developmental relic, but is functionally important in regulation of regional white adipose tissue biology. Combining the *in vitro* experiments with the *in vivo* genotype-phenotype analysis, our work provides evidence that the *HOTAIR* gene is required for maintaining adequate biological function of the gluteal fat depot as a metabolic sink and that loss of *HOTAIR* decreases its capacity for fatty acid storage

with the consequence of increased abdominal subcutaneous fat.

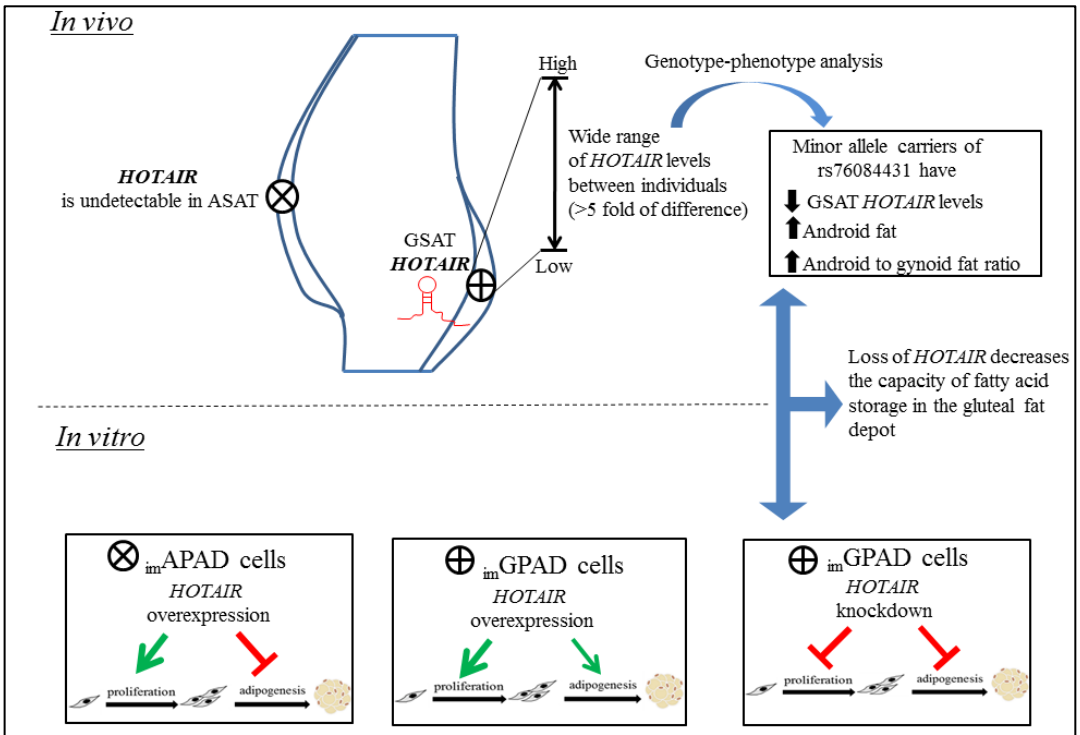


Figure 6-1: Summary of *HOTAIR* functional effects in regional adipose tissue

Schematic illustration of *HOTAIR in vivo* and *in vitro* experiments. *HOTAIR* gene is only expressed in the GSAT with wide range of levels between individuals. *In vitro HOTAIR* overexpression increases cell proliferation rate in both abdominal and gluteal preadipocytes, but specifically suppresses abdominal adipogenesis. *In vitro HOTAIR* knockdown and *in vivo* genotype-phenotype analysis provide evidence that loss of *HOTAIR* decreases the capacity of fatty acid storage in the gluteal fat via decreasing cell proliferation and adipogenesis with the consequence of increase of android to gynoid fat ratio. ⊕ indicates adipose tissue or preadipocyte from gluteal fat depot; ⊗ indicates adipose tissue or preadipocyte from abdominal subcutaneous fat depot. Red line means suppression; Green arrow means stimulation. Thick and thin green arrow for presentation the degree of stimulation.

6.3 Strengths and limitations

There are several strengths in his study. First, we use human sourced cells/tissues for exploring the *HOTAIR* functional roles in human body fat distribution. Second, DXA scan provides accurate estimation of regional fat components which help build up the *HOTAIR* genotype-phenotype association in the large cohort OBB database. Third, the immortalised and primary paired preadipocytes inherit intrinsic fat-depot specific properties which allow us to study *HOTAIR*-involved molecular mechanisms

in a fat depot-specific manner. For example, the exploration of histone marks across *HOTAIR/HOXC* locus via ChIPs provides evidence that abdominal and gluteal preadipocytes have distinct histone marks that make them express differential levels of *HOTAIR* gene. Furthermore, using the cellular model of *in vitro* adipogenesis and co-expression analysis of RNA-seq data during cell differentiation, I detected 28 co-expression patterns from the complex gene network and selected a small cluster of 135 genes that maintained increased expression pattern in the gluteal sh*HOTAIR* cell during adipogenesis. This method identifies the genes that might directly be suppressed by *HOTAIR*, such as protocadherin genes and *HOXD* genes. Moreover, applying ChIP and pyrosequencing, this hypothesis was tested for the *PCDH10* gene and demonstrated that it was epigenetically suppressed by *HOTAIR*. Therefore, other genes in the same group might also be *HOTAIR* target genes and further investigation on these genes could increase our knowledge about *HOTAIR* mediated downstream networks in the gluteal fat depot.

There are also some limitations in this study. First, although several experiments I performed are consistent with *HOTAIR* function being inhibited in the gluteal sh*HOTAIR* cells, the hypothesis that sh*HOTAIR* might interfere *HOTAIR* function via a change in its secondary structure has not been proven yet. To demonstrate this, a new method to determine *in vivo* RNA structure of low-abundance transcripts would be required (Kwok, et al., 2013). Currently, I am collaborating with a research group at the John Innes Centre, Norwich, UK to do this in gluteal sh*HOTAIR* and shControl preadipocytes, but this work is still under experimental optimisation and couldn't be included in this thesis. Second, when exploring *HOTAIR*-mediated epigenetic regulation using H3K27me3/SUZ12 ChIPs and bisulfite pyrosequencing, the examined DNA regions are limited to the promoter regions or CpG islands of some putative target genes. Further advanced methods such as using ChIP-sequencing or whole genome bisulfite sequencing on the gluteal sh*HOTAIR*/shControl cells during *in vitro* adipogenesis would be able to provide a more comprehensive information on

HOTAIR-mediated epigenetic regulation in the gluteal preadipocytes and will be considered within the future plans. Third, although it has been demonstrated in human fibroblasts that *HOTAIR* can recruit the PRC2 complex for silencing target genes *in trans* (Rinn, et al., 2007), this mechanism hasn't been directly validated in the human preadipocytes. To demonstrate this, RNA immunoprecipitation will need to be performed in a tissue-specific manner to examine the physical interaction between *HOTAIR* and PRC2. In this study, although I didn't perform RNA immunoprecipitation to confirm a physical interaction between *HOTAIR* and the PRC2 complex in gluteal preadipocytes, the increased levels of several *HOXD* genes, and decreased presence of H3K27me3/SUZ12 on the *HOXD8*/*HOXD10* promoter regions in the gluteal sh*HOTAIR* preadipocytes, provided indirect evidence to support that a *HOTAIR*/PRC2 interaction also exists in human gluteal preadipocytes.

6.4 Future avenues of the research

Based on the findings of this study, some topics might be of interest for the future.

First, my results show that rs76084431 is associated with decreased GSAT *HOTAIR* expression and increased android to gynoid fat ratio. Exploring the histone marks of *HOTAIR/HOXC* locus in immortalised gluteal and abdominal preadipocytes, I found that rs76084431 is positioned in an open chromatin region, which could be considered as a *HOTAIR* enhancer. Therefore, it will be of interest to perform rs76084431 allele-specific CRISPR gene editing on the immortalised gluteal preadipocytes. Then, the functional impacts including *HOTAIR* expression, histone marks, cell proliferation rate and adipogenic differentiation can be compared between gluteal preadipocytes carrying with homozygous major alleles (CC) and homozygous minor alleles (TT) of rs7084431. This experiment would validate if the minor allele of rs76084431 is directly influencing *HOTAIR* expression and thereby determines the biological activity of the gluteal preadipocytes.

Second, in the *in vitro* experiments using constitutive overexpression of *HOTAIR* in

the abdominal preadipocytes, there was a profound suppression of adipogenesis, whilst the gluteal *HOTAIR* preadipocytes differentiated well. This *HOTAIR* mediated abdominal-depot specific anti-adipogenic effect is intriguing, but the underpinning mechanisms have not been clarified in this study. Therefore, performing co-expression analysis of RNA-seq data in the abdominal *HOTAIR* and Control cells during adipogenesis would potentially disclose the downstream signalling and cellular/molecular mechanisms. Although ASAT doesn't express *HOTAIR* in the normal physiological condition, recently some studies revealed that *HOTAIR* could be secreted from cells/tissues and enriched in the exosomes (Gezer, et al., 2014), which carried the lncRNA into the circulation to influence biological function of distant organs (Lu, et al., 2017). This example was described in patients with malignancy (Cai, et al., 2014), suggesting *HOTAIR* was carried in exosomes (Sun, et al., 2018). Therefore, it could be speculated that *HOTAIR* mediated anti-adipogenic effects in the ASAT might show up in these patients, which could contribute to features of fat loss as cancer cachexia (Liu, et al., 2018) and would deserve further investigation.

Reference:

Akhtar, W., *et al.* (2013) Chromatin position effects assayed by thousands of reporters integrated in parallel, *Cell*, 154, 914-927.

Allan, C.A., *et al.* (2008) Testosterone therapy prevents gain in visceral adipose tissue and loss of skeletal muscle in nonobese aging men, *J Clin Endocrinol Metab*, 93, 139-146.

Alvarado, D.M., *et al.* (2016) Deletions of 5' HOXC genes are associated with lower extremity malformations, including clubfoot and vertical talus, *Journal of Medical Genetics*, 53, 250-255.

Ambros, V. (2004) The functions of animal microRNAs, *Nature*, 431, 350-355.

Aoki, E., *et al.* (2003) Distribution of OL-protocadherin protein in correlation with specific neural compartments and local circuits in the postnatal mouse brain, *Neuroscience*, 117, 593-614.

Arner, P., *et al.* (1990) Adrenergic regulation of lipolysis in situ at rest and during exercise, *J Clin Invest*, 85, 893-898.

Arner, P., *et al.* (1991) Expression of lipoprotein lipase in different human subcutaneous adipose tissue regions, *J Lipid Res*, 32, 423-429.

Avgustinova, A. and Benitah, S.A. (2016) Epigenetic control of adult stem cell function, *Nat Rev Mol Cell Biol*, 17, 643-658.

Ball, M.P., *et al.* (2009) Targeted and genome-scale strategies reveal gene-body methylation signatures in human cells, *Nature Biotechnology*, 27, 361-368.

Bengtsson, B.A., *et al.* (1993) Treatment of adults with growth hormone (GH) deficiency with recombinant human GH, *J Clin Endocrinol Metab*, 76, 309-317.

Bhan, A., *et al.* (2017) Histone methylase MLL1 coordinates with HIF and regulate lncRNA HOTAIR expression under hypoxia, *Gene*, 629, 16-28.

Bhan, A., *et al.* (2013) Antisense transcript long noncoding RNA (lncRNA) HOTAIR is transcriptionally induced by estradiol, *J Mol Biol*, 425, 3707-3722.

Bhan, A. and Mandal, S.S. (2015) LncRNA HOTAIR: A master regulator of chromatin dynamics and cancer, *Biochim Biophys Acta*, 1856, 151-164.

Blouin, K., *et al.* (2010) Effects of androgens on adipocyte differentiation and adipose tissue explant metabolism in men and women, *Clinical Endocrinology*, 72, 176-188.

Bohmdorfer, G. and Wierzbicki, A.T. (2015) Control of Chromatin Structure by Long Noncoding RNA, *Trends Cell Biol*, 25, 623-632.

Boyle, A.P., *et al.* (2011) High-resolution genome-wide in vivo footprinting of diverse transcription factors in human cells, *Genome Research*, 21, 456-464.

Broholm, C., *et al.* (2016) Human adipogenesis is associated with genome-wide DNA methylation and gene-expression changes, *Epigenomics*, 8, 1601-1617.

Buenrostro, J.D., *et al.* (2013) Transposition of native chromatin for fast and sensitive epigenomic profiling of open chromatin, DNA-binding proteins and nucleosome position, *Nature Methods*, 10, 1213-1218.

Burt, M.G., Gibney, J. and Ho, K.K. (2006) Characterization of the metabolic phenotypes of Cushing's syndrome and growth hormone deficiency: a study of body composition and energy metabolism, *Clinical Endocrinology*, 64, 436-443.

Cabili, M.N., *et al.* (2011) Integrative annotation of human large intergenic noncoding RNAs reveals global properties and specific subclasses, *Genes Dev*, 25, 1915-1927.

Cai, B., *et al.* (2014) HOTAIR: a cancer-related long non-coding RNA, *Neoplasma*, 61, 379-391.

Cai, H., *et al.* (2017) LncRNA HOTAIR acts a competing endogenous RNA to control

the expression of notch3 via sponging miR-613 in pancreatic cancer, *Oncotarget*, 8, 32905-32917.
Canoy, D.*, et al.* (2007) Body fat distribution and risk of coronary heart disease in men and women in the European Prospective Investigation Into Cancer and Nutrition in Norfolk cohort: a population-based prospective study, *Circulation*, 116, 2933-2943.
Carr, A. (2003) HIV lipodystrophy: risk factors, pathogenesis, diagnosis and management, *Aids*, 17 Suppl 1, S141-148.
Carrion, K.*, et al.* (2014) The long non-coding HOTAIR is modulated by cyclic stretch and WNT/beta-CATENIN in human aortic valve cells and is a novel repressor of calcification genes, *PloS One*, 9, e96577.
Carroll, S.B. (1995) Homeotic genes and the evolution of arthropods and chordates, *Nature*, 376, 479-485.
Carthew, R.W. and Sontheimer, E.J. (2009) Origins and Mechanisms of miRNAs and siRNAs, *Cell*, 136, 642-655.
Charo, N.L.*, et al.* (2016) Organization of nuclear architecture during adipocyte differentiation, *Nucleus*, 7, 249-269.
Chazenbalk, G.*, et al.* (2013) Androgens inhibit adipogenesis during human adipose stem cell commitment to preadipocyte formation, *Steroids*, 78, 920-926.
Chen, L.*, et al.* (2018) Actin depolymerization enhances adipogenic differentiation in human stromal stem cells, *Stem Cell Research*, 29, 76-83.
Cirulli, E.T. and Goldstein, D.B. (2010) Uncovering the roles of rare variants in common disease through whole-genome sequencing, *Nature Reviews. Genetics*, 11, 415-425.
Collins, J.M.*, et al.* (2010) De novo lipogenesis and stearoyl-CoA desaturase are coordinately regulated in the human adipocyte and protect against palmitate-induced cell injury, *The Journal of Biological Chemistry*, 285, 6044-6052.
Consortium, G.T. (2013) The Genotype-Tissue Expression (GTEx) project, *Nature Genetics*, 45, 580-585.
Cox-York, K.A.*, et al.* (2017) Region-specific effects of oestradiol on adipose-derived stem cell differentiation in post-menopausal women, *Journal of Cellular and Molecular Medicine*, 21, 677-684.
Croft, J.A.*, et al.* (1999) Differences in the localization and morphology of chromosomes in the human nucleus, *J Cell Biol*, 145, 1119-1131.
Daftary, G.S. and Taylor, H.S. (2006) Endocrine regulation of HOX genes, *Endocr Rev*, 27, 331-355.
Danforth, E., Jr. (2000) Failure of adipocyte differentiation causes type II diabetes mellitus?, *Nature Genetics*, 26, 13.
Dankel, S.N.*, et al.* (2010) Switch from stress response to homeobox transcription factors in adipose tissue after profound fat loss, *PLoS One*, 5, e11033.
Darimont, C. and Mace, K. (2003) Immortalization of human preadipocytes, *Biochimie*, 85, 1231-1233.
Divoux, A.*, et al.* (2014) Identification of a novel lncRNA in gluteal adipose tissue and evidence for its positive effect on preadipocyte differentiation, *Obesity*, 22, 1781-1785.
Dorighi, K.M.*, et al.* (2017) Mll3 and Mll4 Facilitate Enhancer RNA Synthesis and Transcription from Promoters Independently of H3K4 Monomethylation, *Molecular cell*, 66, 568-576 e564.
Dou, P.*, et al.* (2017) Long non-coding RNA HOTAIR promotes expression of ADAMTS-5 in human osteoarthritic articular chondrocytes, *Die Pharmazie*, 72, 113-117.
Dunaif, A. (1997) Insulin resistance and the polycystic ovary syndrome: mechanism

and implications for pathogenesis, *Endocr Rev*, 18, 774-800.
Elbers, J.M., *et al.* (1997) Long-term testosterone administration increases visceral fat in female to male transsexuals, *J Clin Endocrinol Metab*, 82, 2044-2047.
Elbers, J.M., *et al.* (1999) Changes in fat cell size and in vitro lipolytic activity of abdominal and gluteal adipocytes after a one-year cross-sex hormone administration in transsexuals, *Metabolism: Clinical and Experimental*, 48, 1371-1377.
Emdin, C.A., *et al.* (2017) Genetic Association of Waist-to-Hip Ratio With Cardiometabolic Traits, Type 2 Diabetes, and Coronary Heart Disease, *JAMA*, 317, 626-634.
Endo, H., *et al.* (2013) Enhanced expression of long non-coding RNA HOTAIR is associated with the development of gastric cancer, *PloS One*, 8, e77070.
Enerback, S. (2009) The origins of brown adipose tissue, *N Engl J Med*, 360, 2021-2023.
Engin, A. (2017) Adipose Tissue Hypoxia in Obesity and Its Impact on Preadipocytes and Macrophages: Hypoxia Hypothesis, *Advances in Experimental Medicine and Biology*, 960, 305-326.
Engler, A.J., *et al.* (2006) Matrix elasticity directs stem cell lineage specification, *Cell*, 126, 677-689.
Fang, Y. and Fullwood, M.J. (2016) Roles, Functions, and Mechanisms of Long Non-coding RNAs in Cancer, *Genomics Proteomics Bioinformatics*, 14, 42-54.
Fawcett, D.W. (1966) On the occurrence of a fibrous lamina on the inner aspect of the nuclear envelope in certain cells of vertebrates, *Am J Anat*, 119, 129-145.
Finkelstein, E.A., *et al.* (2012) Obesity and severe obesity forecasts through 2030, *Am J Prev Med*, 42, 563-570.
Fisher, F.M., *et al.* (2002) Differences in adiponectin protein expression: effect of fat depots and type 2 diabetic status, *Horm Metab Res*, 34, 650-654.
Folguera-Blasco, N., *et al.* (2018) Epigenetic regulation of cell fate reprogramming in aging and disease: A predictive computational model, *PLoS Computational Biology*, 14, e1006052.
Fried, S.K., Lee, M.J. and Karastergiou, K. (2015) Shaping fat distribution: New insights into the molecular determinants of depot- and sex-dependent adipose biology, *Obesity*, 23, 1345-1352.
Fu, W.M., *et al.* (2015) Hotair mediates hepatocarcinogenesis through suppressing miRNA-218 expression and activating P14 and P16 signaling, *J Hepatol*, 63, 886-895.
Gao, L., *et al.* (2017) Circulating Long Noncoding RNA HOTAIR is an Essential Mediator of Acute Myocardial Infarction, *Cellular Physiology and Biochemistry*, 44, 1497-1508.
Gapstur, S.M., *et al.* (2002) Serum androgen concentrations in young men: a longitudinal analysis of associations with age, obesity, and race. The CARDIA male hormone study, *Cancer Epidemiol Biomarkers Prev*, 11, 1041-1047.
Garg, A. (2011) Clinical review#: Lipodystrophies: genetic and acquired body fat disorders, *J Clin Endocrinol Metab*, 96, 3313-3325.
Gavin, K.M., Cooper, E.E. and Hickner, R.C. (2013) Estrogen receptor protein content is different in abdominal than gluteal subcutaneous adipose tissue of overweight-to-obese premenopausal women, *Metabolism: Clinical and Experimental*, 62, 1180-1188.
Gavrilova, O., *et al.* (2000) Surgical implantation of adipose tissue reverses diabetes in lipoatrophic mice, *J Clin Invest*, 105, 271-278.
Gburcik, V., *et al.* (2012) An essential role for Tbx15 in the differentiation of brown and "brite" but not white adipocytes, *Am J Physiol Endocrinol Metab*, 303, E1053-1060.

Gehrke, S.*, et al.* (2013) Epigenetic regulation of depot-specific gene expression in adipose tissue, *PloS One*, 8, e82516.
Genomes Project, C.*, et al.* (2012) An integrated map of genetic variation from 1,092 human genomes, *Nature*, 491, 56-65.
Gery, S.*, et al.* (2005) C/EBPdelta expression in a BCR-ABL-positive cell line induces growth arrest and myeloid differentiation, *Oncogene*, 24, 1589-1597.
Gesta, S.*, et al.* (2011) Mesodermal developmental gene Tbx15 impairs adipocyte differentiation and mitochondrial respiration, *Proceedings of the National Academy of Sciences of the United States of America*, 108, 2771-2776.
Gesta, S.*, et al.* (2006) Evidence for a role of developmental genes in the origin of obesity and body fat distribution, *Proceedings of the National Academy of Sciences of the United States of America*, 103, 6676-6681.
Gesta, S., Tseng, Y.H. and Kahn, C.R. (2007) Developmental origin of fat: tracking obesity to its source, *Cell*, 131, 242-256.
Geuens, T., Bouhy, D. and Timmerman, V. (2016) The hnRNP family: insights into their role in health and disease, *Hum Genet*, 135, 851-867.
Gezer, U.*, et al.* (2014) Long non-coding RNAs with low expression levels in cells are enriched in secreted exosomes, *Cell Biology International*, 38, 1076-1079.
Global, B.M.I.M.C.*, et al.* (2016) Body-mass index and all-cause mortality: individual-participant-data meta-analysis of 239 prospective studies in four continents, *Lancet*, 388, 776-786.
Gonzalez-Muniesa, P.*, et al.* (2017) Obesity, *Nat Rev Dis Primers*, 3, 17034.
Gray, S.L. and Vidal-Puig, A.J. (2007) Adipose tissue expandability in the maintenance of metabolic homeostasis, *Nutr Rev*, 65, S7-12.
Gupta, R.A.*, et al.* (2010) Long non-coding RNA HOTAIR reprograms chromatin state to promote cancer metastasis, *Nature*, 464, 1071-1076.
Guttman, M.*, et al.* (2010) Ab initio reconstruction of cell type-specific transcriptomes in mouse reveals the conserved multi-exonic structure of lincRNAs, *Nature Biotechnology*, 28, 503-510.
Hasegawa, Y.*, et al.* (2010) The matrix protein hnRNP U is required for chromosomal localization of Xist RNA, *Dev Cell*, 19, 469-476.
Hattori, K.*, et al.* (2004) Chart analysis of body composition change among pre- and postadolescent Japanese subjects assessed by underwater weighing method, *Int J Obes Relat Metab Disord*, 28, 520-524.
Hauner, H., Skurk, T. and Wabitsch, M. (2001) Cultures of human adipose precursor cells, *Methods in Molecular Biology*, 155, 239-247.
Heid, I.M.*, et al.* (2010) Meta-analysis identifies 13 new loci associated with waist-hip ratio and reveals sexual dimorphism in the genetic basis of fat distribution, *Nature Genetics*, 42, 949-960.
Hirano, S., Yan, Q. and Suzuki, S.T. (1999) Expression of a novel protocadherin, OL-protocadherin, in a subset of functional systems of the developing mouse brain, *The Journal of Neuroscience*, 19, 995-1005.
Hlobilkova, A.*, et al.* (2003) The mechanism of action of the tumour suppressor gene PTEN, *Biomedical papers of the Medical Faculty of the University Palacky, Olomouc, Czechoslovakia*, 147, 19-25.
Hodson, L.*, et al.* (2015) Menopausal Status and Abdominal Obesity Are Significant Determinants of Hepatic Lipid Metabolism in Women, *Journal of the American Heart Association*, 4, e002258.
Holland, P.W., Booth, H.A. and Bruford, E.A. (2007) Classification and nomenclature of all human homeobox genes, *BMC biology*, 5, 47.

Hong, L., *et al.* (2007) 17-Beta estradiol enhances osteogenic and adipogenic differentiation of human adipose-derived stromal cells, *Tissue Engineering*, 13, 1197-1203.
Huang da, W., Sherman, B.T. and Lempicki, R.A. (2009) Systematic and integrative analysis of large gene lists using DAVID bioinformatics resources, *Nature Protocols*, 4, 44-57.
Hube, F., *et al.* (1996) Difference in leptin mRNA levels between omental and subcutaneous abdominal adipose tissue from obese humans, *Horm Metab Res*, 28, 690-693.
Ikezoe, T., *et al.* (2005) CCAAT/enhancer-binding protein delta: a molecular target of 1,25-dihydroxyvitamin D3 in androgen-responsive prostate cancer LNCaP cells, *Cancer Research*, 65, 4762-4768.
International HapMap, C. (2003) The International HapMap Project, *Nature*, 426, 789-796.
Jin, F., *et al.* (2013) A high-resolution map of the three-dimensional chromatin interactome in human cells, *Nature*, 503, 290-294.
Johnson, J.A., *et al.* (2001) Impaired insulin action in subcutaneous adipocytes from women with visceral obesity, *American journal of physiology. Endocrinology and metabolism*, 280, E40-49.
Julian, C.G. (2017) Epigenomics and human adaptation to high altitude, *Journal of Applied Physiology*, 123, 1362-1370.
Kalwa, M., *et al.* (2016) The lncRNA HOTAIR impacts on mesenchymal stem cells via triple helix formation, *Nucleic Acids Research*, 44, 10631-10643.
Kang, D., *et al.* (2017) Comparative transcriptome analysis reveals potentially novel roles of Homeobox genes in adipose deposition in fat-tailed sheep, *Scientific Reports*, 7, 14491.
Karastergiou, K., *et al.* (2013) Distinct developmental signatures of human abdominal and gluteal subcutaneous adipose tissue depots, *J Clin Endocrinol Metab*, 98, 362-371.
Karpe, F. and Pinnick, K.E. (2015) Biology of upper-body and lower-body adipose tissue--link to whole-body phenotypes, *Nat Rev Endocrinol*, 11, 90-100.
Kelly, T., *et al.* (2008) Global burden of obesity in 2005 and projections to 2030, *Int J Obes (Lond)*, 32, 1431-1437.
Kim, J.Y., *et al.* (2007) Obesity-associated improvements in metabolic profile through expansion of adipose tissue, *J Clin Invest*, 117, 2621-2637.
Kim, K., *et al.* (2013) HOTAIR is a negative prognostic factor and exhibits pro-oncogenic activity in pancreatic cancer, *Oncogene*, 32, 1616-1625.
Kim, S.Y., *et al.* (2011) Non-clustered protocadherin, *Cell Adhesion & Migration*, 5, 97-105.
Klattenhoff, C.A., *et al.* (2013) Braveheart, a long noncoding RNA required for cardiovascular lineage commitment, *Cell*, 152, 570-583.
Klein, R.J., *et al.* (2005) Complement factor H polymorphism in age-related macular degeneration, *Science*, 308, 385-389.
Kogo, R., *et al.* (2011) Long noncoding RNA HOTAIR regulates polycomb-dependent chromatin modification and is associated with poor prognosis in colorectal cancers, *Cancer Research*, 71, 6320-6326.
Koutsari, C., Snozek, C.L. and Jensen, M.D. (2008) Plasma NEFA storage in adipose tissue in the postprandial state: sex-related and regional differences, *Diabetologia*, 51, 2041-2048.
Kretz, M., *et al.* (2013) Control of somatic tissue differentiation by the long non-coding RNA TINCR, *Nature*, 493, 231-235.

Kretz, M., *et al.* (2012) Suppression of progenitor differentiation requires the long noncoding RNA ANCR, *Genes Dev*, 26, 338-343.
Kuroda, M., *et al.* (2004) Alteration of chromosome positioning during adipocyte differentiation, *J Cell Sci*, 117, 5897-5903.
Kwok, C.K., *et al.* (2013) Determination of in vivo RNA structure in low-abundance transcripts, *Nature Communications*, 4, 2971.
Lafontan, M. and Berlan, M. (1993) Fat cell adrenergic receptors and the control of white and brown fat cell function, *Journal of Lipid Research*, 34, 1057-1091.
Langfelder, P. and Horvath, S. (2008) WGCNA: an R package for weighted correlation network analysis, *BMC Bioinformatics*, 9, 559.
Lee, K.Y., *et al.* (2017) Tbx15 Defines a Glycolytic Subpopulation and White Adipocyte Heterogeneity, *Diabetes*, 66, 2822-2829.
Lee, K.Y., *et al.* (2013) Shox2 is a molecular determinant of depot-specific adipocyte function, *Proceedings of the National Academy of Sciences of the United States of America*, 110, 11409-11414.
Lee, M.J., *et al.* (2014) Deconstructing the roles of glucocorticoids in adipose tissue biology and the development of central obesity, *Biochim Biophys Acta*, 1842, 473-481.
Lee, N.K., *et al.* (2016) Promoter methylation of PCDH10 by HOTAIR regulates the progression of gastrointestinal stromal tumors, *Oncotarget*, 7, 75307-75318.
Lefterova, M.I. and Lazar, M.A. (2009) New developments in adipogenesis, *Trends in Endocrinology and Metabolism: TEM*, 20, 107-114.
Lehtovirta, M., *et al.* (2000) Insulin sensitivity and insulin secretion in monozygotic and dizygotic twins, *Diabetologia*, 43, 285-293.
Li, D., *et al.* (2013) Long intergenic noncoding RNA HOTAIR is overexpressed and regulates PTEN methylation in laryngeal squamous cell carcinoma, *The American Journal of Pathology*, 182, 64-70.
Li, J.T., *et al.* (2014) Nuclear factor of activated T cells 5 maintained by Hotair suppression of miR-568 upregulates S100 calcium binding protein A4 to promote breast cancer metastasis, *Breast Cancer Res*, 16, 454.
Li, L., *et al.* (2013) Targeted disruption of Hotair leads to homeotic transformation and gene derepression, *Cell Reports*, 5, 3-12.
Li, R., Zhu, H. and Luo, Y. (2016) Understanding the Functions of Long Non-Coding RNAs through Their Higher-Order Structures, *Int J Mol Sci*, 17.
Lindberg, U.B., *et al.* (1990) Regional adipose tissue metabolism in postmenopausal women after treatment with exogenous sex steroids, *Horm Metab Res*, 22, 345-351.
Liu, H., *et al.* (2018) Identification and functional analysis of a potential key lncRNA involved in fat loss of cancer cachexia, *Journal of Cellular Biochemistry*, 119, 1679-1688.
Liu, Y., *et al.* (2017) Emerging roles and mechanisms of long noncoding RNAs in atherosclerosis, *Int J Cardiol*, 228, 570-582.
Livingston, E.H. (2006) Lower body subcutaneous fat accumulation and diabetes mellitus risk, *Surg Obes Relat Dis*, 2, 362-368.
Local, A., *et al.* (2018) Identification of H3K4me1-associated proteins at mammalian enhancers, *Nature Genetics*, 50, 73-82.
Lovejoy, J.C., *et al.* (2008) Increased visceral fat and decreased energy expenditure during the menopausal transition, *Int J Obes (Lond)*, 32, 949-958.
Lu, X., *et al.* (2017) Sedentary lifestyle related exosomal release of Hotair from gluteal-femoral fat promotes intestinal cell proliferation, *Scientific reports*, 7, 45648.
Luo, S., *et al.* (2013) Adipose tissue-derived stem cells treated with estradiol enhance survival of autologous fat transplants, *The Tohoku Journal of Experimental Medicine*,

231, 101-110.
Ma, H., Siegel, A.J. and Berezney, R. (1999) Association of chromosome territories with the nuclear matrix. Disruption of human chromosome territories correlates with the release of a subset of nuclear matrix proteins, *J Cell Biol*, 146, 531-542.
Ma, L., Bajic, V.B. and Zhang, Z. (2013) On the classification of long non-coding RNAs, *RNA Biol*, 10, 925-933.
Ma, M.Z.*, et al.* (2014) Long non-coding RNA HOTAIR, a c-Myc activated driver of malignancy, negatively regulates miRNA-130a in gallbladder cancer, *Mol Cancer*, 13, 156.
MacArthur, J.*, et al.* (2017) The new NHGRI-EBI Catalog of published genome-wide association studies (GWAS Catalog), *Nucleic Acids Research*, 45, D896-D901.
Mah, K.M. and Weiner, J.A. (2017) Regulation of Wnt signaling by protocadherins, *Seminars in Cell & Developmental Biology*, 69, 158-171.
Majewski, J. and Ott, J. (2002) Distribution and characterization of regulatory elements in the human genome, *Genome Research*, 12, 1827-1836.
Malis, C.*, et al.* (2005) Total and regional fat distribution is strongly influenced by genetic factors in young and elderly twins, *Obesity Research*, 13, 2139-2145.
Manolopoulos, K.N., Karpe, F. and Frayn, K.N. (2010) Gluteofemoral body fat as a determinant of metabolic health, *Int J Obes (Lond)*, 34, 949-959.
Marinou, K.*, et al.* (2014) Structural and functional properties of deep abdominal subcutaneous adipose tissue explain its association with insulin resistance and cardiovascular risk in men, *Diabetes Care*, 37, 821-829.
Mattick, J.S. (2004) RNA regulation: a new genetics?, *Nature reviews. Genetics*, 5, 316-323.
Maurano, M.T.*, et al.* (2012) Systematic localization of common disease-associated variation in regulatory DNA, *Science*, 337, 1190-1195.
Mayes, J.S. and Watson, G.H. (2004) Direct effects of sex steroid hormones on adipose tissues and obesity, *Obes Rev*, 5, 197-216.
Maynard, L.M.*, et al.* (2001) Childhood body composition in relation to body mass index, *Pediatrics*, 107, 344-350.
Messeguer, X.*, et al.* (2002) PROMO: detection of known transcription regulatory elements using species-tailored searches, *Bioinformatics*, 18, 333-334.
Mikkelsen, T.S.*, et al.* (2010) Comparative epigenomic analysis of murine and human adipogenesis, *Cell*, 143, 156-169.
Mohamed-Ali, V., Pinkney, J.H. and Coppack, S.W. (1998) Adipose tissue as an endocrine and paracrine organ, *Int J Obes Relat Metab Disord*, 22, 1145-1158.
Mori, S.*, et al.* (2014) Characteristic expression of extracellular matrix in subcutaneous adipose tissue development and adipogenesis; comparison with visceral adipose tissue, *International Journal of Biological Sciences*, 10, 825-833.
Morrow, E.M.*, et al.* (2008) Identifying autism loci and genes by tracing recent shared ancestry, *Science*, 321, 218-223.
Nakao, S.*, et al.* (2008) Contact-dependent promotion of cell migration by the OL-protocadherin-Nap1 interaction, *J Cell Biol*, 182, 395-410.
Nelson, V.L.*, et al.* (2014) Adipose tissue insulin resistance due to loss of PI3K p110alpha leads to decreased energy expenditure and obesity, *Am J Physiol Endocrinol Metab*, 306, E1205-1216.
Neville, M.J.*, et al.* (2011) Comprehensive human adipose tissue mRNA and microRNA endogenous control selection for quantitative real-time-PCR normalization, *Obesity*, 19, 888-892.
Nguyen, N.T. and Varela, J.E. (2017) Bariatric surgery for obesity and metabolic

disorders: state of the art, *Nat Rev Gastroenterol Hepatol*, 14, 160-169.
Nishizawa, H.*, et al.* (2002) Androgens decrease plasma adiponectin, an insulin-sensitizing adipocyte-derived protein, *Diabetes*, 51, 2734-2741.
Oldenburg, A.*, et al.* (2017) A lipodystrophy-causing lamin A mutant alters conformation and epigenetic regulation of the anti-adipogenic MIR335 locus, *J Cell Biol*, 216, 2731-2743.
Ono, H.*, et al.* (2014) Long noncoding RNA HOTAIR is relevant to cellular proliferation, invasiveness, and clinical relapse in small-cell lung cancer, *Cancer Medicine*, 3, 632-642.
Palin, S.L.*, et al.* (2003) 17Beta-estradiol and anti-estrogen ICI:compound 182,780 regulate expression of lipoprotein lipase and hormone-sensitive lipase in isolated subcutaneous abdominal adipocytes, *Metabolism: Clinical and Experimental*, 52, 383-388.
Papaioannou, V.E. (2014) The T-box gene family: emerging roles in development, stem cells and cancer, *Development*, 141, 3819-3833.
Pasquali, R.*, et al.* (1991) Effect of obesity and body fat distribution on sex hormones and insulin in men, *Metabolism: Clinical and Experimental*, 40, 101-104.
Passaro, A.*, et al.* (2017) Gene expression regional differences in human subcutaneous adipose tissue, *BMC Genomics*, 18, 202.
Patrizi, G. and Poger, M. (1967) The ultrastructure of the nuclear periphery. The zonula nucleum limitans, *J Ultrastruct Res*, 17, 127-136.
Paul, D.S., Soranzo, N. and Beck, S. (2014) Functional interpretation of non-coding sequence variation: concepts and challenges, *Bioessays*, 36, 191-199.
Pearson, J.C., Lemons, D. and McGinnis, W. (2005) Modulating Hox gene functions during animal body patterning, *Nature Reviews. Genetics*, 6, 893-904.
Pers, T.H.*, et al.* (2015) Biological interpretation of genome-wide association studies using predicted gene functions, *Nature Communications*, 6, 5890.
Petrovic, N.*, et al.* (2010) Chronic peroxisome proliferator-activated receptor gamma (PPARgamma) activation of epididymally derived white adipocyte cultures reveals a population of thermogenically competent, UCP1-containing adipocytes molecularly distinct from classic brown adipocytes, *The Journal of biological chemistry*, 285, 7153-7164.
Pfaffl, M.W. (2001) A new mathematical model for relative quantification in real-time RT-PCR, *Nucleic Acids Research*, 29, e45.
Pinnick, K.E.*, et al.* (2012) Gluteofemoral adipose tissue plays a major role in production of the lipokine palmitoleate in humans, *Diabetes*, 61, 1399-1403.
Pinnick, K.E.*, et al.* (2014) Distinct developmental profile of lower-body adipose tissue defines resistance against obesity-associated metabolic complications, *Diabetes*, 63, 3785-3797.
Poulsen, P.*, et al.* (2001) Genetic versus environmental aetiology of the metabolic syndrome among male and female twins, *Diabetologia*, 44, 537-543.
Prestwich, T.C. and Macdougald, O.A. (2007) Wnt/beta-catenin signaling in adipogenesis and metabolism, *Current Opinion in Cell Biology*, 19, 612-617.
Price, T.M.*, et al.* (1998) Estrogen regulation of adipose tissue lipoprotein lipase--possible mechanism of body fat distribution, *American Journal of Obstetrics and Gynecology*, 178, 101-107.
Qiu, J.J.*, et al.* (2015) The long non-coding RNA HOTAIR promotes the proliferation of serous ovarian cancer cells through the regulation of cell cycle arrest and apoptosis, *Experimental Cell Research*, 333, 238-248.
Rada-Iglesias, A. (2018) Is H3K4me1 at enhancers correlative or causative?, *Nature*

Genetics, 50, 4-5.
Rasouli, N.*, et al.* (2005) Pioglitazone improves insulin sensitivity through reduction in muscle lipid and redistribution of lipid into adipose tissue, *Am J Physiol Endocrinol Metab*, 288, E930-934.
Raychaudhuri, S.*, et al.* (2009) Identifying relationships among genomic disease regions: predicting genes at pathogenic SNP associations and rare deletions, *PLoS Genet*, 5, e1000534.
Razavi, S.*, et al.* (2015) Estrogen treatment enhances neurogenic differentiation of human adipose derived stem cells in vitro, *Iranian Journal of Basic Medical Sciences*, 18, 799-804.
Rebuffe-Scrive, M., Basdevant, A. and Guy-Grand, B. (1983) Effect of local application of progesterone on human adipose tissue lipoprotein lipase, *Horm Metab Res*, 15, 566.
Rebuffe-Scrive, M.*, et al.* (1987) Regional adipose tissue metabolism in men and postmenopausal women, *International Journal of Obesity*, 11, 347-355.
Redies, C., Hertel, N. and Hubner, C.A. (2012) Cadherins and neuropsychiatric disorders, *Brain Research*, 1470, 130-144.
Ren, K.*, et al.* (2016) Long Noncoding RNA HOTAIR Controls Cell Cycle by Functioning as a Competing Endogenous RNA in Esophageal Squamous Cell Carcinoma, *Translational Oncology*, 9, 489-497.
Rickels, R.*, et al.* (2017) Histone H3K4 monomethylation catalyzed by Trr and mammalian COMPASS-like proteins at enhancers is dispensable for development and viability, *Nature Genetics*, 49, 1647-1653.
Rinn, J.L.*, et al.* (2007) Functional demarcation of active and silent chromatin domains in human HOX loci by noncoding RNAs, *Cell*, 129, 1311-1323.
Rivera, R.M. and Ross, J.W. (2013) Epigenetics in fertilization and preimplantation embryo development, *Prog Biophys Mol Biol*, 113, 423-432.
Roemmich, J.N.*, et al.* (2001) Alterations in body composition and fat distribution in growth hormone-deficient prepubertal children during growth hormone therapy, *Metabolism: Clinical and Experimental*, 50, 537-547.
Saad, F. (2017) Testosterone Therapy and Glucose Homeostasis in Men with Testosterone Deficiency (Hypogonadism), *Advances in Experimental Medicine and Biology*, 1043, 527-558.
Saad, M.F.*, et al.* (1997) Sexual dimorphism in plasma leptin concentration, *J Clin Endocrinol Metab*, 82, 579-584.
Schmidt, H.H.*, et al.* (2001) Dyslipemia in familial partial lipodystrophy caused by an R482W mutation in the LMNA gene, *J Clin Endocrinol Metab*, 86, 2289-2295.
Scott, M.P. (1992) Vertebrate homeobox gene nomenclature, *Cell*, 71, 551-553.
Segre, A.V.*, et al.* (2010) Common inherited variation in mitochondrial genes is not enriched for associations with type 2 diabetes or related glycemic traits, *PLoS Genet*, 6.
Selby, J.V.*, et al.* (1990) Genetic and behavioral influences on body fat distribution, *International Journal of Obesity*, 14, 593-602.
Shadid, S. and Jensen, M.D. (2003) Effects of pioglitazone versus diet and exercise on metabolic health and fat distribution in upper body obesity, *Diabetes Care*, 26, 3148-3152.
Shadid, S., Koutsari, C. and Jensen, M.D. (2007) Direct free fatty acid uptake into human adipocytes in vivo: relation to body fat distribution, *Diabetes*, 56, 1369-1375.
Shih, Y.R.*, et al.* (2011) Matrix stiffness regulation of integrin-mediated mechanotransduction during osteogenic differentiation of human mesenchymal stem

cells, *Journal of Bone and Mineral Research*, 26, 730-738.
Shlyueva, D., Stampfel, G. and Stark, A. (2014) Transcriptional enhancers: from properties to genome-wide predictions, *Nature Reviews. Genetics*, 15, 272-286.
Shungin, D*., et al.* (2015) New genetic loci link adipose and insulin biology to body fat distribution, *Nature*, 518, 187-196.
Somarowthu, S*., et al.* (2015) HOTAIR forms an intricate and modular secondary structure, *Molecular Cell*, 58, 353-361.
Stephens, M. and Donnelly, P. (2003) A comparison of bayesian methods for haplotype reconstruction from population genotype data, *American Journal of Human Genetics*, 73, 1162-1169.
Stevens, J., Katz, E.G. and Huxley, R.R. (2010) Associations between gender, age and waist circumference, *Eur J Clin Nutr*, 64, 6-15.
Sun, L*., et al.* (2013) Long noncoding RNAs regulate adipogenesis, *Proc Natl Acad Sci U S A*, 110, 3387-3392.
Sun, M. and Kraus, W.L. (2015) From discovery to function: the expanding roles of long noncoding RNAs in physiology and disease, *Endocr Rev*, 36, 25-64.
Sun, X., Haider Ali, M.S.S. and Moran, M. (2017) The role of interactions of long non-coding RNAs and heterogeneous nuclear ribonucleoproteins in regulating cellular functions, *Biochem J*, 474, 2925-2935.
Sun, Z*., et al.* (2018) Emerging role of exosome-derived long non-coding RNAs in tumor microenvironment, *Mol Cancer*, 17, 82.
Szczerbal, I., Foster, H.A. and Bridger, J.M. (2009) The spatial repositioning of adipogenesis genes is correlated with their expression status in a porcine mesenchymal stem cell adipogenesis model system, *Chromosoma*, 118, 647-663.
Tak, Y.G. and Farnham, P.J. (2015) Making sense of GWAS: using epigenomics and genome engineering to understand the functional relevance of SNPs in non-coding regions of the human genome, *Epigenetics & Chromatin*, 8, 57.
Tchoukalova, Y.D*., et al.* (2010) Regional differences in cellular mechanisms of adipose tissue gain with overfeeding, *Proceedings of the National Academy of Sciences of the United States of America*, 107, 18226-18231.
Thompson, D*., et al.* (2012) Physical activity and exercise in the regulation of human adipose tissue physiology, *Physiol Rev*, 92, 157-191.
Todorcevic, M*., et al.* (2017) A cellular model for the investigation of depot specific human adipocyte biology, *Adipocyte*, 6, 40-55.
Tong, Q*., et al.* (2000) Function of GATA transcription factors in preadipocyte-adipocyte transition, *Science*, 290, 134-138.
Tsai, M.C*., et al.* (2010) Long noncoding RNA as modular scaffold of histone modification complexes, *Science*, 329, 689-693.
Uemura, M*., et al.* (2007) OL-Protocadherin is essential for growth of striatal axons and thalamocortical projections, *Nature Neuroscience*, 10, 1151-1159.
Vallis, M. (2016) Quality of life and psychological well-being in obesity management: improving the odds of success by managing distress, *Int J Clin Pract*, 70, 196-205.
Van Harmelen, V*., et al.* (1998) Leptin secretion from subcutaneous and visceral adipose tissue in women, *Diabetes*, 47, 913-917.
Van Pelt, R.E*., et al.* (2006) Acute modulation of adipose tissue lipolysis by intravenous estrogens, *Obesity*, 14, 2163-2172.
Vazquez, G*., et al.* (2007) Comparison of body mass index, waist circumference, and waist/hip ratio in predicting incident diabetes: a meta-analysis, *Epidemiologic Reviews*, 29, 115-128.
Verheijen, R., van Venrooij, W. and Ramaekers, F. (1988) The nuclear matrix: structure

and composition, *J Cell Sci*, 90 (Pt 1), 11-36.
Verstraeten, V.L.*, et al.* (2011) Reorganization of the nuclear lamina and cytoskeleton in adipogenesis, *Histochem Cell Biol*, 135, 251-261.
Vigouroux, C.*, et al.* (2001) Nuclear envelope disorganization in fibroblasts from lipodystrophic patients with heterozygous R482Q/W mutations in the lamin A/C gene, *J Cell Sci*, 114, 4459-4468.
Visscher, P.M.*, et al.* (2017) 10 Years of GWAS Discovery: Biology, Function, and Translation, *American Journal of Human Genetics*, 101, 5-22.
Visser, M., Kayser, M. and Palstra, R.J. (2012) HERC2 rs12913832 modulates human pigmentation by attenuating chromatin-loop formation between a long-range enhancer and the OCA2 promoter, *Genome Research*, 22, 446-455.
Vogelstein, B., Pardoll, D.M. and Coffey, D.S. (1980) Supercoiled loops and eucaryotic DNA replicaton, *Cell*, 22, 79-85.
Wahrenberg, H., Lonnqvist, F. and Arner, P. (1989) Mechanisms underlying regional differences in lipolysis in human adipose tissue, *J Clin Invest*, 84, 458-467.
Wang, C.*, et al.* (2017) LncRNA Structural Characteristics in Epigenetic Regulation, *Int J Mol Sci*, 18.
Wang, K.C. and Chang, H.Y. (2011) Molecular mechanisms of long noncoding RNAs, *Molecular Cell*, 43, 904-914.
Wang, Q.L.*, et al.* (2016) Data analysis in the post-genome-wide association study era, *Chronic Diseases and Translational Medicine*, 2, 231-234.
Wang, R. and Li, X.N. (2017) [Different adipose tissue depots and metabolic syndrome in human], *Sheng Li Xue Bao*, 69, 357-365.
Wei, B.*, et al.* (2017) Long non-coding RNA HOTAIR inhibits miR-17-5p to regulate osteogenic differentiation and proliferation in non-traumatic osteonecrosis of femoral head, *PloS One*, 12, e0169097.
Wells, J.C. (2007) Sexual dimorphism of body composition, *Best Pract Res Clin Endocrinol Metab*, 21, 415-430.
WHO (2017) Obesity and overweight. World Health Organization, http://www.who.int/mediacentre/factsheets/fs311/en/.
Williams, E.P.*, et al.* (2015) Overweight and Obesity: Prevalence, Consequences, and Causes of a Growing Public Health Problem, *Current Obesity Reports*, 4, 363-370.
Wolverton, T. and Lalande, M. (2001) Identification and characterization of three members of a novel subclass of protocadherins, *Genomics*, 76, 66-72.
Wu, J.*, et al.* (2012) Beige adipocytes are a distinct type of thermogenic fat cell in mouse and human, *Cell*, 150, 366-376.
Xiao, T.*, et al.* (2015) Long Noncoding RNA ADINR Regulates Adipogenesis by Transcriptionally Activating C/EBPalpha, *Stem Cell Reports*, 5, 856-865.
Xu, F. and Zhang, J. (2017) Long non-coding RNA HOTAIR functions as miRNA sponge to promote the epithelial to mesenchymal transition in esophageal cancer, *Biomedicine & Pharmacotherapy*, 90, 888-896.
Xu, Y.*, et al.* (2015) PCDH10 inhibits cell proliferation of multiple myeloma via the negative regulation of the Wnt/beta-catenin/BCL-9 signaling pathway, *Oncology Reports*, 34, 747-754.
Yan, H.*, et al.* (2015) Chromatin modifications and genomic contexts linked to dynamic DNA methylation patterns across human cell types, *Scientific Reports*, 5, 8410.
Yan, J.*, et al.* (2018) Histone H3 lysine 4 monomethylation modulates long-range chromatin interactions at enhancers, *Cell Research*, 28, 387.
Yan, J.*, et al.* (2018) Histone H3 lysine 4 monomethylation modulates long-range

chromatin interactions at enhancers, *Cell Research*, 28, 204-220.
Yang, Z.*, et al.* (2011) Overexpression of long non-coding RNA HOTAIR predicts tumor recurrence in hepatocellular carcinoma patients following liver transplantation, *Annals of Surgical Oncology*, 18, 1243-1250.
Yao, K.*, et al.* (2017) A competing endogenous RNA network identifies novel mRNA, miRNA and lncRNA markers for the prognosis of diabetic pancreatic cancer, *Tumour Biology*, 39, 1010428317707882.
Ye, K.*, et al.* (2015) Matrix Stiffness and Nanoscale Spatial Organization of Cell-Adhesive Ligands Direct Stem Cell Fate, *Nano Letters*, 15, 4720-4729.
Ye, M., Li, J. and Gong, J. (2017) PCDH10 gene inhibits cell proliferation and induces cell apoptosis by inhibiting the PI3K/Akt signaling pathway in hepatocellular carcinoma cells, *Oncology Reports*, 37, 3167-3174.
Ying, J.*, et al.* (2006) Functional epigenetics identifies a protocadherin PCDH10 as a candidate tumor suppressor for nasopharyngeal, esophageal and multiple other carcinomas with frequent methylation, *Oncogene*, 25, 1070-1080.
Yokochi, T.*, et al.* (2009) G9a selectively represses a class of late-replicating genes at the nuclear periphery, *Proceedings of the National Academy of Sciences of the United States of America*, 106, 19363-19368.
Yoon, J.H.*, et al.* (2013) Scaffold function of long non-coding RNA HOTAIR in protein ubiquitination, *Nature Communications*, 4, 2939.
Yu, Y.*, et al.* (2017) HOTAIR may regulate proliferation, apoptosis, migration and invasion of MCF-7 cells through regulating the P53/Akt/JNK signaling pathway, *Biomedicine & Pharmacotherapy*, 90, 555-561.
Yusuf, S.*, et al.* (2005) Obesity and the risk of myocardial infarction in 27,000 participants from 52 countries: a case-control study, *Lancet*, 366, 1640-1649.
Zhang, C.*, et al.* (2016) Upregulation of lncRNA HOTAIR contributes to IL-1beta-induced MMP overexpression and chondrocytes apoptosis in temporomandibular joint osteoarthritis, *Gene*, 586, 248-253.
Zhang, H.J.*, et al.* (2017) LncRNA HOTAIR alleviates rheumatoid arthritis by targeting miR-138 and inactivating NF-kappaB pathway, *International Immunopharmacology*, 50, 283-290.
Zhang, S.*, et al.* (2014) Long noncoding RNA HOTAIR as an independent prognostic marker in cancer: a meta-analysis, *PloS One*, 9, e105538.
Zhang, T.*, et al.* (2018) Regulating osteogenesis and adipogenesis in adipose-derived stem cells by controlling underlying substrate stiffness, *Journal of Cellular Physiology*, 233, 3418-3428.
Zhong, X.*, et al.* (2017) Epigenetic silencing of protocadherin 10 in colorectal cancer, *Oncology Letters*, 13, 2449-2453.
Zhou, X., Chen, J. and Tang, W. (2014) The molecular mechanism of HOTAIR in tumorigenesis, metastasis, and drug resistance, *Acta Biochimica et Biophysica Sinica*, 46, 1011-1015.
Zou, Y.F. and Sun, L.Z. (2015) [Long noncoding RNA HOTAIR modulates the function of trophoblast cells in pre-eclampsia], *Sichuan Da Xue Xue bao. Yi xue ban*, 46, 113-117, 122.